MICROMECHANICAL BIOCHEMICAL STUDIES OF MITOTIC CHROMOSOME ELASTICITY AND STRUCTURE

BY

MICHAEL GUY POIRIER
B.S., Northeast Missouri State University, 1995
M.S., University of Illinois at Chicago, 1997

THESIS
Submitted as partial fulfillment of the requirements
for the degree of Doctor of Philosophy in Physics
in the Graduate College of the
University of Illinois at Chicago, 2001

Chicago, Illinois

This thesis is dedicated to my parents Clare and Victor and my wife Ellen, who are always there to provide encouragement and support.

ACKNOWLEDGMENTS

The person I am most grateful to is my advisor, Prof. John Marko. It has been a wonderful opportunity to work for and learn from him. His guidance is what has allowed me to do these experiments and understand some of the physics behind them.

I am grateful to my thesis committee, Prof. Anjum Ansari, Prof. Michael Cho, Prof. Wai-Yee Keung and Prof. Mark Schlossman, for their critical reading of and suggestions about this thesis.

I would like to thank the many people who helped me during my thesis research. Prof. Didier Chatenay was critical in getting Prof. Marko's lab started. Sertac Eroglu, and I worked closely during the initial elasticity experiments. Abihjit Sarkar and Yan Jie, theory graduate students in Prof. Marko's lab, provided many interesting discussions related and unrelated to physics. Abihjit Sarkar kindly took the time to edit this thesis. Yan Jie was particularly helpful when I was studying various aspects of elasticity theory and fixed all of the computer problems I encountered. Prof. Marko's experimental graduate students, Dunja Skoko, Chee Xiong and Pan Yan worked with me in taking care of the day-to-day aspects of the lab. I had many interesting and helpful discussions with Dr. Simona Cocco and Dr. Remi Monasson. The undergraduates in Prof. Marko's lab, Mazen Albaghdadi, Caiti Hammill-Thompson, Prateek Gupta, Tamar Monhait and Ajay Nemani helped in various aspects of this research, especially with maintaining the cell cultures. All of these people combined to make Prof. Marko's lab an exciting place to do research.

I would like to thank Dr. Y. Cui, Dr. S. Dimitrov, Prof. G. Friedman, Dr. T. Hirano, Dr. B. Houchmandzadeh, Prof. F.C. MacKintosh, Prof. A. Maniotis, Dr. W. Marshall, Prof. J. Sedat, Prof. J. Widom and Prof. E.L. Zecheidrich for helpful discussions and advice regarding these

experiments. I am indebted to Prof. D. Reese for generously sending us the TVI cells used in this study.

I also acknowledge the help of the Biology Department and in particular Prof. L. Kaufman, Prof. H. Buhse, Prof. L. Miller, Prof. A. Kaplan, Dr. Adam Markaryan and Bao Song for help with fluorescence, cell culture techniques and gel imaging.

I would like to thank the Whitaker Foundation, which supported me from 1997 to 2001 through Biomedical Engineering Research Grant 20-32/59. This work was also indirectly supported by the National Science Foundation through Grant DMR-973178, by the Research Corporation through a Research Innovation Award, by the Petroleum Research Foundation of the American Chemical Society through Grant 31911-AC7, and by a Focused Giving Grant from Johnson and Johnson Corporate Research.

The physics machine shop was critical for the success of the research. Kevin, Kurt, Bob and the late Rich are amazing machinists. They made many of the critical components of these experiments.

I would like to thank my good friend, Dan Decoursey, who took time out of his busy schedule to edit the introduction of this thesis.

Most importantly, I want to thank my family: my wife, Ellen, my parents, Clare and Vic, my sister, Emily, my brother, David and my in-laws, Marlene, Lester, Colin, Camille and Jamie. They are always there providing all the support and encouragement I could need.

TABLE OF CONTENTS

TABLE OF CONTENTS (continued)

TABLE OF CONTENTS (continued)

TABLE OF CONTENTS (continued)

LIST OF TABLES

LIST OF FIGURES

LIST OF FIGURES (continued)

LIST OF FIGURES (continued)

LIST OF ABBREVIATIONS

bp	base pair of DNA
BSA	Bovine Serium Albumin
DNA	Deoxyribose Nucleic Acid
dsDNA	double-stranded DNA
FBS	Fetal Bovine Serum
GFP	Green Fluorescent Protein
kb	kilobase of DNA
kDa	Kilodalton
MDa	Megadalton
MN	Micrococcal Nuclease
NCCM	Newt Cell Culture Medium
PBS	Phosphate Buffer Saline
RE	Restrictions Enzymes
SFM	Scanning Force Microscope
ssDNA	single-stranded DNA

Summary

This thesis presents characterization of the elasticity of single mitotic chromosomes and its response to shifts in solution conditions and to enzyme modifications. The elasticity experiments were conducted to investigate the structure of mitotic chromosomes.

Our method involves attaching glass micropipettes to either end of a single chromosome to perform mechanical experiments in the extracellular buffer. A third pipette can be used to locally 'spray' reactants in order to carry out dynamical mechanical-chemical experiments. The following elastic properties of mitotic chromosomes are found: Young's modulus, Y = 300 Pa; Poisson ratio, σ = 0.1; Bending rigidity, $B = 1\times10^{-22}$ J·m; Internal viscosity, η' = 100 kg/m·sec; Volume fraction, ϕ = 0.7; Extensions of less than three times the relaxed length are linear and reversible; Extensions beyond 30 fold exhibit a force plateau at 15 nN and convert the chromosome to a disperse ghost-like state with little change in chromatin structure; Mitotic chromosomes are relatively isotropic; dsDNA cuts of at least every 3 kb cause the a mitotic chromosomes to fall apart; dsDNA cuts less frequently than every 50 kb do not affect mitotic chromosome structure.

These results lead to the conclusion that mitotic chromosomes are a network crosslinked every 50 kb between which chromatin is folded by chromatin folding proteins, which are likely condensins.

The results of these chromosome elasticity experiments and their contributions to the understanding of chromosome structure are organized into eight chapters. Chapter 1 introduces background information, reviews related research, describes the motivation behind this research and summarizes the results and conclusions. Chapter 2 describes the techniques and methods that were employed. Chapters 3 through 7 present the experimental results. Chapter 3, 4 and 5 report

the elastic properties of mitotic chromosomes while Chapters 6 and 7 discuss the use of elasticity measurements to monitor the perturbation of mitotic chromosome structure with various ionic conditions and enzymes. Finally, Chapter 8 summarizes these results which form a cohesive story about chromosome structure.

CHAPTER 1

INTRODUCTION

1.1 Overview

This chapter presents background information, reviews related research, describes the motivation behind this thesis and summarizes the results and conclusions. First, a brief discussion of the cell cycle, mitosis, DNA, chromatin and chromosomes is presented. This is followed by a review of the current understanding of mitotic chromosome structure. The theory of linear elasticity of a rod is then introduced. This leads to a description of recent elasticity experiments on single biomolecules that are contained within mitotic chromosomes. A detailed description of the motivation for this research is then included. Finally, the main results and conclusions of this thesis are introduced.

1.2 The Cell Cycle and Mitosis

The cell is the biological unit that contains the entire set of genetic information of an organism in the form of DNA. The dissemination of this information from generation to generation is required for continued existence and is accomplished through the cell cycle, the periodic process by which one cell becomes two. There are four main parts of the cell cycle: S, G2, M and G1 (Figure 1.1). S (synthesis) is the period of the cell cycle when the DNA is replicated. M (mitosis) is the period of the cell cycle when a cell splits the two sets of copied chromosomes into two new cells. G1 and G2 (gap) are the periods following M and S respectively during which the cell recovers from either M or S phase; the cell then performs various functions according to the cell type and prepares for the next period of the cell cycle. Often G1, S and G2 are grouped into one phase of the cell cycle; interphase. This very general

description applies to most cell types from unicellular organisms to cells in multicellular organisms. The following study will focus exclusively on cells from multicellular animals.

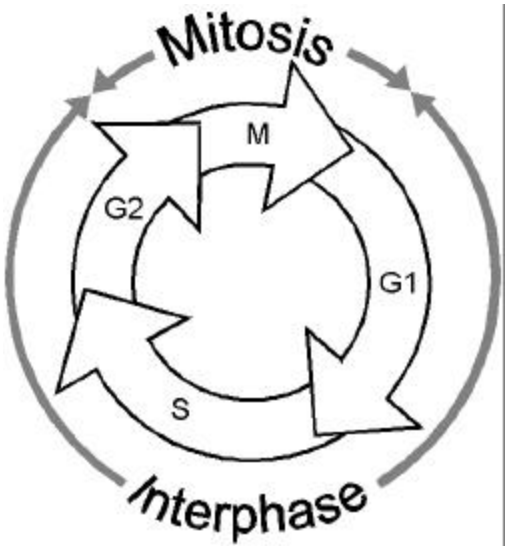

Figure 1.1 The cell cycle is grouped into four periods: S (synthesis), G2 (second gap), M (mitosis) and G1 (first gap). Interphase refers to the three phases S, G1 and G2.

Mitosis is traditionally divided into 6 parts: Prophase, Prometaphase, Metaphase, Anaphase, Telophase and Cytokinesis (Alberts *et al*, 1994). Each of these periods of mitosis is roughly defined by what is observed in the light microscope (Figure 1.2). Prophase occurs when the cell's two sets of chromosomes (which were duplicated earlier in S phase) begin to condense and appear as distinct, worm-like objects in the light microscope. The nuclear envelope remains intact around the worm-like chromosomes. Prometaphase begins when the nuclear envelope disappears. The chromosomes continue to condense as microtubules move them around the cell. Metaphase begins as the chromosomes are aligned along a plane, known as the "metaphase

plate," which is located midway through the cell. The cell then waits for a period of time while the chromosomes continue to oscillate. Anaphase begins as the two sets of chromosomes move toward opposite poles. After the chromosomes are separated, telophase occurs: the chromosomes decondense and the nuclear envelope reappears. Finally, during cytokinesis, the cell cleaves itself into two new cells, each with an identical set of the parent cell's chromosomes. A movie of mitosis can be found at http://safarsquid.phy.uic.edu/~mpoirier/experiments/mitosis.mpg. Clearly, many complicated processes must take place to enable that mitosis be successfully completed.

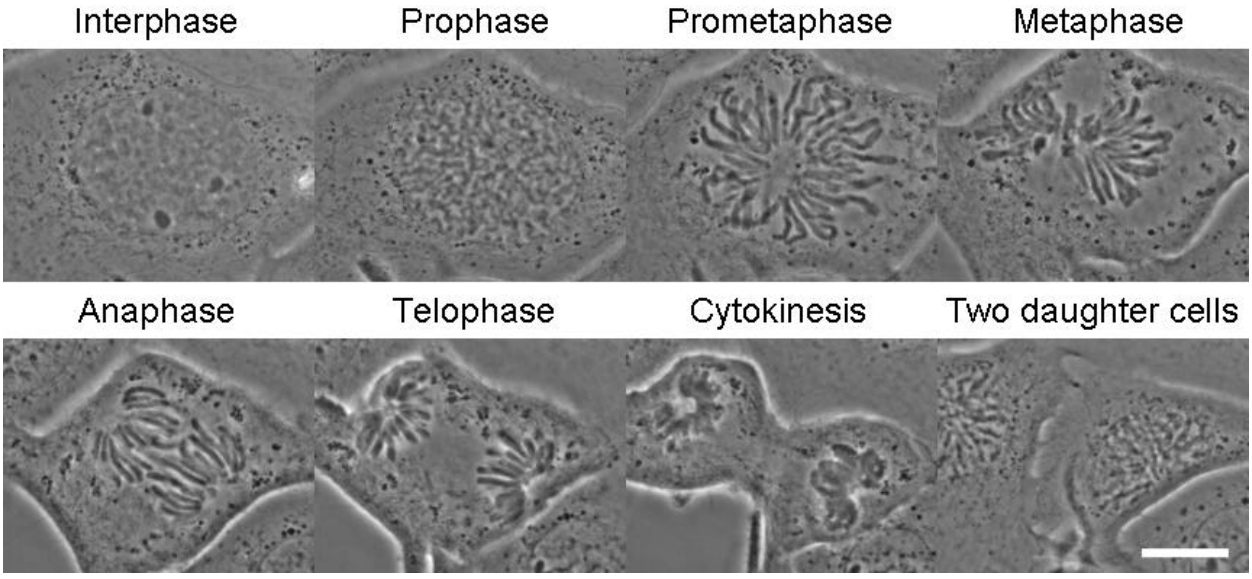

Figure 1.2 Images of a newt lung cell during the different phases of mitosis. Bar = 20 ìm.

Chromosome structure and its modulation are critical to many aspects of cell function. During interphase, control of chromosome structure at the chromatin level is important for the

success and regulation of transcription, replication and recombination (Widom, 1997). As the cell enters mitosis, larger-scale chromosome structure becomes central to disentanglement and compaction of the two chromosome copies, for successful segregation of chromosomes into the daughter cells (Koshland 1994, Heck, 1997). Chromosome structures at these different periods of the cell cycle are intensely studied, yet no clear picture of large-scale structure exists for either interphase or mitotic chromosomes (Koshland and Strunnikov, 1996, Widom, 1998, Hirano, 2000).

1.3 Components of Mitotic Chromosomes

1.3.1 DNA and Histones

A mitotic chromosome is composed of DNA and proteins. DNA consists of a double helix in which the two single strands of DNA are held together by hydrogen bonds and base-stacking interactions (Watson and Crick, 1953). Throughout the cell cycle, chromosomal DNA is organized around an octamer of proteins called core histones (van Holde, 1989). There are four types of core histones: H2A, H2B, H3 and H4 and two of each combine with DNA to form a nucleosome. These core histones form a spool that DNA wraps around about 1.6 times (Figure 1.3). The interaction between DNA and the core histones is mainly electrostatic, since DNA is highly negatively charged and histones are highly positively charged. The diameter of the nucleosome is approximately 10 nm with close to 146 bp of DNA wrapped around the histone spool. The DNA is organized into chromatin by successive nucleosomes separated by about 60 bp of 'linker' DNA, and forms a chromatin structure commonly termed 'beads on a string'.

The structure of the nucleosome is precisely known because single nucleosomes can be isolated with micrococcal nuclease, which cuts only the linker DNA, since the DNA wrapped around the histones is protected (Polach and Widom, 1995). The individual nucleosomes are then

crystallized and the structure is determined by x-ray crystallography (Klug *et al*,1980, Burlingame *et al,* 1985, Lugar, 1997). The beads on a string structure compacts DNA length by approximately 2.5 times.

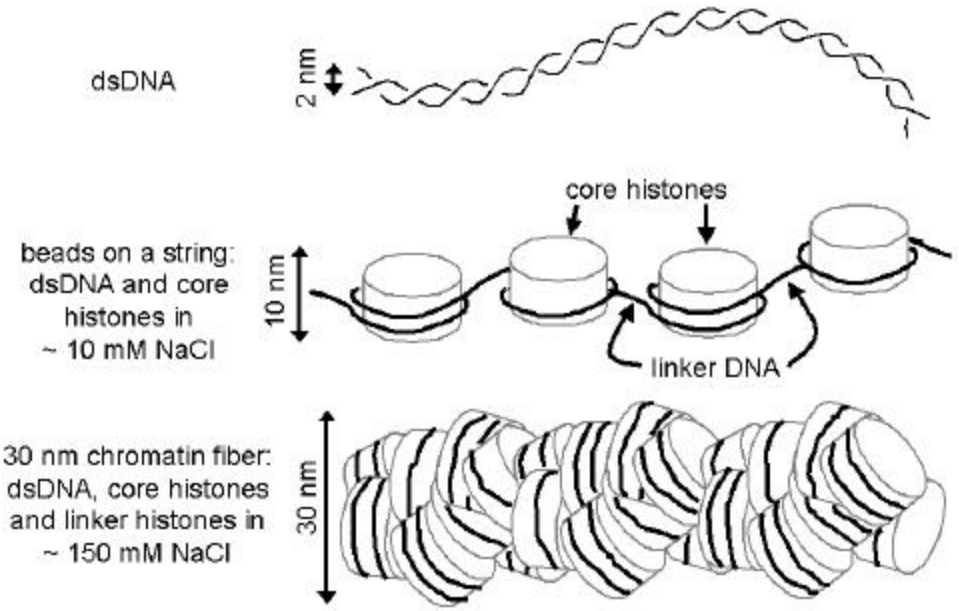

Figure 1.3 Organization of DNA into chromatin. dsDNA wraps around eight core histones to form the 'beads on a string' structure. At physiological ionic conditions with linker histones, the 'beads on a string' condense into 30 nm chromatin fiber.

1.3.2 Chromatin Fiber

The next level of DNA compaction is the 'beads on a string' condensed into the 30 nm chromatin fiber (Figure 1.3). This compaction occurs as a result of interactions between adjacent nucleosomes and the addition of linker histones (van Holde, 1989). The formation of 30 nm chromatin fibers is sensitive to solution conditions, and is most compact at concentrations around 150 mM of univalent salt (van Holde, 1989). This level of DNA folding is not as well understood

as the structure of the nucleosome. There are various models of how the nucleosomes stack into 30 nm chromatin fiber, such as the solenoid model (Widom, 1998). This level of structure is used *in vivo* to regulate transcription and replication by varying the degree of compaction (Widom, 1998). The 30 nm chromatin fiber, not simply dsDNA, is the fundamental fiber of mitotic chromosomes (Figure 1.3).

Not only are histones vital for the formation of 30 nm chromatin fiber, but inter-histone interactions may play a role in large-scale mitotic chromosome condensation and structure. The role of phosphorylation (the addition of a negative charge in the form of a PO_4^-) of linker histone H1 remains unclear, but recent results indicate that it is not required for chromosome condensation (Hirano, 2000). Phosphorylation of histone H3 is tightly coupled to and required for proper chromosome condensation (Hirano, 2000). However, it does not play a role in maintaining mitotic chromosome structure, which suggests that its role in chromosome condensation is indirect (Hirano, 2000).

1.3.3 Topoisomerase II, Condensin and Cohesin

Additional protein factors involved in compacting 30 nm chromatin fiber into a mitotic chromosome are topoisomerase II, condensin and cohesin. Topoisomerase II is well known to resolve dsDNA entanglements (Champoux, 2001) and is required for successful mitotic chromosome condensation (Hirano, 2000). It is found within mitotic chromosomes but the question of what structural role it plays in the assembled mitotic chromosome is somewhat unsettled. Experiments that remove topoisomerase II from *in-vitro*-assembled chromatids suggest that it is not exclusively required for maintenance of mitotic chromosome structure (Hirano and Mitchison, 1993). On the other hand, Bojanowski *et al*, 1998 have shown that topo II can 'rescue' a condensed morphology after protease is used to decondense mitotic

chromosomes removed from metaphase cells, suggesting a possible chromatin-condensing function for topo II.

The condensin complex is a more recently discovered component of mitotic chromosomes (Strunnikov *et al*, 1993). The condensin complex is composed of 5 protein subunits, in which the core of the condensin complex consists of a heterodimer of SMC2 and SMC4 proteins (Structural Maintenance of Chromosomes) (Hirano, 1998). This protein complex is found in mitotic chromosomes every 5-10 kb (Sutani and Yanagida, 1997 and Kimura *et al*, 1999). It is also extremely large: SMC2 and SMC4 have about 1200 amino acids and a molecular weight of about 140 kDa. The *Xenopus* versions of SMC2 and SMC4 are called XCAP-E and XCAP-C, respectively. Both SMC2 and SMC4 have two large coiled-coil domains connected by a hinge (Hirano and Mitchison, 1994). SMC2 and SMC4 associate to form a complex that is about 0.1 microns long (Melby *et al*, 1998). The overall structure of condensin suggests it could fold 30 nm chromatin fiber (Figure 1.4).

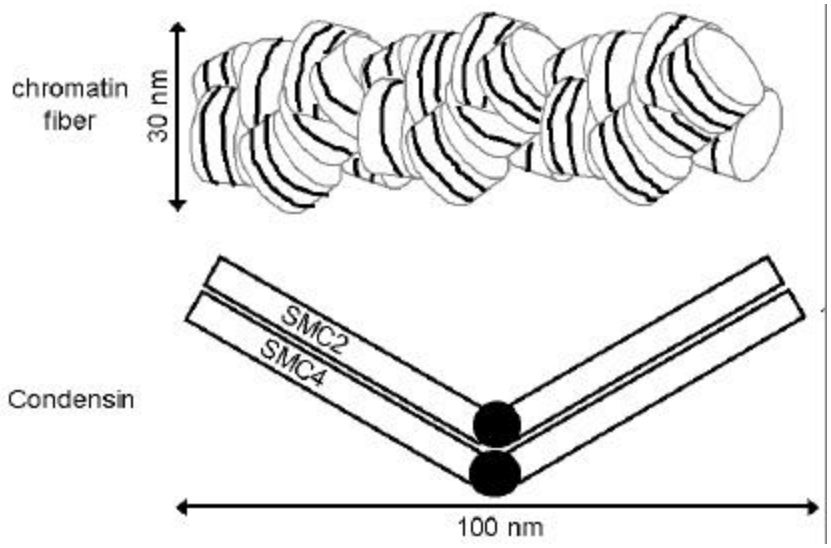

Figure 1.4 The length scales and rough structure of 30nm chromatin fiber and condensin.

Genetic studies in yeast and biochemical studies in *Xenopus* egg extracts have combined to show that the condensin complex is required for the maintenance of mitotic chromosome structure (Hirano, 2000). For example, antibody depletion of certain SMCs from *in vitro* assembled chromatids results in their gradual dissolution into a cloud of chromatin fibers (Hirano and Mitchison, 1994), indicating that those SMCs are chromatin-tethering elements. However, the mechanism by which they condense and maintain chromosome structure is an open question.

The cohesin complex is another recently discovered component of mitotic chromosomes and a close relative of condensin. It is composed of proteins from the SMC family--SMC1 and SMC3--and is required for maintaining connections between daughter chromatids after the chromosomes are duplicated during S-phase (Hirano, 2000). In *S. cerevisiae*, cohesin is responsible for maintaining sister chromatid connects from S phase to the metaphase-anaphase transition (Michaelis *et al*, 1997). In higher eukaryotes, cohesion is more complicated since the measurable amount of cohesin is only observed from S phase to the onset of mitosis (Losada *et al*, 1998). It has been proposed that with higher eukaryotes most of the cohesin during S phase is removed at the onset of mitosis to allow for the larger amount of chromatin compaction as compared to yeast (Hirano, 2000).

1.4 Models of Metaphase Chromosome Structure

The condensation of mitotic chromosomes is widely believed to be based on the folding of chromatin by protein fasteners (Paulson and Laemmli, 1977). The organizational length scale ranges from a few to a hundred nanometers; structure on this scale is difficult to determine. The wavelength of visible light does not allow standard light microscopy techniques to probe this length scale. X-ray diffraction, which can provide Angstrom resolution, is also difficult to apply to the study of chromosome structure, since it generally requires an ordered sample removed

from aqueous solution. Removal of mitotic chromosomes from aqueous solution will likely change their structure. Also, a well ordered structure like a protein crystal is not expected for mitotic chromosomes, making interpretation of a most likely diffuse chromosome diffraction pattern problematic.

Many studies of high-level mitotic chromosome structure are performed with the use of electron microscopy. This technique does probe the length scale of interest: 1nm - 100nm. Results of Paulson and Laemmli, 1977, Earnshaw and Laemmli 1983 and Belmont *et al*, 1987 have led to different models of chromosome structure, including the organization of chromatin around a protein-rich 'scaffold' (Figure 1.5a, Paulson and Laemmli, 1977), or alternately, hierarchies of helical folding (Figure 1.5b, Belmont *et al*, 1987). It has also been suggested that mitotic chromosome structure is a combination of these models (Boy de la Tour and Laemmli, 1988). Interestingly, the possibility that mitotic chromosomes are essentially a three-dimensional crosslinked 'network' (Figure 1.5c) has been largely ignored in the biological literature.

Figure 1.5 Models of high-level mitotic chromosome structure. (a) 'scaffold' model, (b) 'successive coiling or folding of chromatin' model and (c) 'network' model.

Unfortunately, it is unclear whether the structures viewed by electron microscopy are representative of *in vivo* mitotic chromosome structure. Electron microscopy requires elaborate preparations of mitotic chromosomes that involve the plating and drying of chromosomes onto microscope slides and viewing them vacuum, or TEM analysis of thin slices of fixed and densely crosslinked samples (Adolph, 1988). The preparation is likely to change the *in vivo* mitotic chromosome structure, and explains why the use of electron microscopy has led to opposing models of mitotic chromosome structure.

The use of fluorescence microscopy has proven extremely useful in the study of mitotic chromosome structure. Immunolocalization experiments have shown where specific types of molecules are located within a mitotic chromosome (Boy de la Tour and Laemmli, 1988, Hirano and Mitchison, 1994). In the past five years, the intrinsic green fluorescent protein (GFP) has revolutionized fluorescent microscopy (Sullivan and Kay, 1999). This protein, which is found naturally in the jellyfish, *Aequorea Victoria*, can be inserted into an organism's genome with a sequence that codes for the protein of interest. When the protein is synthesized, the GFP protein is thus included, attached to the protein of interest. Now this specific protein is itself fluorescent and can be visualized by fluorescent microscopy.

The incorporation of GFP into the *lac* operator/*lac* repressor reporter system (Robinett *et al*¸ 1996) is proving to be powerful in viewing high-level chromosome structure *in vivo* for both interphase and mitotic chromosomes. This technique involves inserting into an organism's genome both the *lac* repressor gene with the GFP sequence and a 256 tandem repeat sequence of the *lac* operator gene. The cell expresses the *lac* repressor gene producing many copies of a *lac* repressor protein labeled with GFP. These proteins then bind to the *lac* operator repeat sequence making this region of DNA visible by fluorescent microscopy. This new technique has

demonstrated that interphase chromosomes have a relatively large degree of freedom to move within a region of the nucleus (Tumbar and Belmont, 2001). It has also been used to show that the dsDNA folding pattern within mitotic chromosomes changes as the cell goes from prophase to anaphase (Dietzel and Belmont, 2001) and that the folding pattern is inconsistent with a scaffold model. This technique is also very powerful when combined with genetically sequenced and controllable organisms such as *Bacillus subtillis* (Lemon and Grossman, 2000) and *S. cerevesiae* (Pearson *et al*, 2001) where fluorescence microscopy is used as an assay to monitor if mutations in specific genes affect chromosome structure.

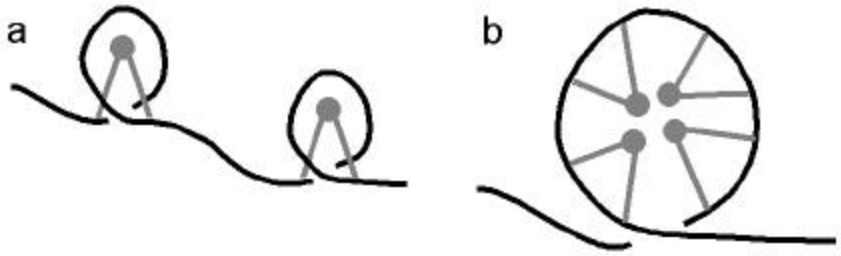

Figure 1.6 Two models of how condensin compacts DNA in chromosomes proposed by Kimura *et al*, 1999.

This chapter has described high-order structure without considering the proteins, which actually maintain the folded chromosome structure. With the discovery of condensin, a model of how it folds up chromatin in mitotic chromosomes structure has been proposed by Kimura *et al*, 1999. They studied, *in vitro*, the topology of circular DNA molecules in the presence of condensin from *Xenopus* egg extracts with either topoisomerase I or II. They conclude that condensin induces a global writhe in dsDNA and propose two ways condensin could compact

DNA: each condensin molecule acts individually to induce and maintain a fold in DNA (Figure 1.6a), or condensin molecules act together to form a large helical wrap (Figure 1.6b). Although preliminary, these are the first models proposed to explain how condensin compacts chromatin into a mitotic chromosome. Additional experiments are needed, especially to address how the interaction of condensin with DNA will change when it acts on DNA within chromatin.

1.5 Linear Elasticity of a Rod

Here we describe the linear elasticity of isotropic rods (Laudau and Lifshitz, 1986), which is used as a framework to describe chromosome elasticity. It is not unreasonable to assume isotropy because proteins and the width of chromatin are small compared to the size of a chromosome. However, the length of chromatin fiber is not, so aspects of the mitotic chromosome structure may not be isotropic. Isotropic elasticity theory is still useful because agreement between measurement and theory point to isotropic aspects of chromosome structure while inconsistencies indicate inhomogeneity of chromosome structure.

A deformation of a continuous elastic body is described by two tensors of rank two, the strain tensor, u_{ij}, and the stress tensor, σ_{ij}, where $i,j = x,y,z$. The strain tensor is defined as $u_{ij} = \frac{1}{2}\left(\frac{\partial u_i}{\partial x_j} + \frac{\partial u_j}{\partial x_i} + 2\frac{\partial u_i}{\partial x_j}\frac{\partial u_j}{\partial x_i} \right)$, where u_i is the position vector. For small deformations, $\frac{\partial u_i}{\partial x_j}$ is small and to lowest order, $u_{ij} = \frac{1}{2}\left(\frac{\partial u_i}{\partial x_j} + \frac{\partial u_j}{\partial x_i} \right)$. The strain tensor is symmetric, unitless and describes how distances change within a deformed body.

The internal stress that develops within a volume element of a deformed object is simply a sum over the force density within the volume, $f_i \, dV$, where f_i is the i^{th} component of the force density. We are considering static deformations, so the sum over the force density must be zero and the resultant force is applied at the surface. From Stokes' theorem, we know that if a volume

integral of a scalar can be converted to a surface integral, the scalar can be written as the divergence of a vector. The integrand, f_i, is a vector, so it is the divergence of a rank two tensor, i.e. $f_i = \frac{\partial \sigma_{ij}}{\partial x_j}$. The stress tensor is in units of energy per volume or pressure, and describes the internal forces that develop as a body is deformed. We will consider deformations in which the change in position between two adjacent points in an object is small compared to the undeformed distance between those two points.

The free energy density, F, to lowest order, is quadratic in terms of the stress tensor since the free energy is a scalar and is of the form: $F = F_0 + \frac{1}{2}\lambda u_{ii}^2 + \mu u_{ij}^2$. λ and μ are called the Lamé coefficients and are in units of pressure. By writing u_{ik} as a sum of a shear and a hydrostatic compression, $u_{ik} = (u_{ij} - \delta_{ij} u_{kk}) + \delta_{ij} u_{kk}$, the free energy density (neglecting F_0) is

$$F = \mu(u_{ij} - \delta_{ij} u_{kk})^2 + \frac{1}{2}K u_{kk}^2, \qquad (1.1)$$

where $K = \lambda + \frac{2}{3}\mu$. The coefficients μ and K are the shear and bulk moduli, and are both in units of pressure. The shear modulus is the energy density of a deformation that changes the shape without changing the total volume. The bulk modulus is the energy density of a change in volume without a change in shape.

A change in the free energy density takes the form, $dF = -S dT + \sigma_{ij} du_{ij}$, and therefore $\sigma_{ij} = (\partial F/\partial u_{ij})_T$. This calculates σ_{ij} in terms of u_{ij}.

$$\sigma_{ij} = K u_{kk} \delta_{ij} + 2\mu(u_{ij} - \tfrac{1}{3}\delta_{ij} u_{kk}) \qquad (1.2)$$

By recognizing that $u_{kk} = \sigma_{kk}/3K$, we can solve for u_{ij}.

$$u_{ij} = \delta_{ij}\sigma_{kk}/9K + (\sigma_{ij} - \tfrac{1}{3}\delta_{ij}\sigma_{kk})/2\mu \qquad (1.3)$$

After inserting (1.2) into (1.1), the free energy density reduces to a simple form of

$$F = \frac{1}{2}\sigma_{ij} u_{ij}. \qquad (1.4)$$

1.5.1 Stretching

These equations describe deformations of any elastic body, which we will now apply to a rod since this is how mitotic chromosomes appear in the light microscope (Figure 1.1). There are three simple types of rod deformations: uniaxial, bending and twisting. We will focus on the first two types: uniaxial and bending deformations.

A uniaxial deformation is simply an extension or compression by a force per area P applied along the rod axis at the ends (Figure 1.7), so the only component of the stress tensor that is nonzero is $\sigma_{zz} = P$. Eq. (1.3) calculates how the strain responds to the applied stress. The off-diagonal terms of u_{ij} are zero and the diagonal terms are:

$$u_{zz} = \frac{\sigma_{zz}}{9K} + \frac{\sigma_{zz}}{3\mu} = \left(\frac{3K + \mu}{9K\mu} \right) P \qquad (1.5)$$

$$\text{and } u_{xx} = u_{yy} = \frac{\sigma_{zz}}{9K} - \frac{\sigma_{zz}}{6\mu} = -\left(\frac{3K - 2\mu}{18K\mu} \right) P \qquad (1.6)$$

Eq. (1.5) simplifies to

$$P = Y u_{zz} = Y\varepsilon, \qquad (1.7)$$

$$\text{where } Y = \left(\frac{9K\mu}{3K + \mu} \right). \qquad (1.8)$$

Y is the Young's modulus and is the extensional stress needed, according to the linear theory, to double the length of a rod. It depends on both the bulk modulus and the shear modulus, since a uniaxial deformation in general is neither a pure shear nor hydrostatic compression. However, if $K << \mu$, than $Y \propto K$ and if $\mu << K$, than $Y \propto \mu$. The Young's modulus can be converted to the characteristic force required to double the length of the rod by multiplying by the cross-sectional area. This characteristic force, f_0, is called the normalized force constant. For

mitotic chromosomes we will find a Young's modulus of 300 Pa, and unlike most media, that the linear theory applies out to u_{zz}=3.

The energy density of a uniaxial deformation can be calculated from (1.4) and is quadratic in e.

$$F = \tfrac{1}{2}Pe = \tfrac{1}{2}Ye^2 \qquad (1.9)$$

How the width changes in response to the change in length is calculated by combining (1.5) and (1.6).

$$u_{xx} = u_{yy} = -su_{zz} = -se, \qquad (1.10)$$

$$\text{where } s = \frac{(3K - 2m)}{2(3K + m)} \qquad (1.11)$$

s is the Poisson ratio and varies between 0.5 ($K >> ì$) and –1 ($ì >> K$). However, the Poisson's ratio typically varies between 0.5 and 0 since an object's width usually decreases as the length increases. For the case that $K = ì$, the Poisson's ratio is 1/8 = 0.12 and the Young's modulus is 9/4 times the bulk and shear modulus. This turns out to be the case for mitotic chromosomes.

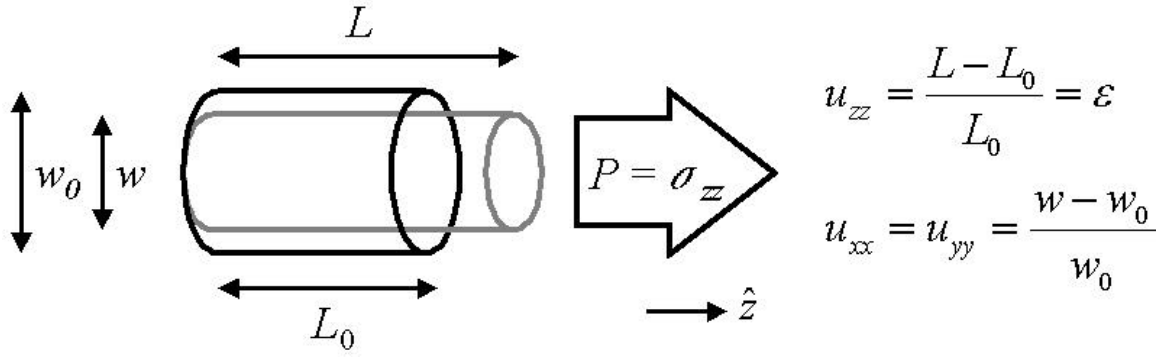

Figure 1.7 A uniaxial deformation of a rod by applying an extensional stress P to the end. The length extends from a relaxed length of L_0 to a length of L, while the width changes from w_0 to w.

Although it is natural to define a general deformation as the sum of a shear and a hydrostatic deformation, it is often easier to measure uniaxial deformations. This is the case for chromosomes, so K and $\grave{\imath}$ are not directly measured. Instead, Y and $\boldsymbol{s}$ are measured and then K and $\grave{\imath}$ can be inferred assuming the object is relatively isotropic.

1.5.2 Bending

Bending deformations are simply uniaxial deformations inhomogeneously distributed along the cross-section of the rod (Figure 1.8). The natural coordinate system to use for a bend is the curvilinear coordinates: $\hat{t}$, the tangent vector to the rod, $\hat{n}$, the normal vector and $\hat{b}$, the binormal vector. Since we will not discuss torsion, $\hat{b}$ is constant, and points out of the page in Figure 1.8 (twists are out-of-plane bends). The cross-section of a bent segment of a rod, extends and contracts with a magnitude of $u_{tt} = d/\hat{\boldsymbol{A}} = d\boldsymbol{k}$, where d is the distance from the axis in the $\hat{n}$ direction, the axis has a radius of curvature, $\hat{\boldsymbol{A}}$, and curvature, $\boldsymbol{k}$ (Figure 1.8). The energy per volume can be calculated from (1.8) and is $\frac{1}{2}Yd^2\boldsymbol{k}^2$. Integrating over the cross-sectional area of a rod with radius R calculates the energy per length of the bend to be $\frac{1}{2}B\boldsymbol{k}^2$, where

$$B = \frac{\boldsymbol{p}}{4} R^4 Y \qquad (1.12)$$

Integrating along the length of the rod calculates the total energy E of the bent rod of length L, and is

$$E = \frac{B}{2}\int_0^L ds\boldsymbol{k}^2 \ . \qquad (1.13)$$

The bending rigidity B is in units of energy×length where B/l is the bending energy of a rod of length l bent into an arc with a radius of curvature of length l.

The bending rigidity of long flexible objects such as biopolymers are often described by a persistence length, A and is equal to B/k_BT . The persistence length is the required length of a rod

so that a bend with a radius of curvature equal to *A* has a bending energy equal to the thermal energy. In Chapter 4, we will find the bending rigidity of mitotic chromosomes to be about 1×10^{-22} J·m. This gives a persistence length of a few centimeters, and is much longer than the chromosome length of 20 ìm. Therefore, *B* is the natural parameter for describing the bending rigidity of a mitotic chromosome and will be used here.

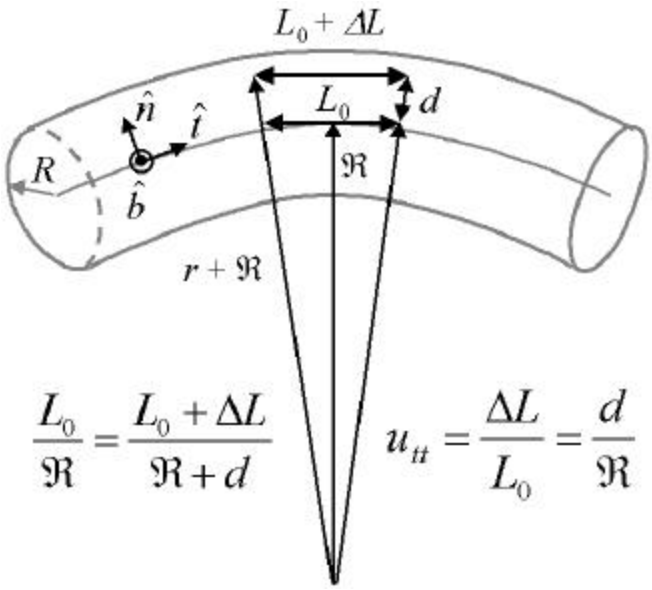

Figure 1.8 Bending of a rod is simply extending and compressing inhomogenously across the cross-section of the rod. Here, we neglect twisting so the binormal vector points out of the page.

Comparing the measured values of *Y, B* and *R* with the Eq. 1.12 estimates the isotropy of the rod. Since *B* scales as R^4, subtle changes in structure can cause large changes in *B*. Chapter 4 shows that mitotic chromosomes roughly obey this relation, indicating that their internal structure is approximately isotropic.

1.5.3 Internal Viscosity

The elasticity theory discussed so far is for deformations that are allowed to reach equilibrium. However, to stretch, compress or bend a rod, it must be initially out of equilibrium. Following a deformation, there is a certain amount of time for the stress and strain to equilibrate. Therefore, when forces are applied faster than the equilibration time, there is energy dissipation from both internal friction and displacement of the surrounding medium. We will focus on the internal dissipation of mitotic chromosomes, since, as will be discussed in chapter 5, they dominate over the dissipative losses of moving the chromosome through the surrounding solution.

The internal dissipation can be described by a dissipative function, *R*, which is a function of $\dot{u}_{ij}$ (Landau and Lifshitz, 1986). For an isotropic elastic body, the dissipative function will have the analogous form to that of the elastic free energy density in Eq. (1.1), where u_{ij}, λ and *K* are replaced with $\dot{u}_{ij}$, η and ζ respectively and so

$$R = \eta\left(\dot{u}_{ij} - \tfrac{1}{3}\delta_{ij}\dot{u}_{kk}\right)^2 + \tfrac{1}{2}\zeta\dot{u}_{kk}^2 \qquad (1.14)$$

Both η and ζ are in units of energy×time/volume and are the viscosities of a pure shear and hydrostatic expansion, respectively. Analogous to $\sigma_{ij} = \partial F/\partial u_{ij}$, the additional strain is calculated with $\sigma'_{ij} = \partial R/\partial\dot{u}_{ij}$ and is therefore,

$$\sigma'_{ij} = 2\eta\left(\dot{u}_{ij} - \tfrac{1}{3}\delta_{ij}\dot{u}_{kk}\right) + \zeta\dot{u}_{kk}\delta_{ij} \qquad (1.15)$$

The total strain is just the sum of σ_{ij}' and σ_{ij}. We can solve for $\dot{u}_{ij}$ in the same way Eq. (1.3) was calculated.

$$\dot{u}_{ij} = \sigma'_{kk}\delta_{ij}/9K + \left(\sigma'_{ij} - 1/3\delta_{ij}\sigma'_{ij}\right)/2\eta \qquad (1.16)$$

When a massless, uniaxially extended rod is allowed to relax, there is balance between σ_{ij}' and σ_{ij}. Therefore the equation of motion is

$$\eta' \frac{d\varepsilon}{dt} + Y\varepsilon = 0 \qquad (1.17)$$

$$\text{where, } \eta' = 9\alpha\nu/(3\nu + \alpha). \qquad (1.18)$$

This effective viscosity for uniaxial dissipation, η', is analogous to the Young's modulus for uniaxial elastic energy. The rod will relax with a characteristic relaxation time of $\tau = \zeta'/Y$.

We can connect this to the complex modulus, $G^*(\omega)$, that is used in chemical physics to describe the solid-like and liquid-like properties of a material. The complex modulus is defined as $G^*(\omega) = G' + iG''$, where G' is the storage modulus and G'' is the loss modulus (Larson, 1999). For reversible, uniaxial deformations, a solid will have a complex modulus of $G^*(\omega) = Y + i\omega\eta'$, as $\omega \to 0$.

The inertial effects are (as usual for this scale of experiment) irrelevant to our results. The chromosome elasticity experiments have a length scale of $l = 10$ µm, and a maximum velocity of $v = 100$ µm/sec. All of the experiments here are done in a fluid with a viscosity, ζ, and density, ρ, similar to water, so the Reynolds number is $\rho v l/\zeta = 10^{-3}$ (Landau and Lifshitz, 1987). The inertial effects are in fact even smaller because, as will be discussed in chapter 5, mitotic chromosomes have such a large internal viscosity that the friction due to the flow near the chromosome is inconsequential. Mitotic chromosomes have a density similar to water since they are neutrally buoyant and the internal viscosity is about 10,000 times larger than water. So, the ratio of the inertial term to the viscous term is more like 10^{-7}.

1.6 Elastic Properties of DNA, Protein and Chromatin

Over the past ten years there have been amazing advances in the study of single biological molecules (Strick *et al*, 2001). These advances have enabled the elasticity measurements of some components of chromosomes: DNA, protein and chromatin. In 1992, Smith *et al* performed the first high-resolution experiments measuring the elasticity of single dsDNA molecules. They found that as dsDNA is extended past its relaxed random coil configuration, it behaves as a linear entropic spring with a force of about 0.1 pN to extend its end-to-end distance to half its contour length (Figure 1.8A). Beyond this, the force response becomes highly nonlinear and is explained by the extensible wormlike chain polymer model (WLC) (Bustamante *et al*, 1994, Marko and Siggia, 1995) in which DNA behaves as an extensible semiflexible polymer with a persistence length of about 50 nm and a normalized force constant of 800 pN (Figure 1.8B).

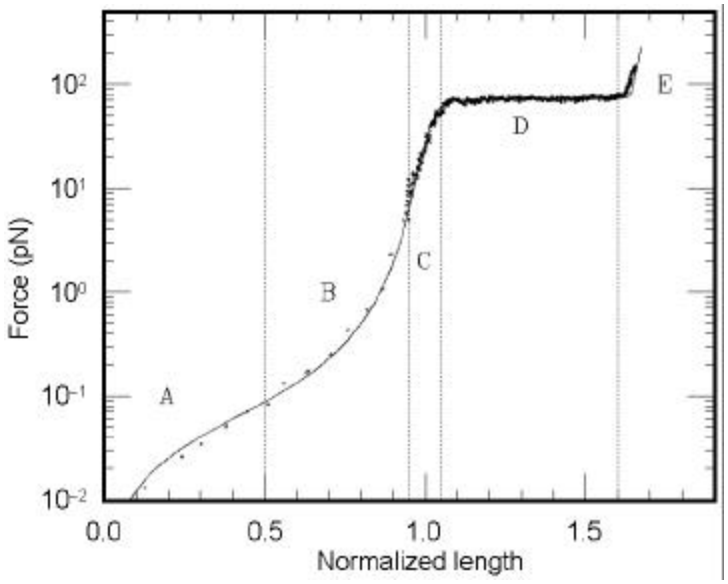

Figure 1.9 The stretching response of a single λ dsDNA molecule. The points are experimental data from Strick *et al*¸1996 and Cluzel *et al*, 1996, and the line is a theoretical fit by Marko, 1998. (Figure courtesy of J.F. Marko)

The extensibility of dsDNA was suggested in the 1992 results of Smith *et al*. A few years later, experiments by Cluzel, *et al*, 1996 and Smith *et al*, 1996 showed that above 10 pN, the DNA molecule does stretch with a normalized stretching force constant of 800 pN (Figure 1.8C). Given dsDNA's width of ~2 nm, the Young's modulus of dsDNA is about 10^8 Pa. At a force of about 60 pN, dsDNA undergoes a structural transition from b-form to an underwound and overstretched structure called S-form (Cluzel, 1996). We will find that this high-force elastic response of dsDNA plays no role in mitotic chromosome elasticity.

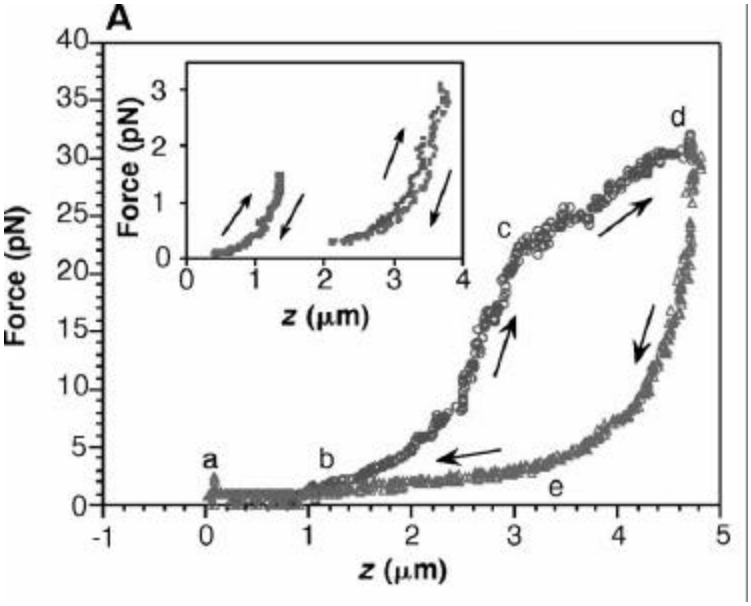

Figure 1.10 Force response of a single titin molecule from the work of Kellermeyer *et al*, 1997. Extensions of less than 2x are reversible, while extensions beyond this exhibit hysteresis. (From Kellermeyer *et al*, 1997. With permission.)

The elastic properties of a single protein, titin, was measured by Kellermeyer *et al*, 1997, Reif *et al*, 1997 and Tskhovrebova *et al*, 1997. Titin is an extremely large protein with a

molecular weight of 3.5 MDa, and a length of about 1 micron. It functions as an elastic spring within muscle cells (Horowits and Podolsky, 1987). Kellermeyer *et al*, 1997 found that titin stretches reversibly out to about double its length, with a normalized force constant of about 1 pN. Beyond this extension, the force response is non-linear and both hysteresis and irreversibility occurs. The force response can be understood as first reversible and then irreversible unfolding of domains within the protein. These results may be particularly relevant for chromosome elasticity because of recent results of Machado *et al*, 1998, which indicate that a protein homologous to muscle titin is found within mitotic chromosomes.

Cui and Bustamante, 2000 and Bennink *et al*, 2001, studied the elasticity of single chromatin fibers. Chromatin is not as well defined as either dsDNA or titin because it is a complex of histone proteins and dsDNA, in which the structure is sensitive to both ionic conditions and the presence of linker histones. Cui and Bustamante reported elasticity experiments of single chicken erythrocyte chromatin fibers in 5 and 40 mM NaCl with linker histones. At a low ionic strength of 5 mM NaCl, they find that chromatin extends reversibly to 7 pN with a persistence length of about 30 nm. Between 7 pN and 20 pN, the force response is no longer reversible since hysteresis is observed; however, multiple extension-retraction cycles are repeatable. The authors also note that at strain rates 6-10 times slower than the data shown, hysteresis is not observed above 7 pN. Above 20 pN, the fiber undergoes an irreversible transition during which sudden drops in force are observed and the fiber becomes permanently lengthened. This transition is interpreted as the force required to remove histone cores. At a higher ionic strength of 40 mM, chromatin fibers extend linearly and then at about 5 pN there is a force plateau. Based on a two state model to explain the transition, the authors estimate the

relaxed length of the chromatin fiber and determine the force constant of the initial response to be about 5 pN. They also report that results at 150 mM NaCl are similar to 40 mM.

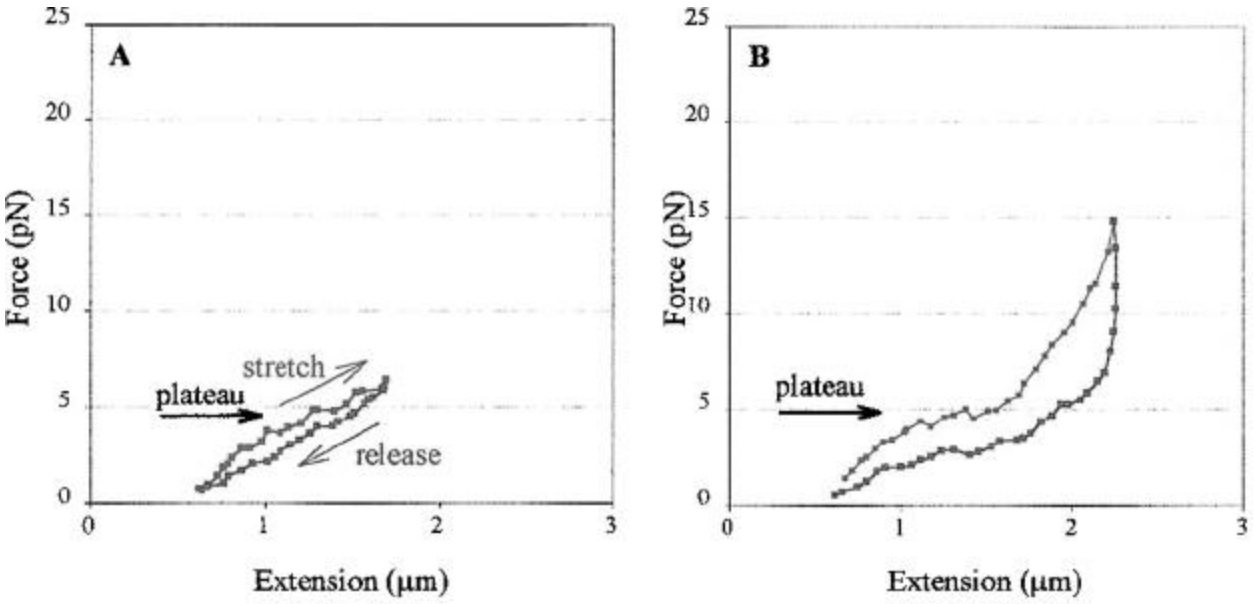

Figure 1.11 The elastic response of single chromatin fibers measured by Cui and Bustamante, 2000. (A) is an extension to about double the initial length, which is reversible with a characteristic force of about 5 pN. (B) is a longer extension that is no longer reversible and exhibits a force plateau at about 5 pN. (From Cui and Bustamante, 2000. With permission.)

Bennick *et al*, 2001 assembled histones on lambda DNA *in vitro* with *Xenopus* egg extracts (Leno, 1998 and Laskey *et al*, 1977). This extract contained core histones and additional nonhistone proteins, but lacked linker histones. These experiments were performed at physiological ionic conditions of 150 mM monovalent salt. They are able to observe the assembly of the histones on a single dsDNA molecule with a maximum compaction of 8 times and find above 10 pN, histone cores do not assemble on dsDNA. Following assembly, forces

between 20 and 60 pN remove histone cores, but by staying below 20 pN of force, the *in* vitro assembled chromatin fibers have a reversible, nonlinear force response. The authors explicitly point out that the load rates used are too fast to allow the fibers to reach equilibrium.

These experiments do not provide precise measurements of the elastic properties of 30 nm chromatin fibers in physiological conditions. Nonetheless, they indicate that it has a persistence length of about 30 nm and a force constant of about 5 pN.

1.7 Why Study the Elasticity of Mitotic Chromosomes?

There are two motivations behind this study of chromosome elasticity. The first is to help understand mechanical processes that occur *in vivo.* Mitosis is an inherently mechanical process, which involves the compaction of its chromosomes from a disperse interphase to a much more compact mitotic state (Figure 1.1). *In vivo,* mitotic chromosomes are bent (Figure 1.1, anaphase) and stretched (Figure 1.12), as they are subject to mechanical forces by polymerizing microtubules (Skibbens *et al*, 1993, Koshland, 1994). The forces exerted on chromosomes *in vivo* are as much as hundreds of piconewtons (Nicklas, 1983). Understanding chromosome elasticity enables estimates of the net forces that mitotic chromosomes are subjected to within the cell by observation of their deformations. Furthermore, many chromosome-reorganization processes *in vivo* may depend on chromosome physical properties. For example, Kleckner, 1996, has argued that chromosome flexibility plays a crucial role in chromosome pairing during meiosis.

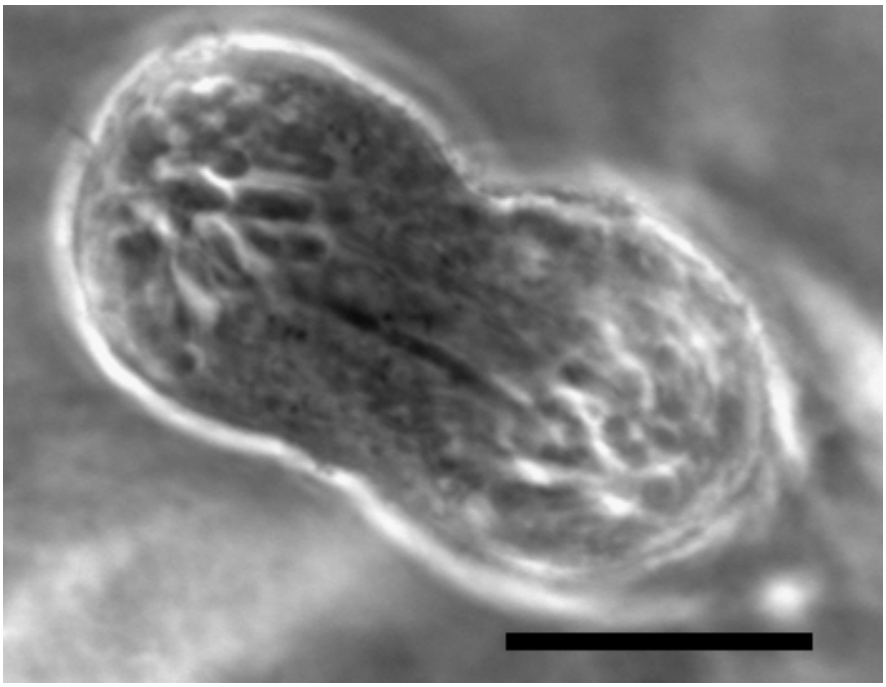

Figure 1.12 Image of newt TVI cell during anaphase in which a chromosome is being stretched with an approximate tension of 1 nN. Bar = 20 ìm.

The second motivation, the focus of this thesis, involves using elasticity measurements to probe chromosome structure. The rest of this section will describe how elasticity measurements can be used in this way.

Bulk elastic properties for various models of chromosome structure can be estimated (Marko and Siggia, 1997) and compared with measurements to either rule out or confirm specific models. For example, as discussed in section 1.5, comparison between measurements and elasticity theory of isotropic rods provides an estimate of mitotic chromosome isotropy. In chapters 4 and 5, we will see that the Young's modulus and bending rigidity of mitotic chromosomes obey the elastic rod relation, $B = \frac{p}{4} R^4 Y$. This indicates mitotic chromosomes are roughly isotropic since the main assumption of the elastic rod relation is isotropy. There is an

analogous relation between μ, the shear modulus, and C, the twist rigidity, i.e. $C = \frac{\pi}{2} R^4 \mu$. In this work, the shear modulus and twist rigidity are not measured directly; these quantities could be studied using specially designed micromanipulators similar to those used for DNA twisting experiments (Leger *et al*, 1999; also see Section 8.6 for more discussion of twist experiments). However, given that our results indicate that mitotic chromosomes are isotropic, the twist rigidity should be similar to the bending rigidity of 1×10^{-22} J·m. A similar argument can be used to estimate the shear and bulk moduli from the results of this thesis.

Small, reversible deformations, which occur *in vivo*, (Nicklas, 1983) indicate how tightly the chromosome is tethered together. An object's elastic response is due to microscopic stresses and strains, which result in measurable quantities such as Y, σ, B and ν. The magnitude of these parameters indicates the microscopic energies and forces that hold an object together. Here are a few examples.

- Covalently bonded solids usually have a modulus between 10^{10} and 10^{11} Pa. The bond energies are about an eV or 1×10^{-19} J and a length scale on the order of a few angstroms. Therefore, a rough estimate of Y is $(1\times10^{-19}\text{ J})/(2\times 10^{-10}\text{ m})^3 \approx 10^{10}$ Pa.
- Molecular crystals and hydrogen-bonded solids such as single molecules of DNA are often found in biological systems and have a modulus between 10^7 and 10^8 Pa. These solids have bond energies of a few k_BT (at room temperature, $k_BT = 4\times10^{-21}$ J) and a length scale of about a nanometer, implying a Y of roughly $(1\times10^{-20}\text{ J})/(1\times10^{-9}\text{ m})^3 \approx 10^7$ Pa.
- Polymer gels are a network of crosslinked polymers and usually have modulus of 10^3 to 10^4 Pa. The elastic energy is due to the removal of polymer entropic degrees of freedom between

crosslinks, so the energy scale is again k_BT. The length scale is usually 10's of nanometers, the typical distance between crosslinks. This predicts a Y of $(4\times10^{-21}\text{ J})/(1\times10^{-8}\text{ m})^3 \approx 10^3$ Pa.

The Young's modulus of 300 Pa for a mitotic chromosome thus suggests a gel-like structure. The modulus of an entropic crosslinked gel is $Y = \frac{k_B T \boldsymbol{j}}{A^3 N}$, in which the volume fraction is $\boldsymbol{j}$, the persistence length of the polymer is A and the number of segments between crosslinks is N (de Gennes, 1979). The polymer within chromosomes is chromatin, which has a persistence length of about 30 nm. As chapter 6 will show, the volume fraction of a mitotic chromosome is approximately 0.7. We can estimate the number of segments between crosslinks from the result that a mitotic chromosome extends linearly and reversibly to about 3 times its relaxed length. A entropic spring is linear out to about half its contour length and its relaxed end-to-end distance is $A\sqrt{N}$. Therefore, the number of segments between crosslinks must be at least 40. This indicates a Young's modulus of about 2 Pa and shows that mitotic chromosomes are not an entropic gel of chromatin. Instead, we will find that a mitotic chromosome is a network of chromatin tightly folded by protein fasteners.

Quantification of the native chromosome elasticity also provides a reference for experiments during which the chromosome structure is altered. There are vast numbers of biomolecules that have well characterized interactions with DNA or protein, such as antibodies, nucleases, topoisomerases, restriction enzymes, proteases, kinases, etc. Since mitotic chromosomes are essentially composed of DNA and protein, these biomolecules can be used to induce a well-defined change in chromosome structure. If a change in chromosome structure is induced, chromosome elasticity will change and elasticity measurements provide a sensitive and quantitative means for directly probing the induced structural change. The results in chapter 6 will show that changes in the elastic properties of a mitotic chromosomes are well correlated

with structural changes and chapter 7 will show that when elasticity measurements monitor structural changes induced by dsDNA cutting enzymes, clear conclusions about chromosome structure are made.

As discussed in section 1.3, fluorescence microscopy is an effective way of detecting structures in aqueous solution. The development of new types of fluorescent molecules such as green fluorescent protein (GFP) and recent improvements in low-light detection has allowed for exciting *in vivo* measurements of chromosome structure (Robinett *et al*, 1996, Lever *et al*, 2000, Misteli *et al*, 2000 and Yin *et al*, 2000). Combination of elasticity measurements and fluorescence techniques will provide additional information about chromosome structure. For example, specific regions of DNA within a chromosome can be labeled. Observation of changes in fluorescent patterns of these regions as a chromosome is stretched or bent should reveal how regions of DNA are folded into the chromosome.

In summary, mitotic chromosome elasticity measurements are motivated in two ways. First, understanding elastic properties of various components of a cell is biologically relevant. There is evidence that forces within a cell are important for various aspects of biological functions (Nicklas, 1997). Therefore, characterization of elastic properties of cell components such as mitotic chromosomes is important. The second motivation, which is the focus of this thesis, is to use elasticity measurements combined with other techniques, such as biochemical modification or fluorescence microscopy to probe the structure of mitotic chromosomes.

1.8 Previous Studies of Mitotic Chromosome Elasticity

Nicklas, 1983, performed the first study of chromosome elasticity. Using glass needles and grasshopper cells, Nicklas measured a Young's modulus of 430 Pa and that the cell can apply forces of up to 0.7 nN. Claussen *et al*¸ 1994 showed that spreads of hydrated human

chromosomes can be stretched more than five times their length. However, they did not measure forces and the mitotic chromosomes were subjected to extreme conditions. Scanning force microscopy (SFM) has been used to image and study human chromosome elasticity (Fritzsche and Henderson, 1997 and Fritzsche, 1999). Unfortunately, it is difficult to determine the elastic modulus from these results since the contact area of the SFM tip is ill-defined.

Newt chromosomes, mechanically removed from mitotic cells, were first studied by Houchmandzadeh *el al*, 1997. By aspirating mitotic chromosomes into a micropipette, they measured a Young's modulus of 5000 Pa for prophase chromosomes and 1000 Pa for metaphase chromosomes. These results provided the starting point for this thesis. A drawback to the aspiration technique is that some of the measured pressure may be due to flow into the pipette, which would cause an over-estimate of the Young's modulus. They also found chromosomes can be extended by up to 100 times and break at a force of 100 nN. The rates used to extend the chromosome were around 20 ìm/sec, implying a strain rate of at least 1 sec^{-1}. As will be discussed in chapters 3 and 5, at these strain rates, the extensions are not in equilibrium, making them difficult to interpret.

Most recently, Houchmandzadeh and Dimitrov, 1999 studied the elasticity of *in vitro* assembled chromosomes in *Xenopus* egg extracts. They measured a Young's modulus of 1000 Pa and a bending rigidity of 1×10^{-26} J·m. A comparison of their results with this thesis, which will presented in chapters 3 and 4, proves very interesting.

1.9 Summary of the Experimental Results

The following is a synopsis of the chromosome elasticity measurements described in chapters 3 through 7. Mitotic chromosomes have a Young's modulus of 300 Pa, a Poisson ratio of 0.1, a bending rigidity of 1×10^{-22} J·m, a step-strain relaxation time is 2 seconds, a thermal

bending correlation time of 0.7 seconds, extensions of up to a three fold are linear and reversible and extensions beyond 3-fold are irreversible with a force plateau occurring of 15 nN at an extension of 30-fold. These measurements provide insight into various aspects of chromosome structure.

The magnitude of the Young's modulus and bending rigidity are consistent with Eq. (1.12). This indicates that mitotic chromosome structure is relatively isotropic. This conclusion is supported by the value of the Poisson ratio, which implies that the bulk and shear moduli are of similar magnitude, again suggesting of isotropy. As discussed in section 1.7, the 3-fold linear response and the magnitude of the Young's modulus rules out the entropic gel model. The relaxation times of step-strains and bending fluctuations both imply that mitotic chromosomes have an internal viscosity of about 100 kg/m·sec. This is 10,000 times larger than the viscosity of water and is likely due to the slow rearrangements of chromatin domains within the mitotic chromosome.

These conclusions regarding mitotic chromosome structure from elasticity measurements are informative but not precise. Combining elasticity measurements with chemical modifications provides a more direct means to measure chromosome structure. Changing the ionic conditions that surround a mitotic chromosome dramatically changes its structure and can be observed through monitoring chromosome elasticity. We find that multivalent ions can reduce mitotic chromosomes volume by 1/3, indicating that 1/3 is aqueous solution. Monovalent ionic conditions above the physiological concentration of 150 mM causes mitotic chromosomes to swell isotropically, indicating structural isotropy.

Using elasticity measurements to monitor how dsDNA cutting enzymes induce structural changes within a single mitotic chromosome provides our most direct chromosome structure

measurements. These experiments show that a protein scaffold is not the contiguous structural element within mitotic chromosomes. Instead, dsDNA provides the structural integrity through a crosslinked networked of high folded chromatin with a crosslink frequency of about one per 50 kb of dsDNA. A more detailed description of this mitotic chromosome structure model is described in Chapter 8.

CHAPTER 2

EXPERIMENTAL TECHNIQUES

2.1 Introduction

This chapter explains the techniques and methods used to study mitotic chromosome elasticity. The general approach to these experiments is to isolate and manipulate single mitotic chromosomes from amphibian cells with micropipettes. The experiments are observed with an inverted light microscope placed on a vibration isolation table. The micropipettes are translated with micromanipulators placed on both sides of the microscope. A PC with Labview and Imaq controls each manipulator and image acquisition during an experiment. The data are in the form of images, which the PC analyzes following an experiment.

The larger the mitotic chromosome, the easier it is to micromanipulate. Therefore, amphibian cells were used since they have some of the largest known chromosomes. The growth conditions for these cells are an additional advantage, because they grow well at room temperature (25 C), in a buffer with univalent ionic strength of about 100 mM, a low concentration of divalent metal ions (0.5 mM Ca^{2+}, 0.9 mM Mg^{2+}) and in contact with room air. This is different than mammalian cells, which typically are grown at 37 C, in an ionic strength of 150 mM, in contact with a gas composition of 5% CO_2, and in culture medium with divalent ion concentrations of 1.8 mM of both Ca^{2+} and Mg^{2+}. For an experiment, the cells are grown in small lab made dishes optimized for micromanipulation on our Olympus IX-70 inverted light microscope.

Micropipettes are used in all aspects of single mitotic chromosome micromanipulation. They isolate single chromosomes, hold them, extend them, measure forces applied to them and

locally introduce changes in buffer conditions or exposures to biochemicals such as dsDNA cutting enzymes. Micropipettes are cheap, simple and very versatile.

The raw data for all of the experiments are in the form of images. The length of the chromosome and the applied forces are measured from the change in position of the pipettes from image to image. The analysis is done following an experiment. Initially, this was done by clicking a mouse on the image. However, this is extremely slow, so the image analysis was automated, allowing for tens of thousands of images to be acquire and analyzed for each experiment.

Forces are measured by observing the deflection of a micropipette fabricated with an extremely small taper. Pipettes can be made to linearly deflect over tens of microns with a force constant of 0.1 nN/ìm. Each force-measuring pipette must be calibrated, and is done by starting with a much stiffer pipette that is calibrated against a scale. This pipette calibrates a flimsier pipette, which in turn calibrates a yet more flimsy pipette. This is repeated until a pipette with a force constant of 0.1 to 1 nN/ìm is measured.

The remaining sections of this chapter describes in detail all of the techniques used to measure elasticity of single mitotic chromosomes.

2.2 Newt Primary Cell Culture and Medium Preparation

Standard protocols for newt lung cell cultures (Rieder and Hard, 1986) adapted for micromanipulation (Houchmandzadeh *et al.*, 1997) were followed. The cells were grown at 25 C and in contact with room air. Male newts (Notophthalmus viridescens, Connecticut Valley) were killed by immersion for 20 minutes in 1 mg/ml tricaine (Acros) and then immediately dissected (Appendix B). Lungs were cut into 1 mm^3 pieces and soaked in culture medium for 24 hrs. The culture medium is 50% L-15 (Cellgro), 46% water (BioWhittaker), 4% FBS (BioWhitaker), 50

units/ml penicillin, 50 µg/ml streptomycin (BioWhitaker) and 5 µg/ml fungizone (BioWhitaker). This culture medium has 0.5 mM $CaCl_2$, 2.5 mM KCl, 0.2 mM KH_2PO_4, 0.5 mM $MgCl_2$, 0.4 $MgSO_4$, 70 mM NaCl, 0.6 mM Na_2HPO_4 and 30 mM of amino acids. Culture dishes (60x15 mm, Falcon) had a 3 cm diameter hole cut out of the bottom, covered with a 4 cm diameter #1 cover glass (Fisher) and sealed with paraffin. Before assembly, the culture dishes were cleaned with a detergent and the cover glass was cleaned with Sparkle; culture dishes, cover glass and Teflon rings were soaked in 70% ethanol for two hours. After drying and assembly, the dishes and Teflon rings were UV-irradiated for 40 minutes. Lung fragments were divided into six dishes, lightly squashed onto the glass, covered by a dialysis filter and held down by a Teflon ring. Epithelial cells began to migrate onto the glass in 3 to 4 days. The culture medium was replaced and the filters removed after seven days. Ten days after culture preparation, mitotic activity reached its peak (Figure 2.1a). Experiments were done between the seventh and fourteenth day.

2.3 Newt TVI and *Xenopus* A6 Cell Line Cultures

TVI newt (*N. viridescens*) epithelial cells (Reese, 1976) and A6 *Xenopus* cells (ATCC) were grown in 75 ml cell culture flasks (Falcon) in 10 ml of cell culture medium at 25 C and exposed to the room air. The culture medium was replaced every four days for TVI and every two days for A6. At 90% confluence, the cells were subcultured (Appendix C) into new flasks with 0.15% trypsin in 60% HBSS (Cellgro). Experiments were done in custom-made culture dishes with a diameter of 20 mm and a depth of 2 mm. These dishes are made of two teflon rings which are stacked on a 40 mm diameter #1 cover slide and attached by paraffin (Appendix D). The cells were subcultured into 1.8 ml of culture medium and grown to about 70% confluence in the small dishes (Figure 2.1a,b). Micromanipulation experiments were done in these dishes while

the cells were between 70% and 100% confluent. Growing the cultures to a point where adjacent cells provided mechanical support to one another was important, since this allowed the appreciable forces necessary for chromosome removal to be applied to mitotic cells without dislodging them.

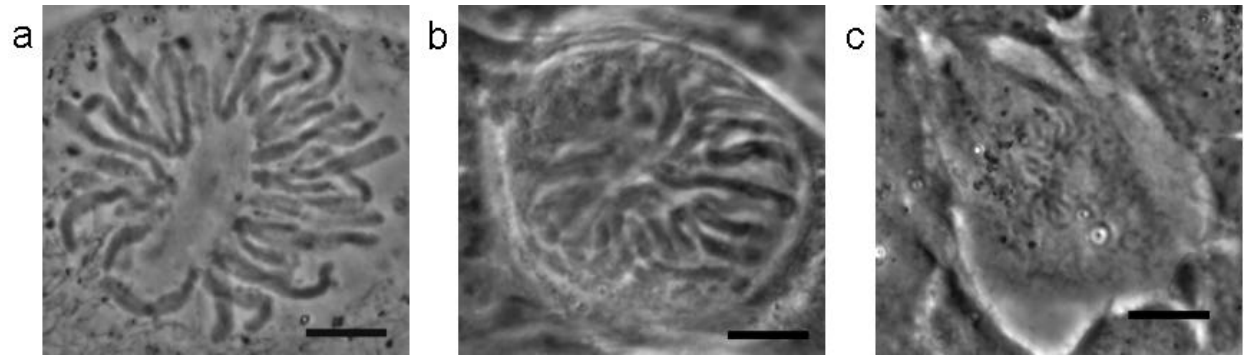

Figure 2.1 Images of a prometaphase newt lung (a), newt TVI (b) and *Xenopus* A6 (c) cells during prometaphase. This is about when a chromosome extraction is attempted. Bar = 10 ìm.

2.4 Experimental Setup

2.4.1 Version 1

Chromosome elasticity experiments were imaged using a DIC inverted light microscope with a 60X, 1.25 N.A. and 10X, 0.3 N.A. objectives (IX-70, Olympus). A three-axis stage-focus control with XY resolution 1 µm and Z resolution 0.1 µm (Prior) was used to position the dish. Chromosome manipulation was done with a pipette mounted to a motorized XYZ micromanipulator with a step size of 0.04 µm (MP-285, Sutter). A second pipette was attached to a manual XYZ micromanipulator (Taurus, WPI), mounted on the microscope. This was all mounted on a vibration isolation workbench (Newport). A 233 MHz Pentium-I PC with

Labview (National Instruments) was used to control the stage and motorized manipulator. Images were recorded by a CCD video camera (Panasonic) and captured with a NI-IMAQ PCI-1408 card and NI-IMAQ (National Instruments) software onto a P.C. This first version was used for the newt lung chromosome experiments. Section 2.11.1 will explain how the data was analyzed and the major sources of experimental uncertainty providing a distance resolution of about 0.1 ìm and force resolution of 0.1 nN.

2.4.2 Version 2

The second version of the experimental setup is simply version 1 with some upgrades. This version was used for the newt TVI and X*enopus* A6 chromosome stretching (chapter 3) and bending (chapter 4) experiments, the step strain experiments (chapter 5) and the experiments measuring how various ionic conditions affect chromosome elasticity (chapter 6). The experiments were done in a much smaller lab made cell culture dishes, since both TVI and A6 cells lines are much less sensitive to their growth conditions than the newt lung cell cultures. The dishes were 10 mm in diameter and 2 mm in height. A second motorized XYZ micromanipulator (MP-285 Sutter) was added, allowing for a third pipette to be positioned by the manual micromanipulator (Taurus, WPI), which was used for the microspraying experiments (Figure 2.2). Also, the objective was replaced by a 1.4 N.A. objective, providing higher image contrast. The P.C. was replaced by one with a 750 MHz processor, 256 mb of RAM and 100 ATA hard drive.

The new culture dishes reduced mechanical vibrations and the slow drift of the force-measuring pipette. The second MP-285 allows for single chromosome isolation using Triton-X (section 2.9.1) and improves the stretching experiments (section 2.11.2). The higher numerical aperture lens improves the computer analysis of the pipette position explained in section 2.11.2.

The new hard drive allows for a time series of images to saved at 10 Hz, which is close to video acquisition rate. The faster processor made the image analysis discussed in section 2.11.2 much faster, allowing for pipette deflections to be monitored in real time at about 5 Hz. This setup provides position resolution of 0.01 ìm and force resolution of 0.001 nN for about 1 minute. Drifts in the force pipette reduce the force resolution for experiments that take longer than about 60 seconds, and will be discussed in more in section 2.11.2.

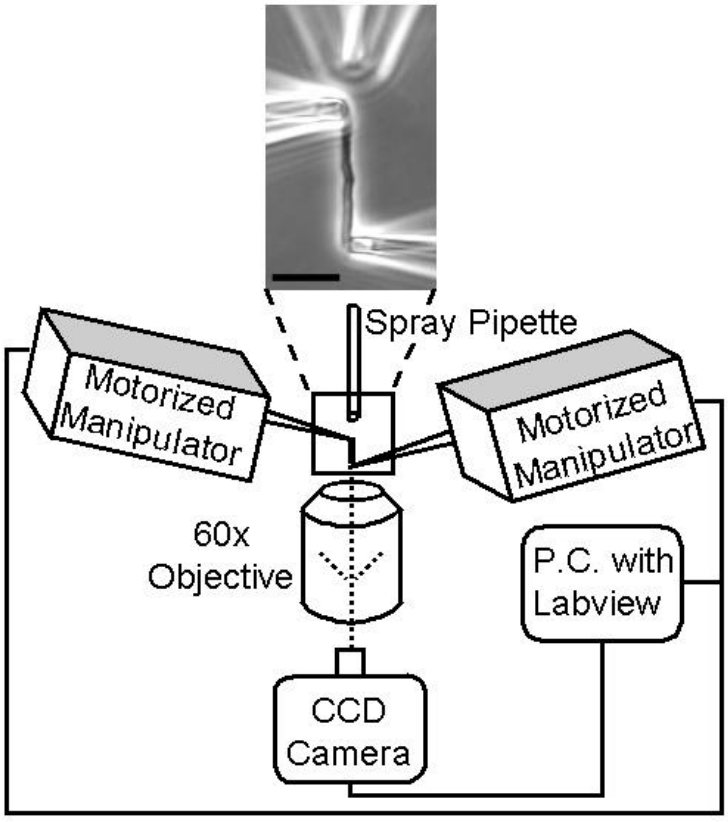

Figure 2.2 Experiments were done on an inverted microscope in cell culture buffer. Two pipettes, positioned by motorized computer controlled manipulators, hold the chromosome for micromechnical-biochemical experiments. A third pipette, positioned close to the chromosome, is used to flow in various buffered solutions. Forces are measured by observing the deflection of the bottom pipette. Bar = 10 ìm.

2.4.3 Version 3

The third version of the experimental setup is the same as version 2, except the force-measuring pipette is directly mounted on the stage and enters the dish through a 1 mm^2 opened on the side of the dish (Figure 2.3). This opening is made by cutting a gap in the rings, which are glued to a cover glass with paraffin. The opening is lined with paraffin, which keeps the cell culture medium from flowing out thanks to the very high water-wax surface tension. The center of the dish is scraped with a micropipette tip to clear an area free of cells and the force-measuring pipette is positioned over this area about 30 microns above the glass. Before a chromosome extraction begins, the force-measuring pipette is tracked to observe drift in the position of the pipette. The microscope stage level is adjusted until the drift is reduced to below 0.02 ìm per minute.

The chromosome experiments are above an area cleared of cells because the background is optically smooth, which improved the pipette deflection analysis described in section 2.11.2. Also, it minimizes the chance of the force-measuring pipette to become clogged with cell junk. Having the force-measuring pipette enter through the side of the dish dramatically reduces by about an order of magnitude the drift of the pipette as compared to the pipette entering through the open, top surface. This setup provides a position resolution of 0.01 microns and a force resolution of 0.001 nN for about 10 minutes. Also, having the force pipette directly mounted on the microscope plate frees up one of the computer controlled manipulators to position a third pipette for microspraying experiments (Figure 2.3).

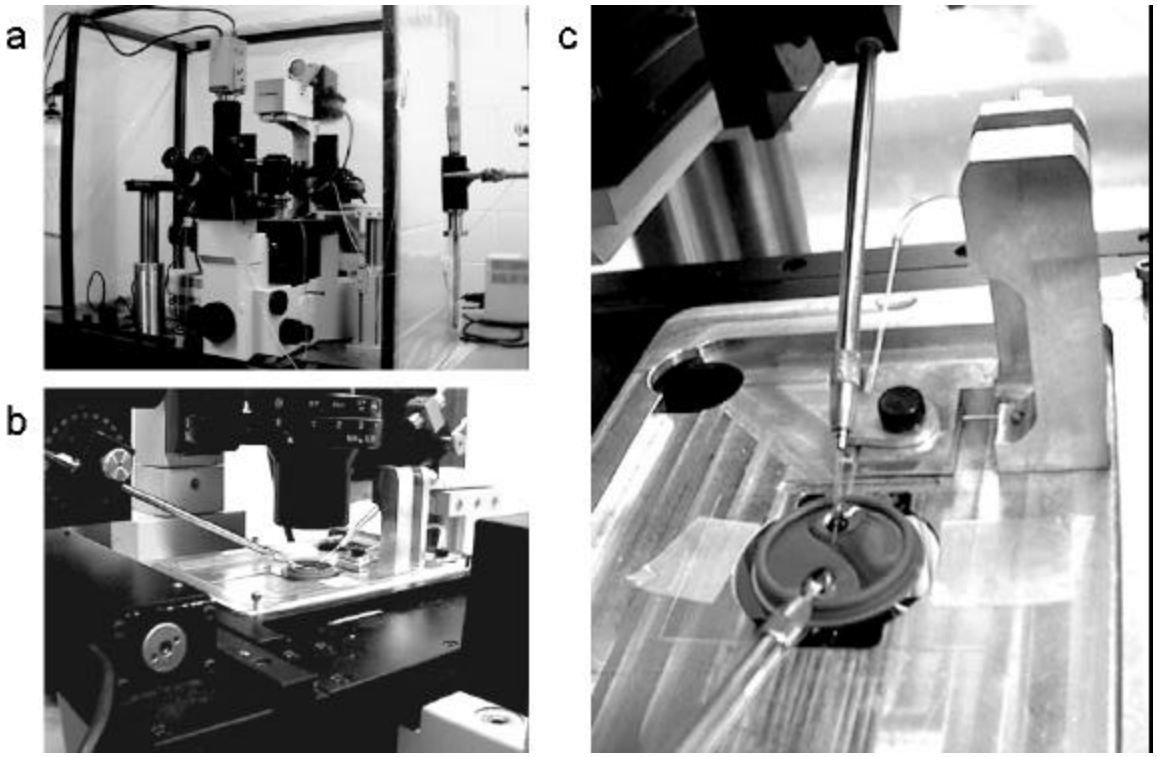

Figure 2.3 Pictures of the Olympus IX-70 microscope with the stage used in experimental setup, version 3. (a) shows the microscope on the vibration isolation work bench. (b) shows the microscope stage with the micromanipulators on both sides of the microscope each holding a micropipette. (c) shows the force measuring pipette mounted directly to the microscope stage.

2.5 Pipette Fabrication

A micropipette puller (P-97, Sutter) pulled borosilicate glass tubes with a 1 mm outer diameter and a 0.7 mm inner diameter (WPI). A micropipette forge was used to cut the tip to have an inner diameter of about 2 microns. The forge is a bright field microscope with a 10X objective, and a 0.5 mm-long, 0.1 mm-diameter platinum wire mounted below the lens. The wire is connected in series with a 16 Ohm, 150 Watt power resister to a power supply. A small (100 ìm wide) drop of borosilicate glass is melted onto the platinum wire. To cut a pipette, the wire is preheated by setting the current to about 2.2 A for at least 1 minute. This causes the wire to

expand out and glow. The current is then turned off, and the micropipette is brought just above the glass bead. The current is then set to about 1.2 A and the glass drop on the wire is raised into contact with the pipette. Immediately after this the current is shut off, causing the wire to retract and cool. This results in a clean break at the point where the pipette was in contact with the glass drop (Brown and Flaming, 1986). Initially, it is difficult to cut pipettes with a 2 ìm tip diameter. After some practice, 2 ìm size tips are cut repeatably by lightly blowing on the pipette held in the micropipette forge and observing the magnitude of the tip fluctuations.

2.6 Pipette Calibration

Pipettes are used as force transducers by fabricating them to have a force deflection constant of 0.1 to 1 nN/µm. They are calibrated by pushing them against a pipette of known force constant. An absolute calibration of a very stiff pipette was directly measured to have a force constant of 2.1 x 10^4 nN/µm by bending it against a precision analytical balance (Denver Instrument Company, TL-64) with a resolution of 0.1 mg or 10^3 nN. A series of successively weaker pipettes were made and calibrated to have force constants of: 3.2 x 10^3 nN/µm, 8.5 x 10^2 nN/µm, 48 nN/µm, 5.8 nN/µm and 0.61 nN/µm. Thus we obtained the force constant of a calibration pipette in the force and distance range we are interested in. A second independent series of calibrations was done. A pipette was then calibrated with a calibration pipette from each series of calibrations. Both gave force constants within 10% of each other, which we estimate to be our uncertainty.

Repeating the experiments on single dsDNA discussed in section 1.6 provided an additional calibration. We observed the elastic response of a single dsDNA molecule, including the transition from B-form dsDNA to S-form dsDNA at 59 pN. This is within 5% of the known

B to S transition of 65 pN (Cluzel *et al*, 1996 and Smith *et al*, 1996) and confirms the pipette calibration.

We can also estimate the force constant of a glass pipette based on its geometry. A force-measuring pipette has a tip radius of about 2 μm and an effective length of about 1 mm. The effective length is the length along the pipette over which the diameter doubles. For small deflections, the rod's force constant is $k \approx B/L^3 \approx R^4B/L^3$. Glass has a Young's modulus of 6×10^{11} Pa (Love, 1944), so the force constant is about 0.6 nN/μm, which is consistent with the measured force constants.

2.7 Pipette Filling

Following fabrication, the pipette must be filled with a solution. There are two ways to fill pipettes, one is through the tip and the other is via the rear of the pipette. The pipettes used to spray solutions such as the dilute solution of Triton-X used to extract single chromosomes only need the tip filled, not the entire pipette. So, after fabrication the pipette is attached to the picopump and the tip is dipped into a tube of the spray solution. A backpressure of about 5000 Pa is applied causing the solution to follow into the pipette via the tip. It usually takes about 10 minutes for enough solution to follow in for an experiment.

The second filling technique is the 'Omega Dot' method (Brown and Flaming, 1986), which fills pipettes used to aspirate on chromosomes. This method is used because they must be completely filled. The solution must run continuously from the pipette tip through a tube to a reservoir, which is raised or lowered to provide forward or back flow. This method requires the pipettes to be pulled from glass tubes with a 100 μm diameter glass filament running along its length. A 10 cm, 28 gauge needle attached to a syringe injects the filling solution from the back. The glass filament creates two channels in which the filling solution can flow down toward the

tip. As the tip fills, small bubbles appear which move away from the tip and eventually work themselves into the main shaft of the pipette. The smaller the taper and the more viscous the solution, the longer the bubbles take to move to the main part of the pipette.

The quickest way to fill pipettes is to combine the two filling techniques. First, connecting it to the picopump, dipping it into a tube with the filling solution and applying some backpressure fill the pipette tip. After a few minutes, the pipette is disconnected from the picopump and the long, thin syringe needle is used to fill the rest of the pipette from the back by the 'Omega Dot' method. This combination of filling techniques must be used for pipettes with small tapers such as the force measuring pipettes and with viscous filling solutions such as 10 mg/ml BSA in 60% PBS.

2.8 Newt Lung Chromosome Isolation

A force measuring pipette filled with 60% PBS was used to tear a hole in the cell membrane of a mitotic cell, about 20 to 30 minutes after nuclear envelope breakdown. Cytoplasm flows out of the cell and typically causes some chromosomes to be partially pushed out of the cell. The pipette is then used to aspirate on the tip of a chromosome with about 500 Pa of suction; the chromosome permanently adheres to the inside of the pipette after 2 minutes of contact. If the chromosome can easily be freed from the cell, a second pipette filled with 60% PBS is then moved nearby and used to aspirate on the its other end. In the event that the chromosome cannot be freed from the cell, the second pipette is used to anchor the chromosome of interest by aspirating near the apparent attachment of it to the other chromosomes. This extraction technique was used exclusively with newt lung cells and experimental setup, version 1. The number of attempts required to isolate a single chromosome is about 50 times. Since there

are only a few mitotic cells at any particular time in a newt lung cell culture, it takes about a week to complete an experiment.

2.9 Newt TVI and *Xenopus* A6 Chromosome Isolation

There are two techniques used to extract mitotic chromosomes from cells. At this point it should be pointed out that the cells appear as shown in Figure 2.1 where the nuclear envelope is gone but the chromosomes are not aligned along the metaphase plate. Therefore the chromosomes are extracted during late prometaphase. So, mitotic chromosomes in this thesis are technically prometaphase chromosomes.

2.9.1 Version 1

Two micropipettes, each attached to a micromanipulator, were used to isolate a TVI or A6 mitotic chromosome. Micropipettes with an inner diameter of 2 µm and a bending rigidity of about 10 nN/ µm were fabricated from borosilicate glass tubes (WPI) as described in section 2.5. One pipette is filled with 0.05% Triton-X (FisherBiotech) in 60% PBS (BioWhittaker) while a second pipette is filled with 60% PBS. After a cell between prometaphase and metaphase is located, the pipette with Triton-X is positioned within a few microns of the edge of the mitotic cell. The Triton-PBS solution is then flowed out of the cell with 5000 Pa of pressure. After 30 to 60 seconds a 5-10 ìm hole in the cell membrane appears and the chromosomes flow out of the cell. Usually the chromosomes are well attached to each other and the cell, but about 1 in 100 attempts, a chromosome floats completely free. When this occurs, the second pipette is positioned within 1 µm of the end of the free chromosome, which is aspirated into the pipette with about 500 Pa of pressure. The chromosome tip permanently adheres to the inner wall of the pipette after 30 to 60 sec of contact, via non-specific adhesion of chromatin to untreated glass.

The cell is then moved away from the isolated chromosome and the chromosome is positioned about 40 µm above the glass surface.

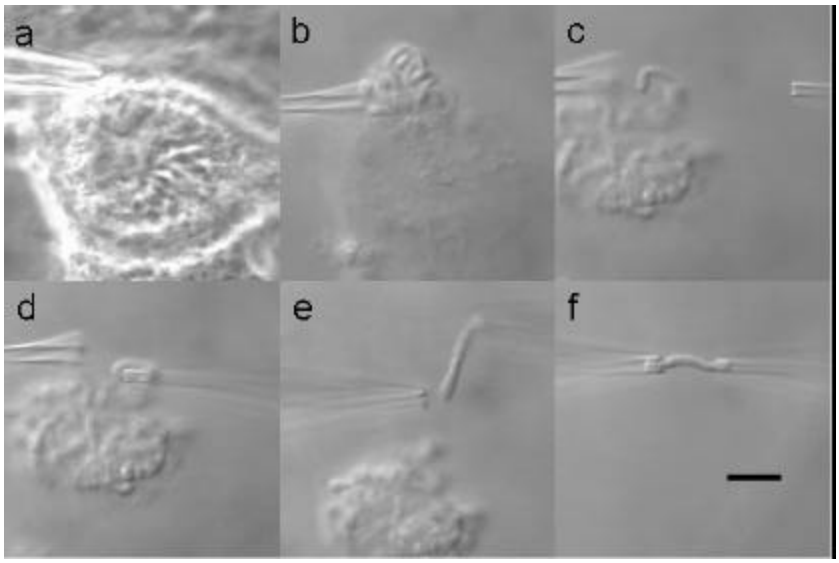

Figure 2.4 Images of a chromosome extraction. (a) is a phase image of a mitotic cell and the pipette filled with 0.05% Triton-X in 60% PBS just before the Triton-X is flowed out. (b) is a DIC image after the 0.05% Triton-X has been flowed out for about 60 seconds. The chromosomes can be seen flowing out of the cell. (c) is a DIC image after most of the chromosomes have flowed out and one in particular appears relatively free. (d) is a DIC image just after the other pipette filled with 60% PBS aspirates the tip of a chromosome into it. (e) is a DIC image after the cell is moved away from the pipette holding the chromosome. Note the chromosome appears straight because there is a thin attachment between the free end of the chromosome and the other chromosomes hanging out of the cell. Also the left pipette with Triton-X has been replaced with a new pipette filled with 60% PBS. (f) is a DIC image after the chromosome is aspirated into the left pipette with 60% PBS. The cell has been moved away from the pipettes, which breaks the thin attachment. The result is a single mitotic chromosome held between two pipettes. Bar = 10 ìm.

More often a chromosome does not float complete free but is connected to a second chromosome and the rest of the cells by a thin fiber (Figure 2.4d), a phenomenon previously

observed by Maniotis, *et al*, 1997. These attachments tend to be at chromosome ends and can support enough stress to extend the chromosome as it is moved away from the cell. Also, the attachments do not break until the chromosome becomes extended by more than 3 times with a force > 3 nN, which irreversibly damages the chromosome (Poirier *et al*, 2000). To avoid this a third pipette is used to aspirate the end of the chromosome anchored by the thin fiber. (This pipette is made relatively flexible because its bending will be used to measure forces as described in section 2.9.) The cell is moved away and the third pipette instead of the chromosome now supports the force applied to the thin fiber. The thin fiber then breaks without damaging the chromosome. (A movie of this procedure is available at http://safarsquid.phy.uic.edu/~mpoirier/experiments/movies/chromo-extract.mpgs). This chromosome extraction technique was used with TVI and A6 cells on experimental setup, version 2.

As will be discussed in chapter 3, the elasticity measurements of chromosomes mechanically extracted from newt lung cells and chemically extracted from both TVI and A6 cells are the same. This indicates that using 0.05% Triton-X to extract chromosomes does not affect their structure.

The success rate of chromosome isolation from both TVI and A6 cell cultures is much better then newt lung cultures. This is due to the vast number of mitotic cells (~1000) in a culture dish. It still takes about 50 attempts to isolate a chromosome, but 100's of isolation attempts can be made in a single day, allowing for one experiment to be done per day. The combination of performing a set of elasticity experiments, calibrating the force-measuring pipette and analyzing the data takes about a day, so chromosome isolation is no longer the limiting step in conducting chromosome elasticity experiments.

2.9.2 Version 2

Experimental setup version 3 has the force-measuring pipette mounted directly on the stage plate (Figure 2.3). Therefore, this pipette cannot be moved near the cell to extract a chromosome. Instead, the chromosome must be moved to the force-measuring pipette. However, the attachments between the chromosome and the rest of the cell do not allow for this. Therefore, a variation of chromosome extraction version 1 is done by using two pipettes, one filled with the 0.05% Triton-X in 60% PBS and the other filled with 10 mg/ml BSA in 60% PBS. The cell is opened up with Triton-X as described above. A relatively free chromosome is then aspirated with the pipette containing 10 mg/ml BSA, which keeps the chromosome from adhering to the inside of the pipette (Houchmandzadeh *et al*, 1997) and the pipette with Triton-X is replaced with a stiff pipette filled with 60% PBS.

Once the pipette with BSA grabs a chromosome, one of two things is done. If the chromosome is not attached to the rest of the chromosomes, the cell is moved away and the force pipette is positioned in the field of view. The free end of the chromosome is aspirated into the force pipette. This is followed by ejection of the other chromosome tip out of the BSA pipette with positive flow and then aspirating it into the 60% PBS pipette. The chromosome usually remains slightly attached to the pipette with BSA so this pipette is carefully moved away, breaking the final attachment between the BSA pipette and the chromosome.

If, after the Triton-X treatment, the chromosome aspirated into the BSA pipette is anchored by a thin fiber, the pipette with 60% PBS is used to grab the end of the chromosome anchored by the thin fiber. The chromosome and thin fiber permanently adheres to the inner wall of the pipette. The microscope stage is then translated so that the cell is moved away from the chromosome, breaking the fiber. The chromosome is not damaged because the third pipette with

60% PBS supports the force that breaks the thin fiber. Now, the chromosome is anchored to two pipettes, permanently to the one filled with 60% PBS and slightly to the pipette filled 10 mg/ml BSA. The microscope stage is positioned so the force-measuring pipette is in the field of view. The chromosome is then pushed out of the BSA pipette with positive flow and aspirated into the pipette with 60% PBS. Again, the chromosome is slightly attached to the pipette with BSA, but this sticking can be broken by carefully moving the BSA pipette away. The result is a chromosome anchored between two pipettes where one is held by a computer controlled micromanipulator with a force constant of about 10 nN/ìm and the other (force-measuring) pipette is mounted on the microscope stage with a force constant of 0.1 to 0.5 nN/ìm. The success rate of this technique is the same as in section 2.7.2. However, since there are so many mitotic cells in both TVI and A6 cell cultures, an experiment is completed in a day.

2.10 *Xenopus* A6 Chromatid Isolation

The technique used to isolate a *Xenopus* chromatid is similar to the technique described above for TVI chromosome isolation, version 1. The difference is that the Triton-PBS solution is sprayed during early anaphase when the chromatids are being pulled to the spindle poles. The chromatids flow out in two groups, but are well attached to each other by end attachments. It is extremely difficult to repeatedly extract isolated chromatids with a free end. Only one Xenopus chromatid was isolated by this technique, and single newt chromatids could not be isolated.

2.11 Force-Extension Experiment and Analyses

2.11.1 Experiments with Setup, Version 1

After a chromosome is isolated and attached to two pipettes, the pipettes are positioned anti-parallel to each other and perpendicular to the chromosome (Figure 2.5). Since experimental setup, version 1, has only the force measuring pipette held by a computer

controlled manipulator, the PC with Labview moves the force-measuring pipette out and back, periodically capturing images to disk. The force-measuring pipette has a force constant of 0.1 to 1 nN/îm, and the bending deflection provides a measure of the force applied to the chromosome. The strain rate of the extension-retraction experiments were done at rates < 0.01 sec^{-1}. The strain rate is the ratio of the linear velocity of the pipette to the native length of the chromosome and is measured in sec^{-1}.

The position of the pipettes and length of the chromosome were determined from the images using a Labview program. The program sequentially opens each image on the monitor, then the computer mouse is positioned to point and click on the same part of the pipette tip in each image. The pixel value that was clicked on is saved providing the pipette tip position for each image with a resolution of 0.1 µm, which is limited by the resolution of DIC and the pixel size of our images. Since the force-measuring pipette was moved, the deflection was deduced from the difference between the recorded position of the manipulator and the image of the pipette tip. Deflections during retraction contain an offset of 1 to 2 µm because of the mechanical backlash of the MP-285. The known force constant of the pipette allows conversion of the deflection into a force providing a force vs. extension plot.

2.11.2 Experimental with Setup, Version 2 and 3

Following chromosome isolation with experimental setup version 2 or 3, the pipettes are aligned so the chromosome is perpendicular to both pipettes (Figure 2.5). While periodically capturing images, the stiff pipette (the right pipette in Figure 2.5) is translated by a Labview program. The force-measuring pipette (the left pipette in Figure 2.5) is held stationary but deflects. Following calibration of the pipette, the deflection monitors the force applied to the

stretched chromosome. A movie of typical extension-retraction cycles showing pipette bending is available at:

http://safarsquid.phy.uic.edu/~mpoirier/experiments/movies/chromo-extend.mpg.

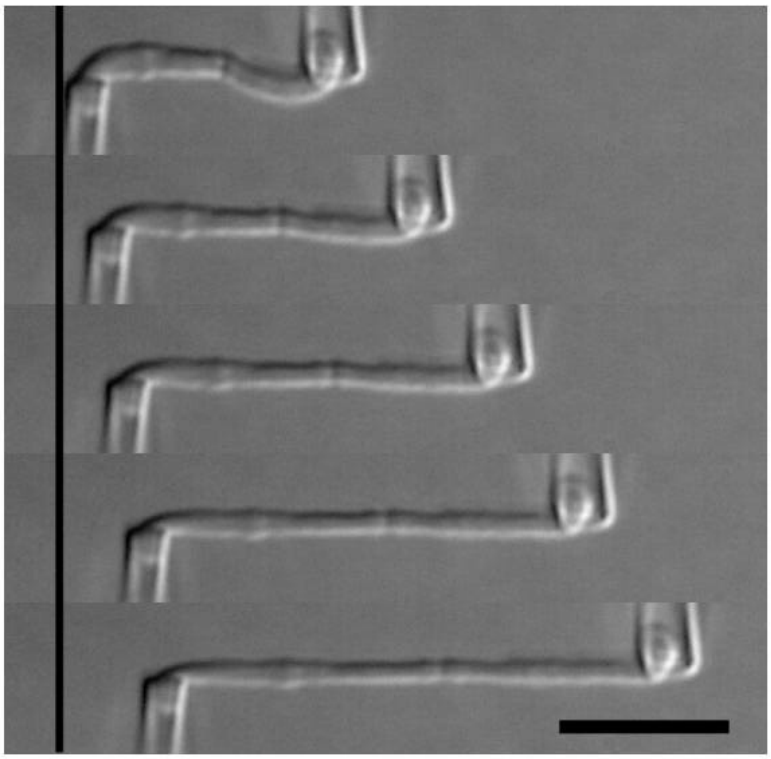

Figure 2.5 DIC images of a single-chromosome stretching experiment where the right pipette is translated 0, 5, 10, 15 and 20 μm. The left pipette is not moved but deflects and is calibrated so the deflection is converted into a force. Bar = 10 μm.

The images were analyzed to measure the change in length of the chromosome as a function of deflection of the stationary pipette. A Labview program extracted a 32×64 or 32×128 pixel image containing one of the pipettes. The initial image is correlated with each

subsequent image in an experiment. The correlation image has a peak, which shifts corresponding to the shift in the pipette position. The image is averaged in the *y* and *x* directions resulting in two 1-D arrays (Figure 2.6). Each array has a well-defined maximum. The peak and its two adjacent points are fit with a parabola, which determines the center of the peak. This measures the pipette deflection to about a 10 nm resolution as determined from unloaded pipette-translation calibrations.

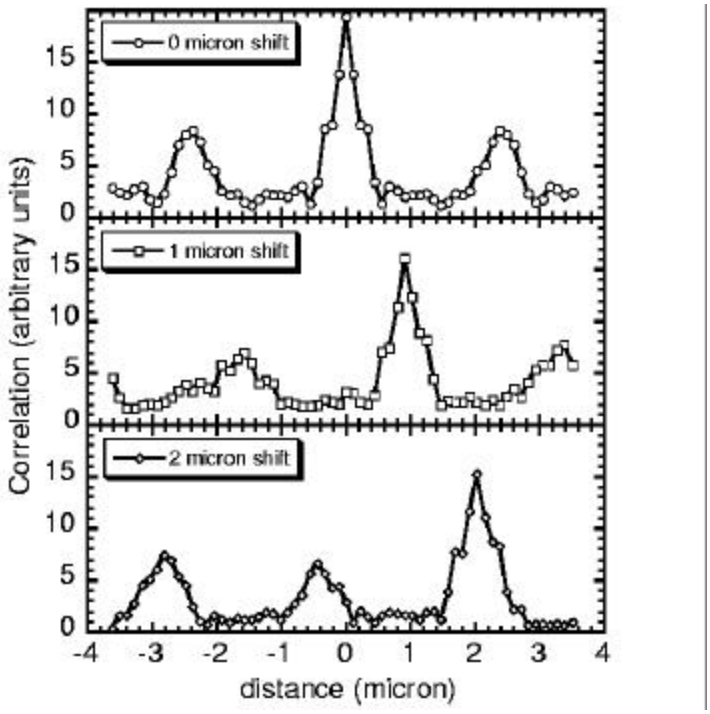

Figure 2.6 Plots of the x correlations (y averaged) for three sets of images. The circles are the correlations for two images where the pipette is not moved. The squares are the correlations of two images where the pipette was moved 1 ìm. The diamonds are the correlations of two images where the pipette was moved 2 ìm. Each plot is averaged in the y direction of the correlation image and by fitting the peak to a parabolic fit; we obtain an accuracy of about 10 nm.

The deflection is converted to a force with the force constant of the force-measuring pipette, which is typical 0.1 to 0.5 nN/îm giving a force resolution of 1 pN. However, mechanical vibrations of the pipette limits the force measurement to ~10 pN. The deflection of the force-measuring pipette does not depend on the position of the manipulator as it did for experimental setup, version 1. The limiting factor in determining the zero force position of the pipette is slow drift, which is mainly due to complicated effects of evaporation at the air-water interface where the pipette enters the cell culture medium. Also, the longer an experiment takes, the more the drift adversely affects the force resolution: for example drift during a 1000 sec period reduces the resolution to as much as 100 pN.

2.12 Bending Rigidity Measurements of Extracted Chromosomes

The bending rigidity was measured by observation of thermal fluctuations of chromosome shape, in a manner similar to that used by Gittes *et al*, 1993 and Houchmandzadeh and Dimitrov, 1999. A mitotic chromosome is isolated by the technique described in section 2.9.1. The chromosome is then held by one pipette leaving one end free. Only chromosomes with no attachments to other chromosomes can be used for bending fluctuation experiments. A Labview program acquired 1500 phase contrast images in 150 sec for different points along the chromosome. An additional lens was added to over magnify the chromosomes by 2.5 times. The resulting images were analyzed by a Labview program to determine chromosome shape fluctuations.

The data analysis used to determine the bending rigidity (described in section 2.12) assumes the chromosome is a straight rod, so it is important that the chromosome be relatively straight and rod like. Therefore, we used chromosomes without strong intrinsic bends. The camera was rotated so the chromosome fluctuations are in the x (horizontal) direction. The

correlation image analysis used for tracking pipettes does not work well for chromosome shape analysis because the contrast of the chromosome is not large enough. Instead, the displacement fluctuations were tracked at various points along the chromosome length by extracting and averaging 10 adjacent line profiles along the chromosome (Figure 2.7a). Each averaged line profiles had two minima, which correspond to the edges of the chromosome (Figure 2.7b). This average line profile is relatively smooth where the shape does not change but shifts from image to image. The shifts in the line profile correspond to the spatial fluctuations, which are determined with parabolic fits of the two minima. This provides two position measurements for each time point, which are averaged to give a single fluctuation time series. The two position measurements at each time point are subtracted, providing an estimate of the change in shape of the line profile and estimates the error of the fluctuation measurement. This was repeated for various points along the chromosome. We can resolve fluctuations as small as 10 nm, much less than the light diffraction limit of our optics (60X Olympus objective, 1.4 N.A.), since the motion of a single isolated object against a smooth optical background is being measured. The center of the resulting smooth density distribution that we observe can be located to a much higher accuracy than its width, given low-noise image data.

After repeating this analysis for many positions along the chromosome length, a set of displacement time series $u(t)$ are obtained at various points along the chromosome. The average of the square of the deflection $\langle u^2 \rangle$ is calculated for each time series. The accuracy of this thermal fluctuation technique is limited by mechanical noise coupled to the pipette by motion of the air-water interface. To eliminate slow drifts caused by evaporation-driven motion of the air-water interface, it was necessary to precisely level the culture dish. Experiments can be carried out for roughly 2 hr before evaporation makes it necessary to add water to the culture dish.

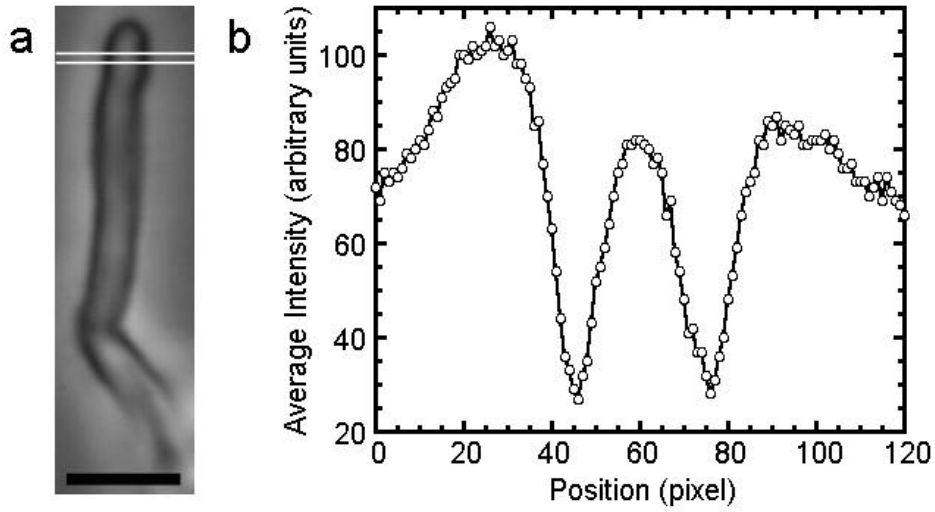

Figure 2.7 Line profile analysis for tracking position of the chromosome. (a) is an image of a chromosome for which 10 horizontal line profiles were extracted between the two white lines. Bar = 4 ìm. (b) is the average intensity line profile of the 10 extracted profiles from the chromosome shown in (a).

Note that the bending measurements are always done before stretching measurements since it requires one of the chromosome ends to be free to fluctuate. A stretching measurement requires both ends of the chromosome are permanently attached to pipettes, which can then not be removed.

The bending rigidity is determined from the root-mean-square amplitude of thermal bending fluctuations, and the absolute temperature of the surrounding medium. By considering the thermal excitation (Appendix A) of the bending modes of a stiff filament (Landau and Lifshitz, 1986), the bending rigidity can be related to the mean-squared deflection a distance x from the fixed end, by

$$\left\langle u^2 \right\rangle = \frac{32 k_B T x^3}{p^4 B}, \qquad (2.1)$$

where k_BT = 4.1 x 10^{-21} J, the thermal energy unit at room temperature. The plot of $<u^2>$ vs. x on a log-log scale will be linear with a slope of 3, and the y-intercept is related to the bending rigidity B. Note that the thermal fluctuations of the chromosome are insensitive to the presence of the pipette apart from its role in immobilizing the chromosome end.

2.13 Bending Rigidity Measurement for Chromosomes in Colchicine Arrested Cells

Newt cells were grown to confluency and then incubated in culture medium with 0.1 mg/ml colchicine for 60 minutes. The mitotic cells become arrested in metaphase and chromosome movement stops. The cell culture is then scanned for metaphase arrested cells, which has a 4-5 μm segment of a metaphase chromosome projected in the plane of the microscope. A 100 second time series of images was acquired at a frame rate of 10 frames per second. Changes in cell shape, which occur on the minute time scale, cause non-thermal changes in chromosome shape. To reduce the effect of these fluctuations of the cell shape, about 20 seconds of the 100 second time series was used for data analysis. Three points along the chromosome were tracked which parameterized the chromosome segment into 2 line segments. A change in angle, $\Delta\theta$, between the lines was computed vs. time.

The bending rigidity can be calculated from $\langle \Delta\theta^2 \rangle$. The bending energy of the chromosome segment is approximated by $E = \frac{B}{2L}\Delta\theta^2$, where L is the line segment. The bending-angle fluctuations will have a Maxwell-Boltzmann distribution in thermal equilibrium.

$$P(\Delta\theta) = \frac{e^{\frac{-\Delta\theta^2}{2\langle \Delta\theta^2 \rangle}}}{\sqrt{2\pi\langle \Delta\theta^2 \rangle}} \qquad (2.2)$$

$$\text{where } \langle \Delta\theta^2 \rangle = \frac{k_BTL}{B} \qquad (2.3)$$

$P(\Delta q)$ is the probability (per unit angle) of the rod segment having a bending-angle fluctuation Δq. $\langle \Delta q^2 \rangle$ can be determined directly from the time series or from a 1 parameter fit of Eq. 2.2 to a normalized histogram of Δq^2. The bending rigidity is then found with Eq. 2.3.

2.14 Step-Strain Experiment

Step-strain experiments were used to quantify the relaxation rate of chromosomes. A chromosome was extracted from a mitotic cell with pipettes as described above in section 2.9.1; experimental setup, version 2 was used for these experiments where each end of the chromosome was strongly anchored to a pipette. The MP-285 controller was used to step the stiffer pipette at a rate of 100 µm/sec while a Labview program was used to acquire images of the experiment at a rate of 20 frames per second for a total of 30 to 60 seconds. The pipette positions were measured as described in section 2.11.2. The relaxation time of the pipettes themselves was measured to be < 0.05 sec.

2.15 Microspray Experiments

The effect of changes in ionic conditions on mitotic chromosome structure was studied by locally spraying a chromosome held in the two pipettes (Figure 2.2). A spray pipette was fabricated as described in section 2.5 and then filled with various concentrations of NaCl, $MgCl_2$, $CaCl_2$ or $Co(NH_3)6Cl_3$ in 50 mM Tris, pH = 8.0. These experiments were done with experimental setup version 2, so a third manual manipulator (Taurus, WPI) was used to position the spray pipette between 10 and 70 microns of the chromosome. The chromosome was then stretched and the pipette position was monitored was described in section 2.11.2. A 40 second time series of images was acquired at 10 frames per second after the chromosome was extended and under tension. Five seconds into the time series the salt solution was sprayed for 10 seconds. This was repeated on the same chromosome with increasing salt concentrations, which was done

by varying the distance between the chromosome and the pipette. Determination of the salt concentration as a function of distance is described below.

2.16 Microspray Concentration Calibration

The concentration of ions decreases as one moves away from a pipette with a solution flowing out. To calibrate the concentration as a function of distance from the pipette we used fluorescence of ethidium bromide, which has a diffusivity similar to the salts used in this study. Fluorescence allows for an estimate of the concentration of ethidium bromide molecules because it absorbs a photon with a wavelength of around 520 nm and then emits one with a wavelength of about 610 nm. The microscope has the correct combination of filters so only photons with a wavelengths around 520 nm are exposed to the sample with ethidium bromide molecules, while only the emitted photons with wavelengths of about 610 nm make it to the camera. The camera captures images of the fluorescent intensity, which is proportional to the number of fluorescent molecules.

Pipettes with diameters of 1.4, 1.6, 1.8, 2.5, 2.6, 2.8 and 3.1 were fabricated and filled with 0.3 mM ethidium bromide diluted in PBS. A 40-second-long time series of images was acquired, where a 10 sec spray of ethidium bromide exposed to excitation light was initiated 5 sec into the time series. Four time series were acquired for each pipette, where two were with 25% excitation intensity and two were with 10% excitation intensity. The intensity decreased by about 2.5 times for the time series with 10% excitation light. This shows the CCD camera is linear over the intensity range we are using. Also, the fluorescence intensity was similar for pipettes with similar diameter.

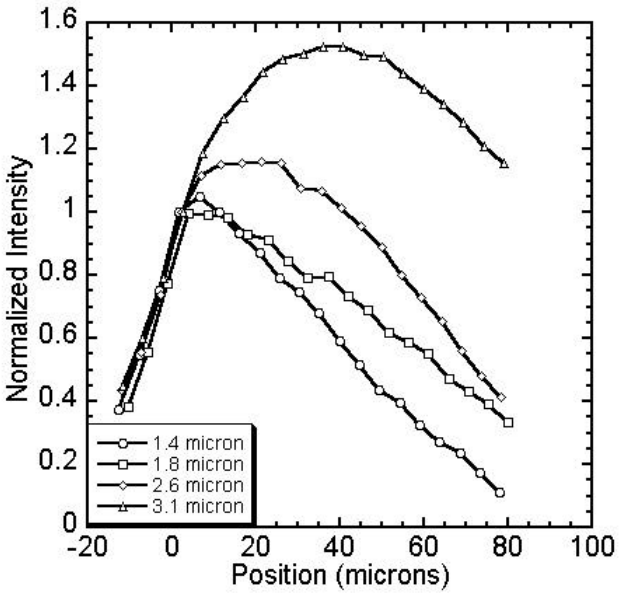

Figure 2.8 Intensity of the fluorescence vs. axial position from the pipette. The intensity is normalized to the intensity at the pipette tip. These plots serve as calibration curves for the concentration of ions as a function of distance from the pipette tip with known pipette tip inner diameter.

The spray pattern observed in fluorescence equilibrated in a few seconds and was predominantly forward, with the fluorescence typically opening up with a ~45 degree angle. A plot of fluorescence intensity vs. distance from a pipette with a diameter similar to the one used in a given experiment was used as a calibration curve (Figure 2.8). This calibration is rough since out-of-focus light contributes to the measured pixel intensity. For wide pipettes (3 µm), it is therefore possible for the observed fluorescence intensity to rise slightly as one goes away from the pipette opening. In this case, the fluorescent intensity initially increases to a maximum 40 ìm from the tip with an intensity double of that at the tip of the pipette. This occurs because the concentration initially decreases slowly enough that the increasing volume over which the fluorescent molecules are spread causes the apparent intensity to increase. From this, we estimate

the error of the concentration calibration to be as large as a factor of two, however changes in concentrations are more accurately known with an uncertainty of about 20%. A more precise calibration could be obtained using a confocal microscope.

2.17 Microdigestion Experiments

These experiments are similar to the microspray experiments described above. However, there are some differences. They were done with experimental setup version 3, which provides the best force resolution and the least amount of pipette drift. After a chromosome was isolated and attached to 2 pipettes, a few extension-retraction experiments were done to characterize the native elasticity of the chromosome. An enzyme was then prepared in the appropriate reaction buffer then a spray pipette was fabricated and filled with the enzyme-buffer solution. One of the MP-285 manipulators positioned the spray pipette ~50 ìm away from the chromosome. Another extension-retraction experiment was done to see if the chromosome elasticity had changed. The chromosome is then extended by about 1.5 times the native length. 2000 images are then acquired at 2 frames per second. After about 100 to 200 seconds, flow out of the spray pipette was initiated with ~ 1000 Pa of pressure and then the pipette was moved ~10 ìm from the chromosome. After an additional 300 seconds, the flow was turned off and the pipette was moved 50 microns away from the chromosome. Images continued to be acquired for up to 500 additional seconds. The chromosome was then retracted slowly back to zero force. The pipette positions were measured as described in section 2.11.2. A comparison of the force response out, before acquiring the 2000 images, and the force response back, following the image acquisition, allows for the drift of the force-measuring pipette to be determined. Only the time series with drifts causing a force shift of < 0.05 nN were used.

2.18 Preparation of Micrococcal Nuclease and Restriction Enzymes

For each microdigestion experiment the enzyme solution was prepared after a chromosome was isolated and its force constant measured. This minimizes degradation in activity of the enzyme before it is used to microdigest a chromosome. There are two types on double stranded DNA (dsDNA) cutting enzymes used: micrococcal nuclease and type II restriction enzymes. Micrococcal nuclease cuts dsDNA at any exposed site in the presence of mM concentrations of $CaCl_2$. The spray solution was 1-10 nM micrococcal nuclease in 60% PBS with 1 mM $CaCl_2$.

Restriction enzymes (RE) are found within most prokaryotic organisms and function as part of a protection system from invading DNA (Pingoud and Jeltsch, 2001). These enzymes are of great importance to genomic analysis and cloning because they make dsDNA cuts at specific sequences in the presence of millimolar amounts of $MgCl_2$. The recognition sites are usually 4 to 8 base pairs and palindromic. Some RE's cut leaving 2 to 4 bp overhangs, while others cut leaving blunt ends. The restriction enzymes used were Alu I (AG^CT, Promega), Hae III (GG^CC, Roche), Cac8 I (GCN^NGC, New England Biolabs), Hinc II (GT(T/C)^(A/G)AC, Promega), Hind II (GT(T/C)^(A/G)AC, Roche), Dra I (TTT^AAA, Promega), Stu I (AGG^CCT, New England Biolabs) and Pvu II (CAG^CTG, Promega), which all produce blunt ends following dsDNA cleavage. The letters describes the enzyme's recognition sequence and '^' indicates where the sequence is cleaved. N indicates that A, G, C or T is allowed for recognition and (T/C) indicates recognition occurs for either T or C. The enzymes were sprayed in the reaction buffers provided by the company. The reaction buffers used were Promega's Buffer B (50 mM NaCl, 6 mM Tris-HCl, 6 mM $MgCl_2$, 1 mM DTT and pH 7.5) Roche's Buffer M (50 mM NaCl, 10 mM Tris-HCl, 10 mM $MgCl_2$, 1 mM DTT and pH 7.5) and New England Biolab's

Buffer 2 (50 mM NaCl 10 mM Tris-HCl, 10 mM $MgCl_2$, 1 mM DTT and pH 7.5) and 3 (100 mM NaCl, 50 mM Tris-HCl, 10 mM $MgCl_2$, 1 mM DTT and pH 7.9).

2.19 Assay of Enzyme Activity

Within 12 hours following a microdigestion experiment the restriction enzyme activity was assayed by digesting either 0.02 ìg/ìl of pBR322 (Promega) or 0.01 ìg/ìl of λ DNA (Promega) with the remaining enzyme in the appropriate reaction buffer at 25 C for 15, 30 and 60 minutes. Alu I, Hae III, Cac8 I, Hinc II and Hind II were assayed with pBR322, since it contains between 2 and 30 cut sites for these enzymes. λ DNA was not used to assay these enzymes because it contains hundreds of cut sites making it nearly impossible to determine when digestion was complete and if there was over digestion (star activity) occurring. Dra I, Pvu II and Stu I were assayed with λ DNA because pBR322 does not contain cut sites for these enzymes. The digested DNA was then analyzed with ethidium bromide gel electrophoresis (Figure 2.9). Only restriction enzymes, which completely digest pBR322 or lambda at 25 C in less than 30 minutes were used. None of the restriction enzymes used exhibited star activity, cutting at sites other than their recognition sequence, after the 60 minute incubation.

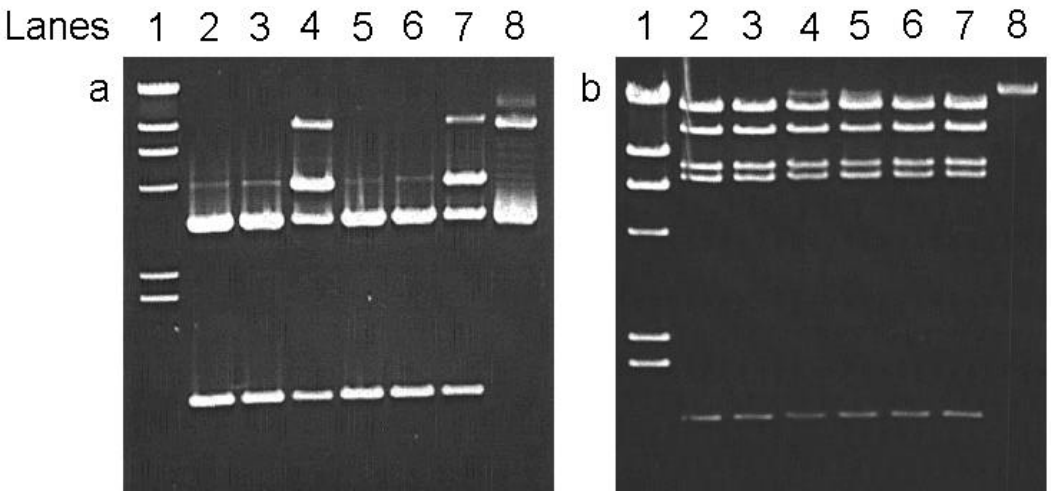

Figure 2.9 Images of the electrophoresis gels stained with ethidium bromide, which assay the activity of restriction enzymes. (a) is a gel of a digestion of pBR322 DNA with Hinc II. (b) is a gel of a digestion of λDNA with Stu I. Lane 1 of each gel is linear DNA of six known lengths and is used as a reference to determine the length of the bands in the other lanes. Lanes 2, 3 and 4 of each gel are digestions for 60, 30 and 15 minutes respectively with the 12 hour old enzyme used in a microdigestion experiment. Lanes 5, 6 and 7 of each gel are the digestions with freshly prepared enzyme for 60, 30 and 15 minutes respectively. Lanes 8 of each gel is the DNA without enzyme. Note that pBR322 is initially supercoiled which explains why lane 8 in (a) has two bright bands. The lower band is supercoiled and the upper band is nicked.

2.20 Preparation of Fluorescein-Labeled Anti-Histone

Anti-histone, pan (Lot # 1492 519, Boehringer-Mannheim) was prepared at a concentration of 0.04 mg/ml with 1 mg/ml of BSA in PBS (BioWhitaker). FLUOS (5 (6)-Carboxyfluorscein-Nhydroxysuccinimide ester, Boehringer Mannheim) was prepared at a concentration of 0.2 mg/ml in PBS and 1 µl was added to 50 µl of anti-histone solution. The mixture was gently stirred for 2 hours at room temperature. Labeled protein was separated from free fluorescein on a column (Microspin G-25, Amersham Pharmacia Biotech) by 1000 g centrifugation for 2 minutes (Appendix E).

2.21 Anti-Histone Labeling Experiments

A pipette was fabricated with a 3 micron size tip, which was filled with about 1 µl of FLUOS labeled anti-histone solution using a microinjection pump (PV830, WPI). The pipette was moved to about 20 µm from the chromosome with the manual micromanipulator, and then was sprayed with anti-histone for about 1 min at a pressure of 1 psi. The spray was then turned off and the pipette was moved away. We waited about 15 minutes before imaging the chromosome to allow unbound protein to diffuse away. The bound antibodies are localized on the core histones because of their high affinity for the core histones: H2A, H2B, H3 and H4. Since the antibodies are labeled with a fluorescent molecule, fluorescent microscopy is used to measure the fluorescent intensity, which is proportional to the number of antibodies bound to core histones. The fluorescence images were recorded with a CCD camera (Pictor 416XT, Meade) to a PC.

CHAPTER 3

MITOTIC CHROMOSOME STRETCHING ELASTICITY

3.1 Introduction

During mitosis, as chromosomes are mechanically moved around and eventually transported to opposite poles of the cell, they are stretched with as much as a nanonewton of force (Figure 1.6, Nicklas, 1983). This chapter describes force-extension measurements for single mitotic chromosomes removed from newt lung cells, newt TVI cells and *Xenopus* A6 cells. Glass micropipettes extract and manipulate chromosomes from live cells as described in Chapter 2. This technique was developed previously and used to carry out rough measurements of chromosome elasticity by Houchmandzadeh *et al.*, 1997; however, dynamics of extension and relaxation were not studied, and no systematic measurements of the elastic response during chromosome unfolding were done. The results of this section are important because they provide information on chromosome elasticity relevant to understanding *in vivo* chromosome movement. However, our main motivation for precise elastic measurement is to provide a quantitative baseline for measurements made after structural modifications (e.g. by enzymes) that will allow inference of chromosome structure (Chapters 6, 7).

An important aspect of these experiments is to ensure the chromosome is close to equilibrium while being stretched. If one carries out experiments at too large an elongation rate, a complicated combination of elasticity and relaxation dynamics are measured instead of the intrinsic chromosome quasi-static elastic response. This dynamical aspect of chromosome elasticity will be discussed in chapter 5. It is important to note that strain rates of $< 0.01\ sec^{-1}$ are used in all of the experiments reported in this chapter, which is sufficiently slow to observe quasi-static behavior. We find that mitotic chromosomes mechanically isolated from newt lung

cells display reversible and linear elasticity for extension to less than 3 times native length. In addition, chromosomes isolated with dilute Triton-X 100 from the newt TVI and the *Xenopus* A6 cells also display the same elastic response. For extreme stretching at slow elongation rates, we observe a new unfolding behavior: after an elongation-retraction cycle to > 30 times native length, mitotic chromosomes become not only permanently stretched, but also swollen. Antibody labeling indicates that even after such dramatic extensions, native quantities of histones remain on chromosomes. This supports the hypothesis that mitotic chromatids are held together by chromatin-tethering elements, and that the chromatin disperses as those elements are broken.

3.2 Short Extensions.

Extension-retraction cycles were done using experimental setup version 1, which is described in section 2.11.1. Extensions up to three times the original length are fully reversible and linear for strain rates less than 0.04 sec^{-1} (Figure 3.1). This experiment was repeated 7 times giving elastic constants: 1.5 ± 0.2 nN, 1.1 ± 0.2 nN, 1.0 ± 0.2 nN, 0.9 ± 0.2 nN, 0.6 ± 0.1 nN, 0.4 ± 0.1 nN, 0.4 ± 0.1 nN. Eight additional extension-retraction experiments were done with one pipette, where one end of the chromosome was anchored inside the cell. Again, extensions up to three times the native length are fully reversible and linear. The elastic constants were measured to be: 1.4 ± 0.3 nN, 1.0 ± 0.2 nN, 0.8 ± 0.2 nN, 0.6 ± 0.2 nN, 0.3 ± 0.1 nN, 0.2 ± 0.1 nN, 0.2 ± 0.1 nN. There was an appreciable variation in the elastic constant from chromosome to chromosome, possibly due to our sampling at different times between the end of prophase and the end of metaphase. Sometimes the pipette aspirates and attaches only one of the two chromatids; it is conceivable (but not obvious from the microscope images) that this has led to some of the run-to-run scatter. Finally, it is possible that different chromosomes have different

elasticity. In general however, the stretching constant of metaphase chromosomes is roughly 1 nN, in accord with measurements of Houchmandzadeh *et al.*, 1997.

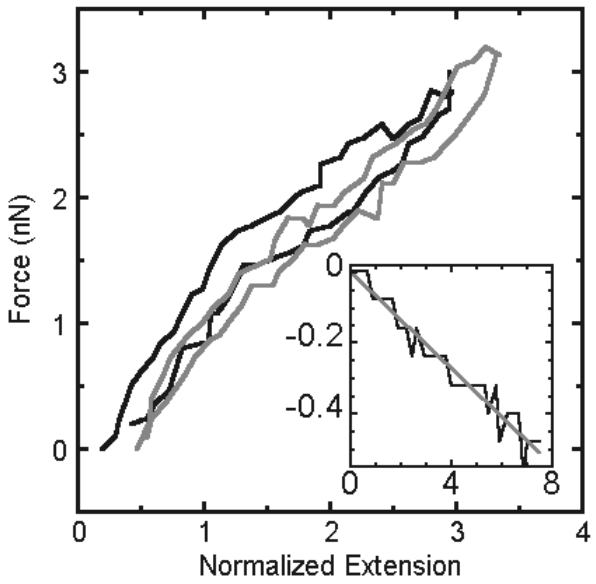

Figure 3.1 Force vs. Extension of a chromosome for 3-fold extensions and retractions. The native length of the chromosome is 7.5 μm. The strain rates are 0.007 sec^{-1} (black), and 0.03 sec^{-1} (gray).

Inset: The normalized change in width vs. normalized change in length of the same chromosome. The black line is the data and the gray line is the linear fit (y=-0.005+0.067x).

A linear decrease in chromosome width was observed to occur with increasing extension (Figure 3.1, inset), as is usual for an elastic object (Landau and Lifshitz, 1986). The ratio of the reduction in width to extension, the Poisson ratio, was $0.069 \pm .005$ during the run of Figure 3.1, a rather small value.

3.3 Intermediate Extensions.

Once a chromosome is extended beyond three to thirty times its original length, irreversibility and hysteresis occur. Figure 3.2 shows repeated extensions out to 10 times the original length. Initially, hysteresis occurs, but by the fourth cycle extension and retraction plots converge to a single curve. The final relaxed length is three times the original length, and most of this lengthening occurs during the first three extensions. Also, the force-extension curves change from nearly linear and slightly concave to a very nonlinear convex shape.

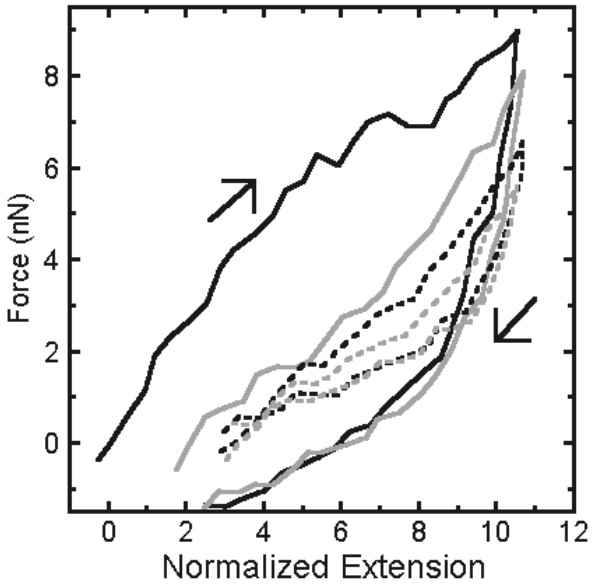

Figure 3.2 Repeated extension-relaxation curves to an extension of 10 times the native length of 3.8 μm. Each extension and relaxation was done at a strain rate of 0.008 sec^{-1}; shown are the first (black), second (gray), fourth (black-dashed) and sixth (gray-dashed) extensions.

Figure 3.3 shows repeated extensions out to gradually increasing lengths. Hysteresis occurs in each extension-retraction cycle and the initial slope decreases for each extension. Also,

the final chromosome length after each cycle increases. The final state of the chromosome is also optically distinct from the initial native state (Figure 3.4); when imaged by DIC, the contrast between the final chromosome and the surrounding medium is much less than the native chromosome. Phase contrast shows the final chromosome to be inhomogeneous on the micron scale, unlike the native chromosome. Also, the chromosome with a native width of 2.3 microns is swollen to a width of 3.3 microns. The elastic constant is reduced from 1.9 nN to less than 0.1 nN, as can be seen from Figure 3.3.

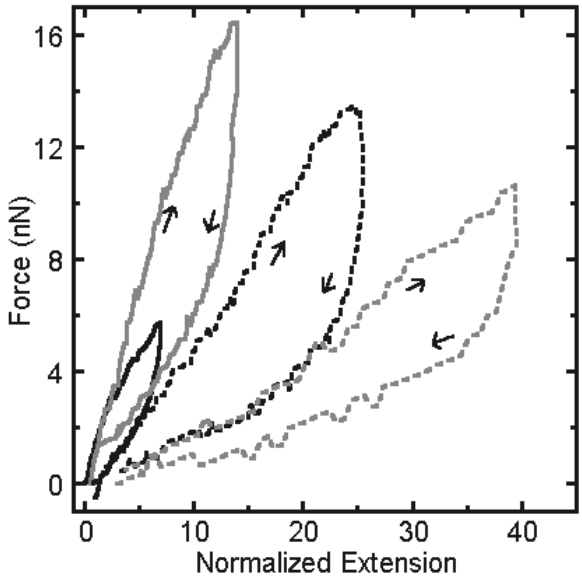

Figure 3.3 Force vs. Extension of a chromosome to increasing maximum extensions. The strain rates for all loops were 0.008 sec^{-1}. The order of maximum extensions was 7 times (black), 14 times (gray), 26 times (black-dashed), and 40 times (gray-dashed) the native length of 7.5 μm.

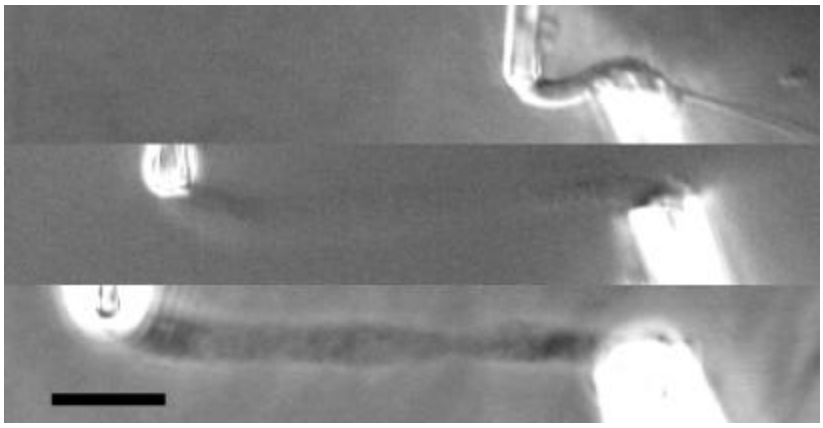

Figure 3.4 Images of the chromosome following the experiment plotted in Figure 3.3. (a) is a DIC image of the chromosome before the experiment; (b) is a DIC image and (c) is a phase contrast image of the chromosome after the experiment. Bar = 10 μm.

3.4 Long Extensions

Chromosomes break when extended to roughly 100 times their original length (Houchmandzadeh *et al.*, 1997). In the experiments of this chapter, chromosomes were stretched to up to 80 times without breakage. The force-extension response during stretching, at a strain rate of 0.008 sec^{-1}, continues to be linear to an extension of 30, after which the slope gradually reduces to a plateau (Figure 3.5). This plateau begins at a force varying from 15 to 20 nN. Chromosomes with lower plateaus display smaller elastic constants. Following retraction after a single long extension, the 'ghost' state of a chromosome is produced with characteristics similar to those described in the previous section.

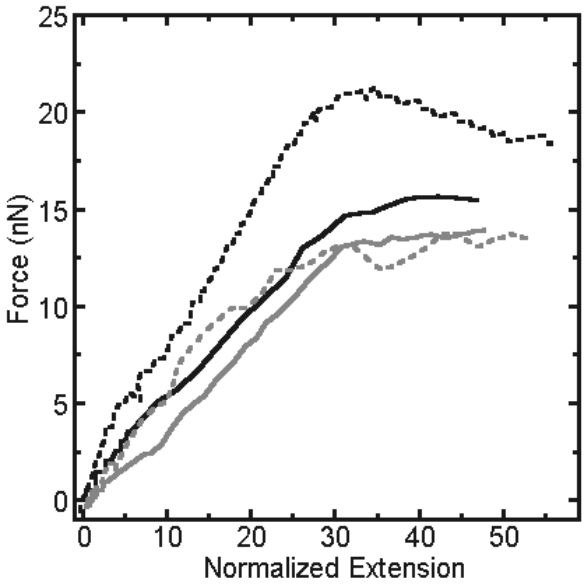

Figure 3.5 Force vs. Extension of chromosomes for large extensions. These extensions were all done with a strain rate of 0.008 sec^{-1}. The native lengths of each chromosome were 2.5 μm (black), 6 μm (gray), 4 μm (black-dashed) and 5.5 μm (gray-dashed).

3.5 Force-Extension Experiments on Anti-Histone Labeled Chromosomes.

Force-extension experiments were done on a newt chromosome before and after labeling it with FLUOS-labeled anti-histone. The elastic constant before labeling was measured to be 0.6 ± 0.2 nN. The chromosome was then sprayed with anti-histone and incubated for 15 minutes. Fluorescent images were then taken to show that anti-histone localized on the chromosome. The force-extension experiments were done again and the elastic constant was 0.8 ± 0.2 nN; chromosome elasticity was thus not strongly altered by the addition of anti-histone.

3.6 Measurement of the Number of Histones Before and After Long Extensions

Two chromosomes were stretched at rates of 0.003 sec^{-1} and 0.007 sec^{-1} to 23 and 50 times the original length, respectively, in separate experiments. The chromosomes were then

sprayed with FLUOS labeled anti-histone. In the 23× run we were able to simultaneously spray a nearby, native and unstretched chromosome. Fluorescent images (Figure 3.6) were collected, and after subtracting out background, the fluorescence intensity density (counts per pixel) of the native chromosome was 4600 ± 700, while the 23× stretched chromosome gave 1600 ± 300 counts. The 50× stretched chromosome had a fluorescent intensity per area of 1400 ± 300.

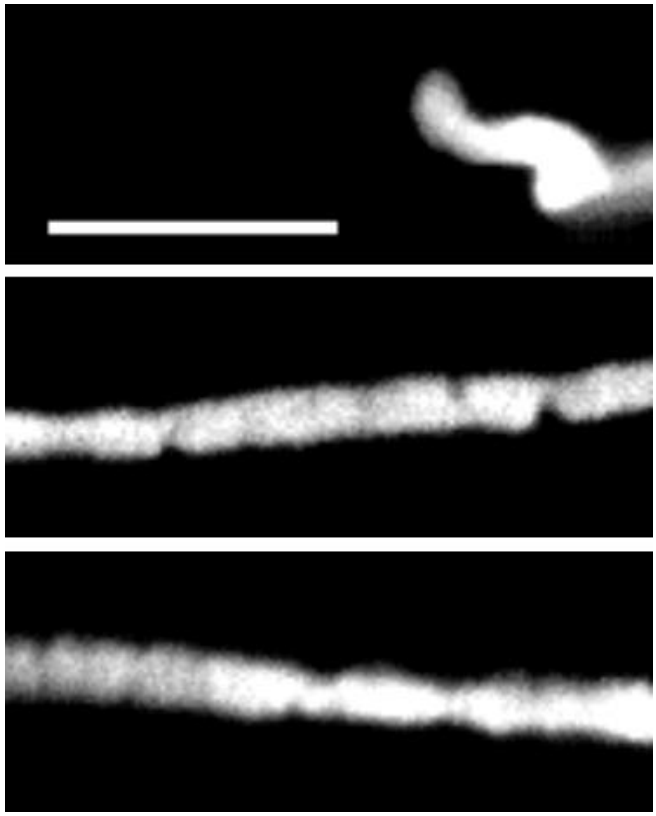

Figure 3.6 Immunolocalization of anti-histone on newt chromosomes. (a) is a native chromosome; (b) is a chromosome labeled after a 23x extension and (c) is a chromosome labeled after a 50x extension. Bar = 10 μm.

There is a decrease of about 3 fold in the fluorescence intensity per pixel as a result of stretching. However, the increased volume of the stretched chromosomes accounts for this. The initial volume of the portion of the chromosome extended to 23x was 70 ± 10 μm^3 and the final volume was 290 ± 40 μm^3. This gives a total volume-integrated fluorescence intensity which changes by a factor of 1.3 ± 0.3. The initial volume of the portion of the chromosome extended to 50× was 20 ± 5 μm^3 while the final volume was 220 ± 30 μm^3. In this case, the total volume-integrated fluorescence intensity increased by 3.5 ± 1.0 times. These results indicate that native numbers of histones remain bound to the chromosomes after being stretched as much as 50×. In the 50× case, the increase in total fluorescence suggests that the completely opened chromosome is able to bind even more antibody than in the compact native state.

3.7 The Stretching Elasticity of Newt Lung, Newt TVI and *Xenopus* A6 Chromosomes Are the Same

The results described so far are for chromosomes extracted from primary cultures of newt lung epithelial tissue. These chromosomes are from healthy animals and are extracted without any chemical treatment. Two changes in our method, the use of TVI cell cultures, and use of 0.05% Triton-X in 60% PBS to soften the cell membrane, tremendously increased the rate at which non-damaging extractions of single chromosomes could be done. A TVI cell culture has a large number of mitotic cells at any particular time, providing many more opportunities for chromosome isolation as compared to a primary cell culture. However, we needed to check that there were no significant differences between the elastic properties of chromosomes from primary cell cultures and TVI chromosomes extracted using diluted Triton-X.

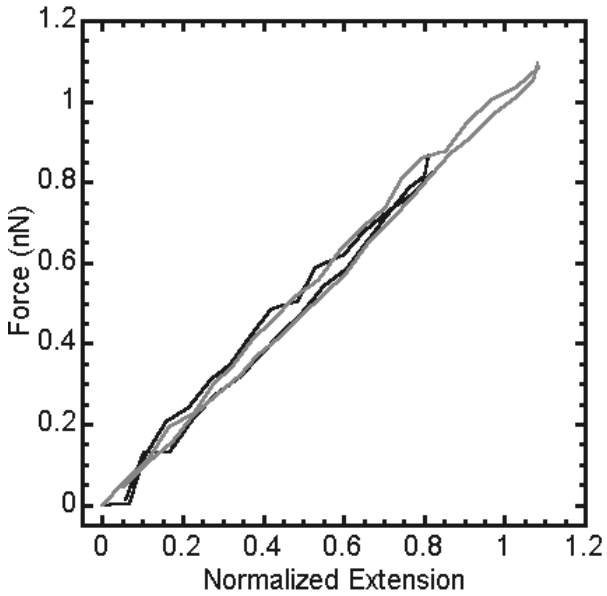

Figure 3.7 Two force vs. extension curves for a TVI chromosome extended and retracted at a strain rate of 0.01 sec^{-1}. The response is reversible and linear with a characteristic force of f_0=1 nN to double the length of the chromosome.

Figure 3.7 shows the response of a TVI chromosome during an extension-retraction cycle. The response is linear with a characteristic force of 1 nN to double the length, and the extension and retraction curves overlap. This response is similar to that of newt chromosomes from explanted cells (Houchmandzadeh *et al*., 1997, Poirier *et al*., 2000, Figure 3.1). The force constant can be converted to a Young's Modulus of 500 Pa by dividing by the cross-sectional area. The modulus is consistent with earlier results on newt chromosomes (Houchmandzadeh *et al*., 1997) and *Xenopus in vitro* assembled chromatids (Houchmandzadeh and Dimitrov, 1999).

The TVI chromosome elastic response for extensions larger than 3 times native length was also measured. Slow extension at a strain rate of 0.01 sec^{-1} shows a force plateau at an extension of about 30x and at a force of about 10 nN (Figure 3.8). Also, repeated extension-

retraction cycles to increasing maximum extension display hysteresis and the following extension curve has a decrease in the force response (Figure 3.8, inset). These results are identical to the stretching elasticity of chromosomes removed from newt lung cells.

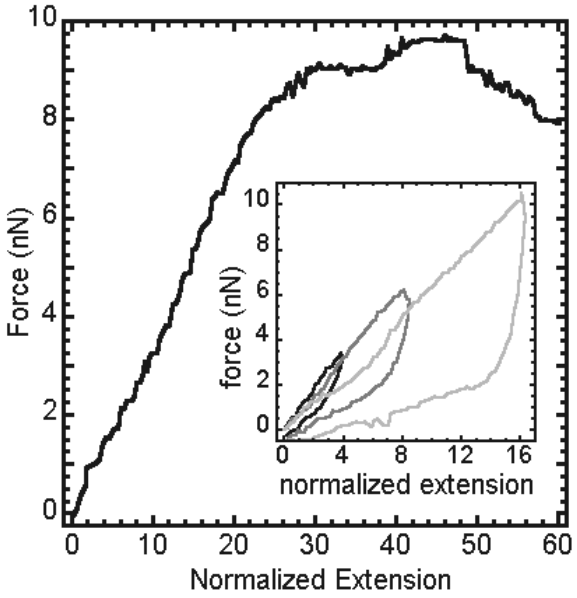

Figure 3.8 Force vs. normalized extension for a TVI chromosome to 60 time native length at a strain rate of 0.01 sec^{-1}. The response is linear out to 30 times extension at which a force plateau occurs at a force of 10 nN. This response is similar to newt lung chromosomes.

Inset: 3 Force vs. extension curves for a TVI chromosome. Each curve is out to an increased maximum extension. The appearance of hysteresis for extensions beyond 3 times and the reduction of the force response for successive extensions are identical to the force response of newt lung chromosomes.

The force response and Young's modulus of *Xenopus* A6 chromosomes were measured by the same technique as newt chromosomes. Figure 3.9 shows a typical force extension curve for a *Xenopus* A6 chromosome. Four separate A6 chromosomes were measured to have Young's

moduli of 200, 400, 400 and 800. These values are similar to previously measured chromosome moduli (Houchmandzadeh *et al.*, 1997, Poirier *et al.*, 2000) and to moduli of *Xenopus* chromatids assembled in egg extract (Houchmandzadeh and Dimitrov, 1999).

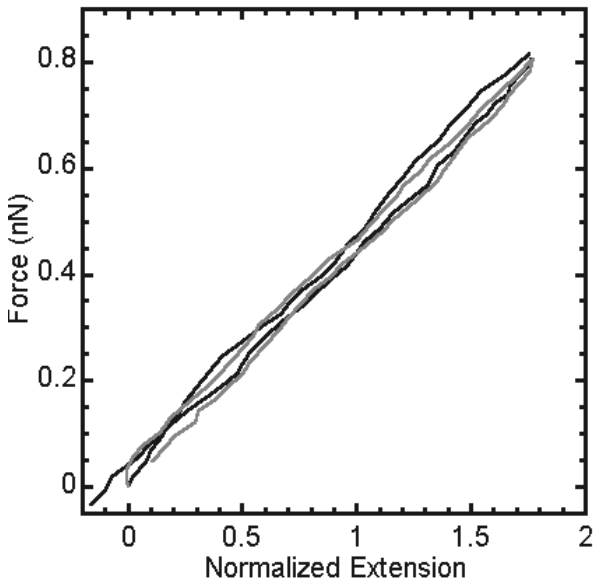

Figure 3.9 Force vs. Extension of a *Xenopus* A6 chromosome extended and retracted at 0.03 sec^{-1}. The force response is similar to chromosomes removed from newt lung cells and newt TVI cells.

3.8 Triton-X 100 Does not Affect Chromosome Elasticity

We have found that the minimum concentration of Triton-X 100 required to extract chromosomes is 0.05%. TVI chromosomes, which are extracted with this concentration, have the same elastic response as chromosomes extracted from newt lung cells. This indicates that using 0.05% Triton-X does not affect chromosome elasticity.

3.9 Extensions Up to Three-Fold are Reversible

Mitotic chromosomes display reversible and nearly linear elasticity for extensions up to 3 times native length (Figure 3.1, 3.7 and 3.9). By comparison, most solid materials fracture if extended by more than a small fraction of their initial length; polymer gels can sometimes show this kind of extensibility (Houchmandzadeh *et al.*, 1997). Chromosome linear elasticity is described by a force constant of roughly 1 nN. The variability from chromosome to chromosome was roughly 0.5 nN; this is larger than our experimental error, and must be intrinsic to the chromosomes themselves or to the precise time in cell cycle when they are extracted. Houchmandzadeh *et al.*, 1997 reported a five-fold decrease in force constant from prometaphase to metaphase.

The chromosome force constant of 1 nN may be expressed as a Young modulus Y by dividing it by the cross-sectional area of the unstretched chromosome, $3x10^{-12}$ m^2, giving Y=300 Pa. This is a very low modulus; covalently bonded solids usually have a modulus near 10^{10} Pa; molecular crystals and hydrogen-bonded solids such as single molecules of DNA have a modulus near 10^8 Pa; polymer gels usually have moduli of 10^3 to 10^4 Pa. This again suggests a comparison of a mitotic chromosome to a polymer gel. However, as discussed previously (Houchmandzadeh *et al.*, 1997) and in section 1.7, the scale of the Young's modulus is too large to be associated with the elasticity of a gel of chromatin fiber.

Another possible origin of the reversible elasticity is stretching and reversible modification of chromatin fiber structure. This explanation requires chromatin fibers themselves to have a force constant of less than 1 pN to explain the 1 nN chromosome force constant, since there should be at least 1000 chromatin fibers piercing a given cross section of chromosome with an area of 4 μm^2. First, this is a rather low value for a chromatin force constant since a doubling

of length would require disruption of linker histones; preliminary data on single chromatin fibers suggests that forces in the 5 pN is required to double chromatin length (Cui and Bustamante, 2000). Our result that anti-histone has no effect on chromosome elasticity also suggests that we are not observing principally chromatin elasticity. Instead, we propose that chromosome linear elasticity is mainly due to reversible unfolding of compacted chromatin by reversible deformation of chromosome-folding proteins.

3.10 Extension Beyond Three-Fold are Irreversible

The elasticity of chromosomes becomes irreversible, i.e. the force observed during retraction is below that found during extension, following extensions > 3x at strain rates (< 0.01 sec^{-1}) small enough to allow stress relaxation to occur (Figure 3.2). Following such irreversible extension-retraction cycles, chromosomes are permanently lengthened; for example, an 8x extension-retraction cycle results in the chromosome being permanently lengthened by 2x when relaxed; following a 25x extension-retraction, a 4x permanently extended chromosome is obtained. The force at which this hysteresis begins is a few nN, indicating that a structural element that holds the chromosome together is failing when the chromosome as a whole is under about 3 nN of stress.

There is no obvious signature of this 3 nN transition such as a force plateau that can be seen during initial extension beyond 3x. Instead a smooth, first linear and then slightly concave force-distance response is observed during initial extensions of up to 30x (Figure 3.5). The first sign of the 3 nN transition is irreversibility during retraction and then a modified elastic response if extension-retraction cycles are then repeated (Figure 3.2, 3.3). This suggests that the failure occurring near 3 nN is probably not due to breaking of chromosome-folding proteins or protein-chromatin connections; breaking should result in a plateau or drop in force as the chromosome is

extended. Instead, this irreversibility is possibly due to irreversible unfolding of proteins or protein-chromatin folds to the point where they are unable to recover their native conformation. Repeated extension-relaxation cycles to e.g. 10x extension (Figure 3.3) result in a gradual transformation of the force vs. distance from a slightly concave shape, to a highly convex shape typical of the polymer elasticity of stiff biopolymers (Smith *et al.*, 1992; Kellermayer *et al.*, 1997; Reif *et al.*, 1997; Tskhovrebova *et al.*, 1997). Modifications of nucleosome structure are most likely not contributing to this irreversibility, since anti-histone binding does not significantly change for a chromosome extended to 23 times its native length.

3.11 A Force Plateau Occurs Beyond 30-Fold Extensions

A force plateau at 15-20 nN (Figure 3.5) begins at 30x extension and can go out to 100x extension; extensions beyond this break the chromosome. Dramatic changes in the chromosome coincide with this force plateau: the chromosome is transformed to a dilute 'ghost' state with a low elastic modulus. This state was produced by both slow repeated extension-retraction cycles out to increasing extensions (Figure 3.4) and by a single, slow extension (Figure 3.5). There are two requirements for transforming a native chromosome into this new state. First, the chromosome must be elongated past 30x. Secondly, the chromosome must be extended at strain rates of less than 0.01 sec^{-1}. If the chromosome is extended too quickly, a stiff 'thin fiber' is produced instead (Houchmandzadeh *et al.*, 1997). Repeated extension-relaxation cycles as in Figure 3.3 are not required to produce a ghost state: a single elongation and retraction produce the same state, while repeated cycles to extensions of less than 30x do not (Figure 3.2).

A 'ghost' chromosome is up to 10 times longer than native length and swollen to 1.5 times the native width. There is a severe reduction in the optical contrast of the chromosome viewed in DIC and phase contrast (Figure 3.4). The force constant of a ghost chromosome is

less than 1/20 of its native value. The total fluorescent antihistone intensity of a chromosome extended to 23×, and then relaxed to zero force, shows almost no change. The fluorescent anti-histone intensity of a chromosome extended to 50x, and then relaxed to zero force, shows a 3.5 ± 1.0 fold increase in total fluorescence intensity. This suggests the swelling is not due to a loss of histones. The increase in fluorescence is possibly due to increased accessibility to histones as a result of the chromosome swelling. All of the above changes are consistent with breakage of the connector proteins discussed above starting at a force of 15 nN.

3.12 Comparison of the Stretching Elasticity of Chromosomes Assembled *In Vivo* and *In Vitro*

Houchmandzadeh and Dimitrov, 1999, recently studied the elasticity of "artificial" chromosomes assembled using Xenopus egg extracts by a method similar to this study. Much of the force-extension behavior of the two systems agree: extensions of less than 3x are reversible, repeated extensions to increasing maximum lengths result in hysteresis and a gradual reduction in the Young modulus, and single long extensions result in a force plateau. However, there are some differences between the two systems. The average Young modulus of an in vitro assembled chromosome is about 4 times higher than the average Young modulus of an in vivo assembled chromosome. This difference may be due to the *in vivo* and *in vitro* chromosomes being derived from different animals. It could also be explained by cell cycle differences, since a five-fold decrease in the Young modulus from prometaphase to metaphase has been observed for newt chromosomes (Houchmandzadeh *et al*, 1997). Also, Houchmandzadeh and Dimitrov do not observe swelling or a "ghost" morphology when a chromosome is extended into the force plateau region. Instead, thinned regions of the chromosome are produced. This could be a result of

extending the chromosome quickly; strain rates of about 0.1 sec^{-1} were used. Indeed, when we stretch newt chromosomes at a rate of 0.1 sec^{-1} we observe permanent thinning and no "ghost".

3.13 Conclusions

Mitotic chromosomes from newt lung, newt TVI and *Xenopus* A6 cells display linear-reversible elasticity for extensions < 3 times native length. Associated with this reversibility are a Young's modulus of about 300 Pa and a Poisson ratio of about 0.1. Larger extensions are no longer reversible and there is a force plateau of about 15 nN at a normalized extension of 30. Associated with these long extensions is a radically changed chromosome: the Young's modulus is reduced by more than twenty times, the volume swells by about twenty times (the length is increased by 10 times and the width increases by 1.5 times), and the image contrast is dramatically reduced. These results indicate the chromosome fills with the surrounding medium.

Labeling with fluorescent anti-histone shows there is no loss of histones after the chromosome is transformed into this ghost state, suggesting these dramatic changes in chromosome structure are not due to disruption of chromatin structure. Instead these deformations unfold a higher level of chromosome structure, which is presumably maintained by chromatin tethering proteins. Extensions of less than 3 times reversibly unfold this level of chromosome organization while larger extensions permanently unfold it.

Finally, these elastic measurements provide a well-defined baseline for experiments in chapters 6 and 7, where elasticity experiments are used to monitor changes in internal structure. In Chapters 6, force measurements detect structural changes induced by changes in ionic conditions, and in Chapter 7, force measurement provides a sensitive probe into the how chromosome structure is changed by dsDNA cutting enzymes.

The contents of this chapter were originally published as Poirier *et al*, 2000.

CHAPTER 4

MITOTIC CHROMOSOME BENDING ELASTICITY

4.1 Introduction

Chromosomes are bent as well as stretched during mitosis (Figure 1.1 and Figure 2.1), and a question relevant to the biomechanics of the cell cycle and to chromosome structure is how their bending rigidity compares to their stretching elasticity. The bending flexibility of rod-shaped objects is described by a stiffness B with dimensions of force times length-squared, or energy times length. For a rod of length ℓ, B/ℓ^2 gives approximately the force that must be applied at the rod ends to deform it into a U-shape. The utility of the bending rigidity B is that it provides a measure of rigidity, which is independent of the length. However, the bending rigidity of a rod does depend on its cross section.

For a rod composed of an ideal, isotropic elastic medium, the bending rigidity B is $B = \frac{\pi}{4} Y R^4$, where R is the cross-sectional radius and Y is the Young's modulus. The Young's modulus is independent of an object's dimensions and is a measure of a material's intrinsic elasticity. Doubling R increases B by a factor of 16 since the bending rigidity scales as R^4. Therefore, we will use $Y_B = \frac{4B}{\pi R^4}$, the Young's modulus inferred from the bending rigidity, to compare bending rigidities of chromosomes in a way that removes the dependence of B on chromosome radius expected for simple elastic materials. For example, bending rigidity measurements for chromosomes assembled in *Xenopus* mitotic egg extracts, $B = 1.2 \times 10^{-26}$ J·m (Houchmandzadeh and Dimitrov, 1999), lead to $Y_B = 0.6$ Pa, given the radius of 0.4 μm. Recent measurements of $B = 6 \times 10^{-25}$ J·m for metaphase chromosomes in colchicine arrested *Drosophila* embryo cells (Marshall *et al*, 2001) lead to a value of $Y_B = 40$ Pa.

During the mechanical experiments on mitotic newt chromosomes described in chapter 3, we noticed that thermally excited bending fluctuations were small, but measurable. This chapter reports measurements of thermal bending fluctuations of single newt and *Xenopus* chromosomes removed from mitotic cells. The bending fluctuations were used to find a bending rigidity of B = 1×10^{-22} to 3×10^{-22} J·m and 0.5×10^{-23} to 2×10^{-23} J·m for newt and *Xenopus* chromosomes, respectively.

To directly address the question of whether chromosomes extracted into the cell culture medium have mechanical properties and structure representative of those occurring *in vivo*, bending-fluctuation measurements were done with mitotic chromosomes inside living cells. However, bending fluctuations in native cells cannot be easily related to chromosome bending stiffness because the mitotic spindle (composed of motors on an array of microtubules) applies large forces to mitotic chromosomes (Marshall *et al*, 2001). In fact, the bending fluctuations of mitotic chromosome in native cells are to the eye clearly non-thermal, and instead are due to the ~nN forces generated by the spindle microtubules and motors (Nicklas, 1983).

In order to examine thermal bending fluctuations of chromosomes inside living cells, we used a drug, colchicine, which depolymerizes microtubules but otherwise does not affect live cell processes. After colchicine treatment, we observe small bending fluctuations *in vivo*, consistent with those of our extracted-chromosome experiments. While intrinsically less precise than the measurements on isolated chromosomes, *in vivo* measurements on colchicine-treated metaphase arrested cells gave $B = 2 \times 10^{-23}$ J·m, in good agreement with the isolated-chromosome measurement. The similar bending rigidities obtained from measurements *in vivo* and on extracted chromosomes indicate that the extraction and exposure to the cell culture buffer does not dramatically alter chromosome mechanical properties.

This study also provides the first combined stretching and bending experiments on the same chromosome. The measurements of B give values of Y_B = 500 Pa for newt chromosomes and 1000 Pa for *Xenopus* chromosomes. We also directly measured a Young's modulus of about 500 Pa for both newt and *Xenopus* chromosomes in which the bending rigidity was measured. These results indicate that the elastic rod relation, $B \gg YR^4$, holds for the chromosomes we have studied, indicating in turn that their structure is not highly anisotropic, and that the interior of a mitotic chromosome behaves as an isotropic elastic medium.

4.2 Bending Rigidity of Extracted Newt Chromosomes

Our measurement of B is based on measurement of the amount of thermal bending that occurs along a newt chromosome, following the method of Gittes *et al*, 1993, and Houchmandzadeh and Dimitrov, 1999. One pipette holds a single chromosome about 40 µm above the glass surface. While held at one end in the cell buffer (Figure 4.1), the free end of the extracted chromosome undergoes submicron fluctuations.

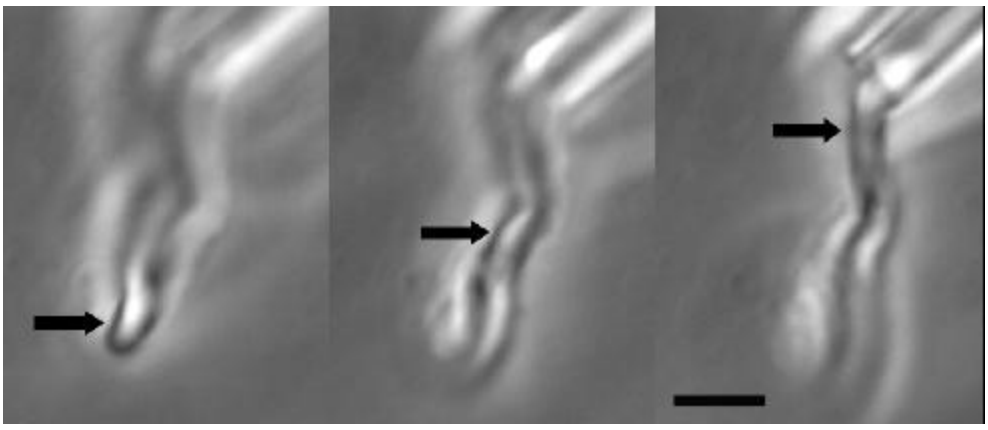

Figure 4.1. Phase-contrast images of different segments of a chromosome for which thermal bending fluctuations were measured. Arrows show where the fluctuations were measured, 15.6 µm, 8.7 µm and 0.9 µm from the pipette tip. Note that the chromosome extends slightly out of plane, so the focus is different for each image. Bar = 4 µm.

To quantify the fluctuation amplitude, we acquired two 150 sec time series at 10 frames per second of phase-contrast video photomicrographs at different points along the chromosome as described in section 2.12. The resulting photographs were digitally analyzed to determine the chromosome fluctuations relative to the anchored end. Three of the resulting time series are shown in Figure 4.2. The top and middle panels show the relatively large fluctuations occurring near the free end and near the middle of the chromosome.

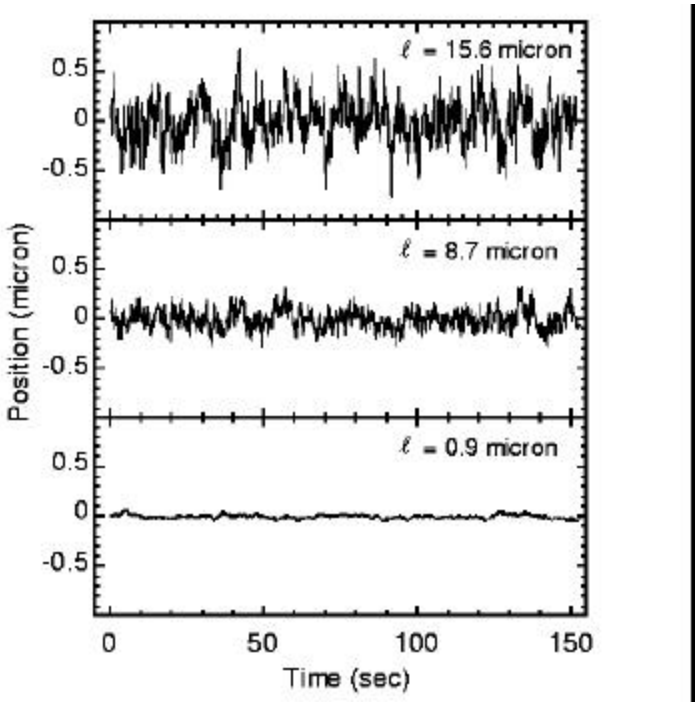

Figure 4.2 Thermal fluctuations at three positions along the chromosome shown in Figure 4.1. The fluctuation amplitudes increase with distance from the pipette. The fluctuations very near to the pipette are non-thermal in character, and give an estimate of mechanical noise.

The bottom time series in Figure 4.2 shows the relatively low-amplitude fluctuations 0.9 μm from the pipette. These fluctuations are different in character from the much 'noisier' ones further down the chromosome, and are non-thermal fluctuations of the pipette, i.e. mechanical noise. The slow and smooth variations are most likely slow drifts caused by lab temperature variations and air currents. Observation of this low fluctuation amplitude near the pipette is important since it indicates that we have reduced the level of mechanical noise to where it does not move the pipette relative to the rest of the microscope by more than ~ 0.01 microns, allowing thermal bending fluctuations to dominate. This low remnant mean-squared mechanical noise was subtracted from the other mean-square amplitudes.

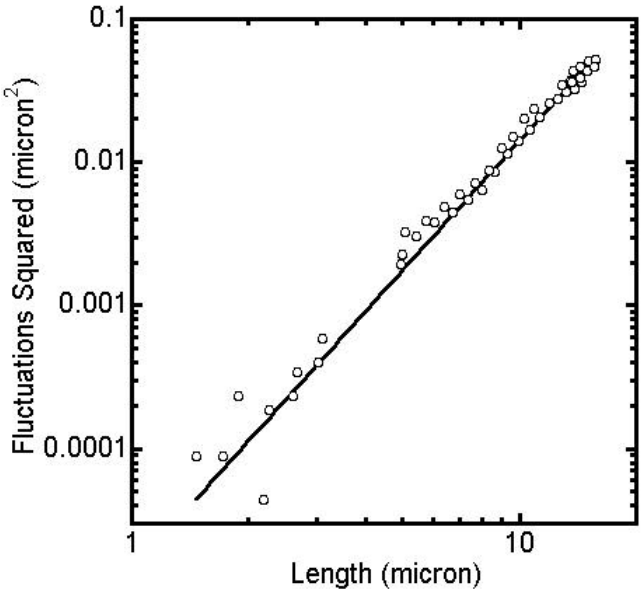

Figure 4.3. Mean-square fluctuations (μm^2) vs. position (μm) along the chromosome of Figure 4.1. This log-log plot shows the expected cubic dependence of mean-squared fluctuations on distance from the pipette (clamped end). The measured positions have an uncertainty of ± 0.1 μm and the measured mean-squared fluctuations have an uncertainty of ± 10%. The data are fitted to $\langle u^2 \rangle = Cx^3$, with $C = 1.4 \times 10^{-5}\ \mu m^{-1}$, giving a bending rigidity of 1×10^{-22} J·m.

The thermal fluctuation amplitudes as a function of position along the chromosome length are shown in Figure 4.3 on a log-log plot with a fit to the functional form $\langle u^2 \rangle = Cx^3$. The one fit parameter is C=1.8 x 10^{-5} μm^{-1}. Using Eq. (2.1) with k_BT = 4.1 x 10^{-21} J, we find a bending rigidity B of 1 x 10^{-22} J·m, resulting in a calculated Young's modulus Y_B = 500 Pa. Following the thermal fluctuation measurements, the characteristic force was measured via an extension experiment to be 1.0 nN, which converts to a Young modulus of 500 Pa. We repeated the thermal fluctuation measurements on three additional chromosomes, each time obtaining a bending rigidity $B \approx 10^{-22}$ J·m (Table I).

Table I

Elastic properties of mitotic chromosomes

Chromosome Type	Bending Rigidity, B (J·m)	Young's Modulus, Y (Pa)	Calculated Young's Modulus, Y_B (Pa)
Newt chromosome extracted	100×10^{-24}	500	500
Newt chromosome extracted	150×10^{-24}	400	500
Newt chromosome extracted	300×10^{-24}	1000	1500
Newt chromosome extracted	300×10^{-24}	300	900
Newt chromosome *In vivo*	20×10^{-24}	N.D.	130
Newt chromosome *In vivo*	20×10^{-24}	N.D.	110
Newt chromosome *In vivo*	30×10^{-24}	N.D.	90
Newt chromosome *In vivo*	50×10^{-24}	N.D.	160
Xenopus chromosome extracted	5×10^{-24}	300	200
Xenopus chromosome extracted	6×10^{-24}	N.D.	500
Xenopus chromosome extracted	10×10^{-24}	800	400
Xenopus chromosome extracted	20×10^{-24}	200	1300
Xenopus chromosome extracted	20×10^{-24}	400	2000
Xenopus chromatid extracted	5×10^{-24}	300	1500

N.D. indicates the experiment could not be done on that chromosome.

4.3 Bending Rigidity of Newt Chromosomes in Colchicine Arrested Cells.

The bending fluctuations for chromosomes extracted from cells show exactly the expected relationship between the mean-squared thermal fluctuations and distance from the anchor point. This provides a reliable measure of the bending rigidity of extracted chromosomes. However, the extracted chromosome has been moved from the *in vivo* environment to the cell culture buffer. This change in buffer may induce a change in chromosome structure and its physical properties. To check this, we measured chromosome fluctuations inside cells arrested in metaphase by colchicine in the manner similar to experiments carried out by Marshall *et al*, 2001. Colchicine treatment blocks polymerization of microtubules, eliminating the mitotic spindle. However, chromosome condensation is essentially unaffected. Thus we obtain mitotic chromosomes, while eliminating their large-amplitude mechanical bending by the mitotic spindle. Only small-amplitude thermal bending fluctuations remain.

Bending fluctuations of mitotic newt chromosomes inside metaphase arrested cells were measured for 4 separate chromosomes. Figure 4.4 shows the time series for one of these chromosomes. The time series for the other three chromosomes give the same result. We were concerned that the other chromosomes and the cell membrane would restrict bending fluctuations: to check this, we show a histogram of the bending amplitudes extracted from one of the time series (Figure 4.5, 25 bins). Unconstrained thermal bending fluctuations will have a Gaussian distribution according to Eq. 2.2. Alternately, if the fluctuations are constrained, the tails of this distribution should be suppressed, making the distribution more ‘square’.

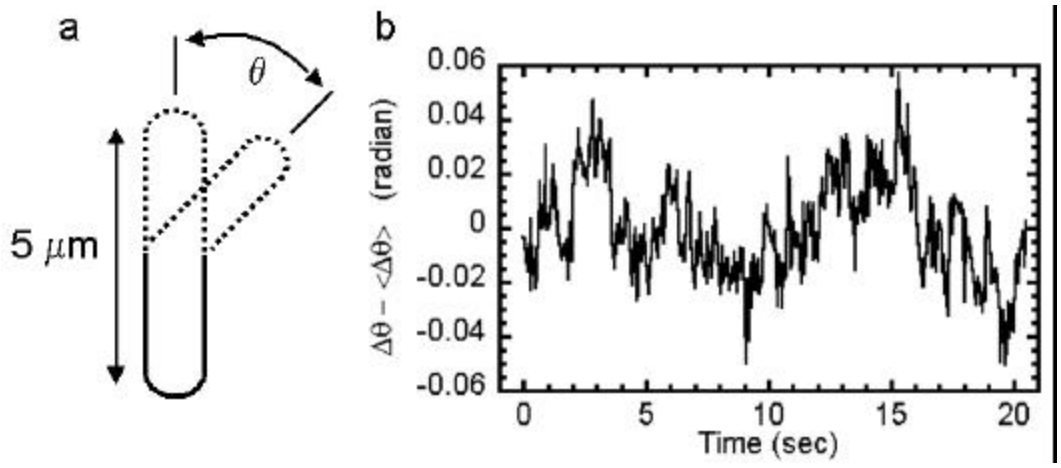

Figure 4.4 Angle fluctuations of an *in vivo* chromosome segment. (a) sketches how the change in angle is calculated for a segment of a mitotic chromosome. (b) is the change in angle (radians) vs. time for 5 μm chromosome segment in a colchicine arrested cells.

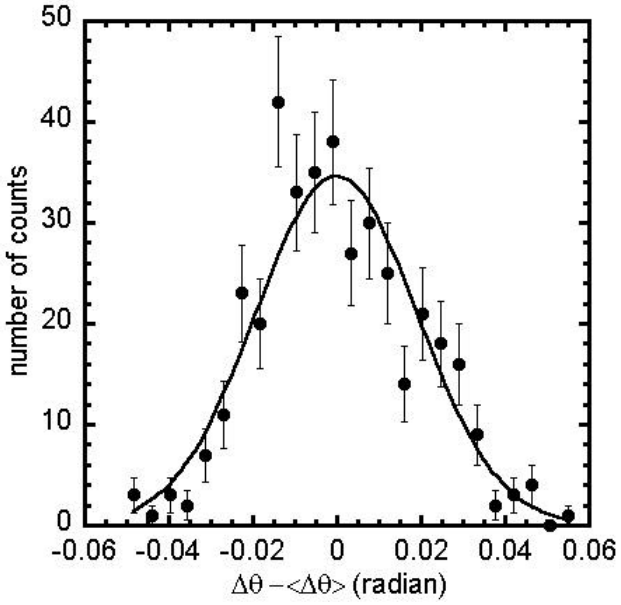

Figure 4.5 Histogram of the angle fluctuations $\Delta\theta$ with 25 bins between 0.05 and –0.05. A normalized gaussian distribution (Eq. 2) is used for the 1 parameter fit where $\langle \Delta\theta^2 \rangle$ = 3.7 x 10^{-4} radian^2. Using Eq. 2.3, we find $B = 5 \times 10^{-23}$ J·m.

We used Eq. 2.2 to fit the histogram with one parameter, $\langle \Delta q^2 \rangle$ = 3.7 x 10^{-4} radian^2. The tails of the histogram fit well to this distribution, indicating that the bending fluctuations are unconstrained. Eq. 2.3 is then used to calculate the bending rigidity, B = 5 x 10^{-23} J·m using the thermal energy, k_bT = 4.1 x 10^{-21} J and the length of the segment of chromosome analyzed, L=2.3 μm. The bending rigidities of the three other *in vivo* chromosomes are listed in Table 1.

This analysis assumes that all of the fluctuations measured are thermal, a hypothesis made reasonable by the expected shape of the fluctuation distribution (Figure 4.5), and the reasonable value of B thereby obtained. However, there are likely sources of mechanical agitation remaining which give additional contributions to the measured fluctuations. Slow changes in cell shape and the other chromosomes within the cells distort the image of the chromosome in focus causing the bending fluctuation to be over estimated. These additional fluctuations cause the measured bending rigidity to be less than its true value. Therefore, the in vivo results provide a lower limit on the actual bending rigidity. However, based on examination of the time series, we estimate that the true value of B in vivo is within a factor of 2 of our measured value.

4.4 Bending Rigidity of Extracted *Xenopus* A6 Chromosomes.

We also measured the bending rigidities for chromosomes removed from *Xenopus* cells. We used the same technique to measure the bending rigidity as with newt chromosomes by measuring thermal fluctuations along the length of the chromosome. The bending rigidity was measured for 5 chromosomes with values of 5x10^{-24} J·m, 6x10^{-24} J·m, 10x10^{-24} J·m, 20x10^{-24} J·m and 20x10^{-24} J·m.

4.5 Elastic Response and Bending Rigidity of an Extracted Xenopus Chromatid

Chromosomes extracted during metaphase are composed of two chromatids. A direct measurement of the bending rigidity of a single chromatid extracted from a cell in anaphase would test whether connections between the two chromatids in the single chromosome significantly contribute to the chromosome bending rigidity. We attempted this by extracting chromatids during anaphase. Although it is nearly impossible to isolate an individual chromatid, the group of chromatids, which could be repeatedly extracted, displayed submicron fluctuations, similar to the quantified fluctuations for newt and *Xenopus* chromosomes. In addition, one *Xenopus* chromatid was isolated, for which a Young's of 300 Pa and a bending rigidity of 5×10^{-24} J·m was measured, which is similar to the elastic constants found for *Xenopus* chromosomes.

4.6 Bending Rigidities of *In Vivo* and Extracted Chromosomes are Similar

The measurements of chromosome elastic properties of chromosomes inside and outside the cell have advantages and disadvantages that complement each other. Measurements inside the cell allow us to study the native *in vivo* structure. A problem with these measurements is that other components of the cell may add 'noise' to the supposed thermal fluctuation measurement. On the other hand, measurements on chromosomes extracted from a cell allow more precise measurements which are unaffected by the mechanical limitations of the *in vivo* experiments. Also, extracellular measurements are much more precise because the position of the chromosome is measured against an optically smooth background. However, the extracellular buffer may dramatically affect the chromosome's internal structure. An essential point of this chapter is that there is good agreement between bending rigidities measured by these two approaches, indicating that the effects of cell-generated forces in vivo, and the change to the extracellular buffer, are both small.

We find a bending rigidity between $3x10^{-22}$ and $1x10^{-22}$ J·m for chromosomes removed from cells. The bending rigidity of chromosomes in colchicine arrested cells was measured to be between $5x10^{-23}$ and $2x10^{-23}$ J·m. The bending rigidity for chromosomes removed from cells and in metaphase arrested cells are within an order of magnitude of each other, indicating that removing a chromosome from the cell and exposing it to cell culture buffer does not drastically alter the bending rigidity. Since the measurements in metaphase arrested cells provide a lower limit on of the bending rigidity, we conclude that our measurements on extracted chromosomes are relevant to chromosomes *in vivo.*

It is also possible that extracted chromosomes are up to 5 times stiffer than *in vivo* chromosomes. This is suggested by the experiments of Marshall, *et al*, 2001. They measured a bending rigidity of 6×10^{-25} J·m for *Drosophila* embryo chromosomes which gives Y_B = 40 Pa. This is about 10 times less than our measurements. However, Marshall, *et al* 2001 also point out that *Drosophila* embryo chromosomes may be less tightly compacted explaining this ten-fold difference. Therefore, we interpret our mechanical measurement of chromosomes removed from a cell as representative of the *in vivo* chromosome bending rigidity of $\sim 10^{22}$ J·m.

4.7 The Elastic Rod Model Predicts the Measured Bending Rigidity

The stretching and bending elastic constants can be used to extract information about the structures responsible for the elastic response. In general, rod-shaped biopolymers and biopolymer complexes have bending rigidities *B*, which are approximately related to their stretch modulus *Y* by the formula $B = \frac{p}{4} Y R^4$ where *R* is the cross-sectional radius of the rod (Landau and Lifshitz, 1986). For example, the radius, R=1 x 10^{-9}, and stretch modulus, $Y \approx 3 \times 10^8$ Pa (Smith *et al*., 1996), of dsDNA give a bending rigidity, *B* = 2.5 x 10^{-28} J·m, within 25% of the bending rigidity measured for dsDNA. Note that DNA bending rigidity is usually described in

terms of its persistence length, which is just $B/k_BT \approx 50$ nm (Hagerman 1988, Bustamante *et al.*, 1994).

A newt chromosome was measured to have a bending rigidity of $B = 1 \times 10^{-22}$ J·m, a force constant of $f_0 = 1.0$ nN and a radius of 0.75 μm. This gives a Young's modulus of $Y = 500$ Pa and a Young's modulus calculated from the bending rigidity of $Y_B = 500$ Pa, the same value. The three other newt chromosomes have similar calculated and measured bending rigidities (Table 1). Xenopus chromosomes also roughly obey the elastic rod relation between force constant and bending rigidity (Table 1). Therefore, chromosomes can be roughly thought of as solid, elastic rods.

4.8 Mitotic Chromosomes Are Not Hinged at the Kinetochore.

The kinetochore is the region of a mitotic chromosome that functions as the major point for microtubule attachment and is important for ensuring that the correct number of chromosomes are separated into each daughter cell (Nicklas, 1997). The structure around the kinetochore is different than the rest of the mitotic chromosome (Reider and Salmon, 1998). If there were large-scale structural differences, a different elastic behavior would be observed for this region of the chromosome. During anaphase, mitotic chromosomes are mostly bent at the kinetochore; suggesting the region around the kinetochore is very flexible and creates a hinge in the chromosomes (Figure 1.1). However, Figure 4.3 shows that the fluctuations along the length of the chromosome scale with a power law of nearly three, which is predicted for a homogeneous rod. A hinge in the chromosome would not fit to this power law of three. This shows that the kinetochore region of mitotic chromosomes does not have large-scale isotropies and does not create a hinge in the chromosome.

4.9 Chromosomes From Cells are Much Stiffer Than *Xenopus* Egg Extract Chromatids

Houchmandzadeh and Dimitrov (1999) measured the bending rigidity and the force constant of chromatids assembled *in vitro* using *Xenopus* egg extracts. The force constant of these chromosomes was measured to be $f_0 \approx 0.6$ nN and $Y = 1000$ Pa. This is similar to the force constant and Young's modulus for newt and *Xenopus* chromosomes. However, they measured $B = 1.2 \times 10^{-26}$ J·m giving a calculated Young's modulus of $Y_B = 0.4$ Pa, three orders of magnitude smaller than the Y_B found for newt and *Xenopus* chromosomes. This dramatic difference suggests there are important structural differences between chromosomes assembled in somatic cells and chromatids assembled in *Xenopus* egg extract. The differences must allow the egg extract chromatids to be much more easily bent than chromosomes in somatic cells, while giving the two systems similar force constants.

A possible explanation of the difference in bending rigidity is the *in vivo* chromosomes contain two tethered chromatids, while the egg extract chromosomes are single chromatids. Therefore, the egg extract chromatids lack interchromatid attachments, which could generate the increase in bending rigidity, through the coupling of chromosome bending to chromatid stretching. Candidates for the interchromatid attachments are protein complexes formed of cohesins. These have been found in different species, such as S. cerevisiae (Guacci *et al*., 1997) and *Xenopus* (Losada *et al*., 1998), and are required for maintaining connections between sister chromatids until anaphase (Michaelis *et al*., 1997). However, our estimates of the bending rigidity of individual chromatids, from observation of fluctuations of groups of isolated chromatids, and measurement of the bending rigidity of a chromatid extracted from an anaphase cell, indicate that this is not the case.

A second, more likely explanation is that the stiffness we observe is intrinsic to the *in vivo* chromatids, indicating that there must be inherent differences between them and chromatids assembled in the *Xenopus* egg extract. The chromosomes assembled from *Xenopus* egg extracts may represent an embryonic chromosome structure different from our somatic tissue culture cells. Also, the egg extract reaction does not undergo replication and thus, does not require resolution of two chromatids, which may be coupled to chromosome condensation (Hirano, 2000). This could result in a different chromosome structure, allowing it to be much more flexible. Another possibility is that the egg extract reaction may produce chromatids that are not completely condensed, with small but highly flexible regions along the chromatid length. If such uncondensed regions were small and closely spaced, they would be unobservable in the light microscope except through the flexibility they would impart to the chromatids.

A further experiment could help address the above explanations. Two-chromatid chromosomes can be produced *in vitro*, by the use of 'mitotic' or 'cycling' extracts which actually carry out nuclear assembly, DNA replication, and then chromosome condensation (Smythe and Newport, 1991). A measurement of the bending rigidity of such chromosomes would be extremely interesting. However, preliminary results communicated to us by E. Salmon show large bending fluctuations of chromosomes in cycled extracts, relative to those observed during mitosis in Xenopus cells. This suggests that in vitro chromosomes are anomalously flexible even after one cell cycle.

4.10 Conclusions

The bending rigidity for newt and *Xenopus* mitotic chromosomes was measured both *in vivo* and after extraction into cell culture buffer. The bending rigidities of extracted and *in vivo* chromosomes are consistent indicating that extracting chromosomes into the cell culture buffer

does not significantly alter *in vivo* chromosome structure. Therefore, extracted chromosomes are representative of their *in vivo* structure. The bending rigidity of newt chromosomes are found to be ~10^{-22} J·m and for *Xenopus* chromosomes to be ~10^{-23} J·m. These values are consistent with the elastic rod model, $B \gg YR^4$, given the measured radius and Young's modulus of each type of chromosome. This indicates mitotic chromosomes can be thought of as being made of roughly isotropic elastic media and also that the use of this idea to estimate mechanical properties within cells is reasonable.

CHAPTER 5

MITOTIC CHROMOSOME INTERNAL VISCOSITY

5.1 Introduction

This chapter presents the characterization of the dynamics of stress relaxation in mitotic chromosomes. Initially, step- strain experiments were done to determine the strain rate necessary for the extension-retraction experiments discussed in Chapter 3 to be quasi-static. We find that mitotic chromosomes reversibly relax in a characteristic time of ~2 seconds for quick extensions of < 3x. This implies that a strain rate < 0.1 sec^{-1} should be used to ensure that the chromosome is in equilibrium during extension-retraction experiments. Interestingly, this time scale is orders of magnitude larger than what is expected for viscous drag dominated stress relaxation. To explain the relaxation time scale by viscous drag, a chromosome with length $L=10^{-5}$ m and a relaxation time τ = 1 sec, which is attached to a pipette with a force constant k = 1 nN/micron requires the surrounding fluid to have a viscosity $\eta = k \cdot \tau / L$ = 100 kg/m·sec. Therefore, viscous drag on the chromosome does not play a role in the measured relaxation time. Instead, this viscosity is due to internal dissipation, which we can characterize with an internal viscosity $\eta_i \approx$ 100 kg/m·sec.

We carried out experiments to study this long relaxation time. Experimentally we find that both the stress transfers along the chromosome length and its width equilibrates in < 0.05 seconds. This shows that stress propagation down the length of the chromosome or flow of the surrounding fluid into the chromosome as it is elongates are not responsible for the observed response time. Instead, the relaxation time is consistent with the dynamics of polymers tethered to and threaded through a polymer network (de Gennes, 1975) with 0.5 micron loops of chromatin, which contain about 80 kb of DNA.

The large internal viscosity observed for uniaxial extensions should also play a role in the dynamics of bending deformations, since a bend is simply a uniaxial deformation inhomogeneously distributed along the cross-section of the chromosome, as discussed in section 1.5. In chapter 4, the bending rigidity of mitotic chromosomes was measured by observing the mean-squared thermal shape fluctuations. A large internal viscosity will not affect this equilibrium measurement as long as the time series are at least a few time correlations long. However, the magnitude or scaling behavior of the time correlations may point to a large internal viscosity. To understand how the internal viscosity affects the thermal fluctuation correlation time, a theory is presented to describe the dynamics of chromosome thermal fluctuations with an additional internal viscous term in the usual Langevin equation for bending fluctuations (Doi and Edwards, 1988). We find that internal dissipation dominates over hydrodynamic friction for wavenumbers $q > (\kappa/\kappa_i)^{1/4}/r$, where ζ is the viscosity of the surrounding solution, and the relaxation time of bending modes is independent of q in this wavenumber regime. This is in opposition to the usual result $\tau \sim 1/q^4$ obtained from external hydrodynamic damping of filament bending modes (Harnau and Reineker, 1999). Mitotic chromosomes are expected to show this q independent result for $q > 0.05\ \mu m^{-1}$ or with a length, $L < 100$ microns, which is always the case for newt mitotic chromosomes. We find that mitotic chromosomes display this q independent result and that internal dissipation is so large that the external hydrodynamic damping usually considered in theories of filament dynamics is immaterial.

This internal viscosity term may also be important for other biofilaments, e.g. double-stranded dsDNA (Marko and Siggia, 1995), actin (Gittes *et al*, 1993), intermediate and other protein filaments (Hohenadl *et al*, 1999), composite fibers such as dsDNA coated with RecA protein (Hegner *et al*, 1999), or semiflexible virus particles (Schmidt *et al*, 2000). These

biofilaments are all rather stiff, with thermal persistence lengths of roughly a micron, and rather thick, with cross-sectional diameters larger than a few nanometers. They also have many internal conformational degrees of freedom, and are relatively soft (< GPa elastic moduli). An estimate for actin indicates it may display this q independent relaxation for bending mode wavelengths > 100 nm.

5.2 Step-Strain Experiments

To quantify the stress relaxation, we performed dynamical experiments (Figure 5.1), as described in section 2.14. An isolated chromosome suspended between two micropipettes was rapidly stretched by stepping one pipette (v=100 μm/sec) by 5 to 100 microns, while deflection of the other pipette was used to measure the dynamical force response (section 2.16). Using Labview and IMAQ software (National Instruments), digitized video frames were acquired at 20 frames/sec. Step-relaxation cycles were done to 1.4, 1.7, 2, 2.4, 2.7, 3, 3.4, 3.7, 4, 4.4, 5.1, 5.8, 6.5, 7.2 and 7.9 times chromosome initial length. Two stretch-release cycles were done for each of these final lengths. We focus mainly on results of one experiment; the same results were obtained from 3 separate runs on chromosomes from different cells.

5.3 Dynamic Response for Extensions <3x

Figure 5.1 shows the dynamical response of a chromosome stretched to various lengths. The force-measuring pipette shows an initial force jump, followed by a decay to a smaller final force. The force decays in Figure 5.1 were extracted and normalized so they each decay from 1 to 0 (Figure 5.2). These decays have three important features. First, an initial decay of ~0.5 sec is observed for each elongation (note elongation refers to total length divided by initial length). Second, for an elongation less than 3 times initial length (3x), the initial decay is followed by an exponential decay with a decay time ~2 sec. Third, after being rescaled in force, the decays after

extensions of < 3x are the same (note that the thin black and thin dark gray lines show different extensions in Figure 5.2). This superposition and final exponential decay is characteristic of linear elastic response.

The viscous relaxation time of a chromosome of length ℓ_o~10 μm attached to the pipette with spring constant k~1 nN/μm with effective viscosity η' is $\tau \sim \eta'\ell_o/k$. This implies an effective viscosity η'~100 kg/(m sec), about 10^5 times that of water. Thus, the relaxation dynamics are unrelated to viscous flow of the buffer past the chromosome.

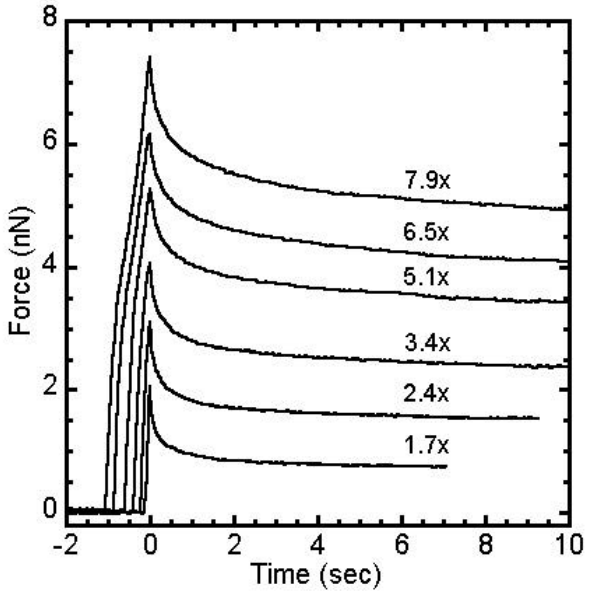

Figure 5.1 Dynamics of force relaxation for a mitotic chromosome following step strains to lengths of 1.7, 2.4, 3.4, 5.1, 6.5 and 7.9 times initial length. The length change is listed just below the corresponding time series. Initial force jumps are followed by force decays to a final force. For the longer extensions, only part of the decay curves is shown.

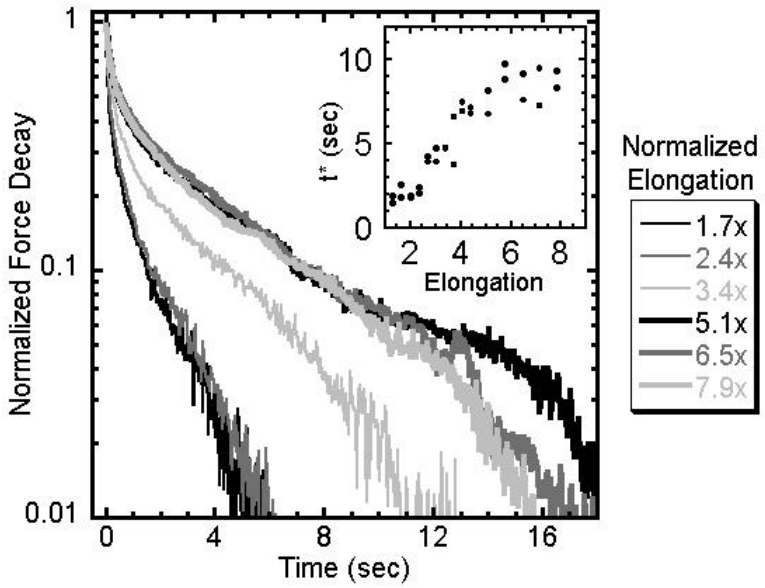

Figure 5.2 The normalized force decays, $\frac{force - final\ force}{inital\ force\ after\ step - final\ force}$, from Figure 5.1 are plotted so that the stress decays from 1 to 0. The plots correspond to the extension shown in Figure 5.1 of 1.7 (thin black), 2.4 (thin dark gray), 3.4 (thin light gray), 5.1 (thick black), 6.5 (thick dark gray) and 7.9 (think light gray). The decays all follow roughly the same behavior to 50% of the transient force has relaxed. This is followed by a slower decay, which increases for extensions beyond 3x.

Inset: The time in which 90% of the transient force has decayed, t*, versus elongation (length in units of the initial length). The low-extension curves in the reversible regime show a final exponential decay with a lifetime comparable to t*. The higher-extension results show a non-exponential final decay.

5.4 Dynamic Response for Extensions >3x

For jumps to >3x, the duration of the characteristic decay time gradually increases (Figure 5.2, inset). A permanent increase in the relaxed chromosome length following release of applied stress coincides with this increase in the decay time (data not shown), indicating that irreversible damage occurs during jumps to >3x initial length. This is consistent with quasi-static elongations beyond 3x being irreversible (Poirier *et al*, 2000, chapter 3). In the irreversible

regime, the terminal force relaxation no longer fits an exponential (Figure 5.2). For the longer steps to >6x initial length, force ~ constant – ln(time) describes the entire decay range.

5.5 Step-Strain are Reversible for Extensions < 3x

Following each step we determined the final force versus extension after the decays (Figure 5.3, points). The resulting force-extension behavior is linear to 3x initial length with a slope of 1 nN/um, in accord with previous results for chromosome elasticity (Houchmandzadeh *et al*, 1997, Houchmandzadeh and Dimitrov, 1999, Poirier *et al*, 2000).

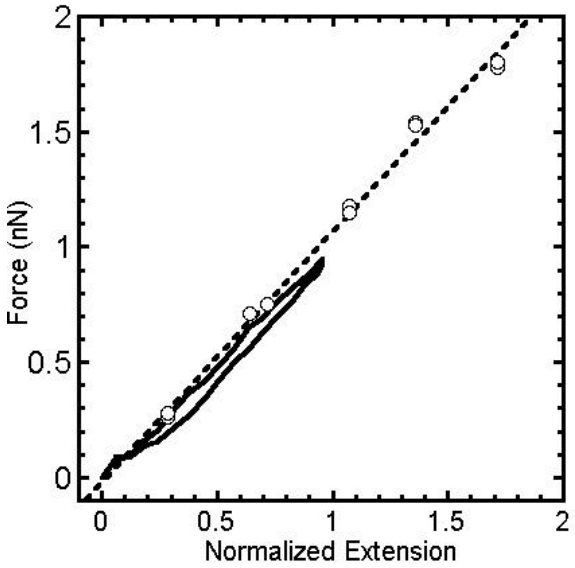

Figure 5.3 Force (nN) vs. extension (change in length in units of initial length) derived from the final extensions observed following the step strains (points), which have a linear fit of y = 1.1x (dashed line). Before the step strain experiments a quasi-static extension-retraction experiment was done on the same chromosome (solid curve). There is excellent agreement between the two force-extension results, showing that up to 2x extensions, the chromosome reaches its equilibrium elongation in the step-strain experiments

The force-extension curve derived from the step experiments matches the result of a quasi-static force-extension measurement done just before the dynamic experiments (Figure 5.3, solid curve). This shows that quick extensions are reversible for extensions of less than three times the chromosome relaxed length.

5.6 The Force Transfer Along the Length of the Chromosome

One explanation for the relaxation time scale of 2 seconds might be a slow force equilibration over the length of the chromosome. However, the stationary pipette responds within 0.05 seconds to the step of the other pipette, and the decays of both pipettes overlap, following the step extension (Figure 5.4).

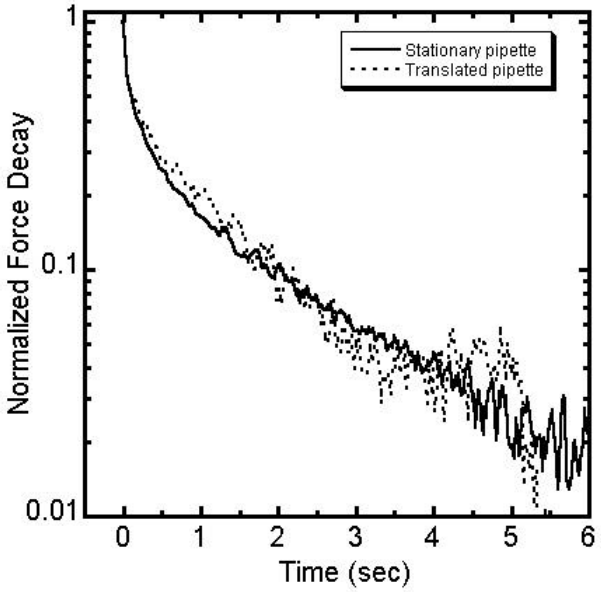

Figure 5.4 The force relaxation of both pipettes during a stress-strain experiment. The dashed line the force response of the pipette, which was stepped at 100 ìm/sec. The solid line is the force response of the stationary pipette. The pipettes show the same response within our resolution of 0.05 sec. There is no delay in the force response of the stationary pipette. This shows that there is force balance and the decay time is not due to the time the force takes to propagate along the length of the chromosome.

Therefore, stress is supported uniformly throughout the chromosome throughout the decay. This rules out the time for stress to transfer along the chromosome length as the reason for the 2 sec decay time.

5.7 Chromosome Width Equilibration

Another explanation for the scale of the relaxation time in the reversible, linear relaxation regime (< 3x final length) is the squeezing of fluid through interstices between chromatin fibers, as would occur in a gel following a step-strain (Geissler and Hecht, 1981). Such flow certainly occurs because chromosomes remain nearly the same diameter even when doubled in length: the Poisson ratio of a mitotic chromosome is ~0.1 (Poirier *et al*, 2000). Chromosomes thus appreciably increase in volume when stretched, requiring an inflow of fluid.

In separate experiments we simultaneously measured chromosome width and force relaxation. Chromosome width reaches its final value within 0.05 sec of being stretched (Figure 5.5). This is during the early stages of the force relaxation, so all bulk flow into the outer region of the chromosome is finished well before the transient stress has decayed. This eliminates the time for the surrounding solution to flow into the chromosome as the source of the 2 second time decay.

By estimating the time required for the solution to flow into the middle of the chromosome, a lower limit can be placed on the pore size, d, of mitotic chromosomes. As discussed in section 1.5, the Reynolds number, $\mathbf{R} << 1$, so the inertial terms of the Navier-Stokes equation can be ignored. There is a balance between the viscous term and the pressure term, $\eta\nabla^2 v = \nabla P$, as the surrounding solution fills the chromosome. The typical velocity of the solution as it fills the chromosome is the radius of the chromosome, R, divided by the width equilibration time, τ. Similar to Poiseuille flow, the change in the velocity occurs over the length

of the pore size, d. The pressure is set by the stretching modulus of 300 Pa and changes over the radius of the chromosome. Therefore, the pore size is $d = \sqrt{\frac{\eta R^2}{Y\tau}}$. Since $\eta \approx 10^{-3}$ kg/m·sec, $R \approx 1\times10^{-6}$ m, $Y \approx 3\times10^{2}$ Pa and $\tau<0.1$ sec, d is greater than 50 nm. This lower limit is reasonable since the pore size should be at least as large as 30 nm, the chromatin fiber diameter.

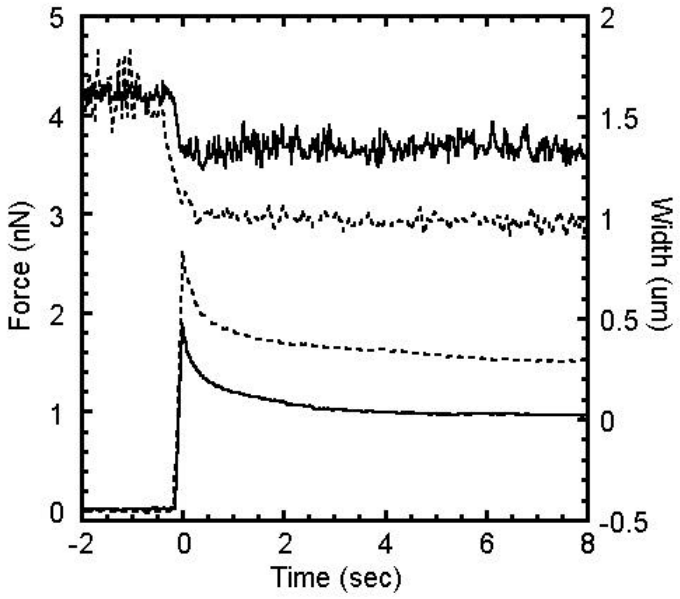

Figure 5.5 Comparison of force (lower curves) and width relaxation (upper curves) for a mitotic chromosome following a step strain to 1.8 (solid) and 2.2 (dashed) times native length. Force and width were simultaneously measured at a ~20 Hz rate by analysis of digitized video images. Due to inhomogeneities in chromosome width, the width was averaged over 1 micron lengths for which it is constant. One width section for each extension is shown; each width section equilibrated in less than 0.05 seconds. The width and therefore chromosome volume is seen to equilibrate on a timescale short compared to the force. This indicates that the force relaxation is not due to the hydrodynamics of liquid being squeezed out of the chromosome by the applied stress, and is therefore due to reorganization of the chromosome fibers themselves. A movie of this experiment is available on-line at
http://safarsquid.phy.uic.edu/~mpoirier/experiments/relax.mpg

5.8 Chromosome Dynamics is due to Small-Scale Internal Reorganization

Having ruled out inhomogeneous relaxation and solvent flow, the observed slow stress relaxation for an elongation <3x must be due to reorganization of chromosome structure at scales much smaller than the chromosome length. We see two possibilities: first, we may be breaking crosslinks (bonds) between chromosome fibers (Fig 5.6d). However, a crosslink-breaking picture suggests that there should be either irreversibility for small < 2x strains, or a slow 'healing' process following each stretch-release cycle, as the crosslinks find their partners and relink. Instead of this, we find that chromosomes return to their native lengths immediately as stress is removed.

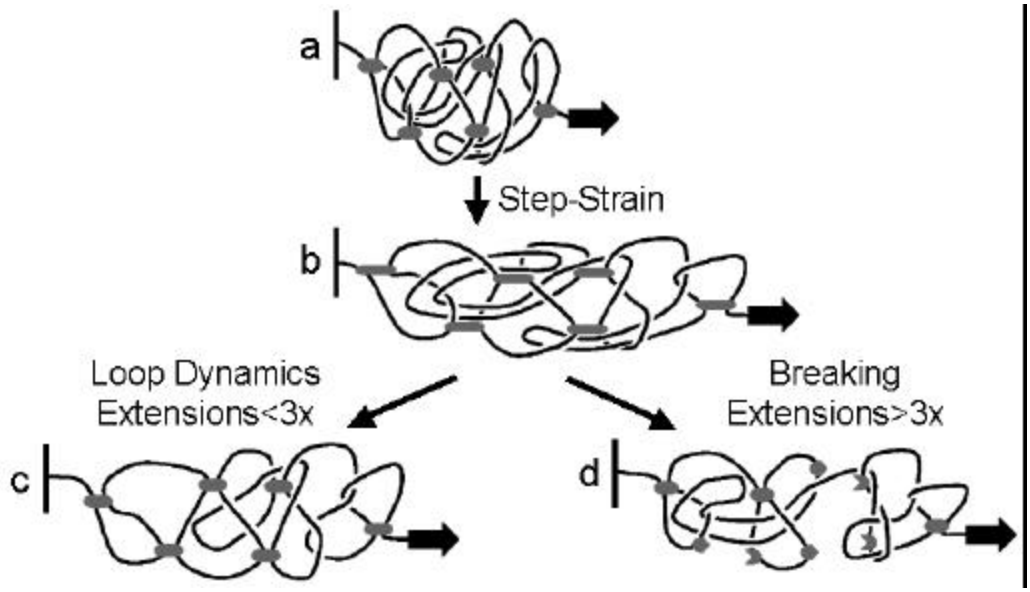

Figure 5.6 Models of stress relaxation inside a mitotic chromosome. A chromosome consists of a long (10 cm for TVI cells) chromatin fiber, tethered to itself to form a compact mitotic chromatid (a). To form such a structure, there must be 'loop domains' which will be entangled with the surrounding chromatin. Immediately following a step strain, the network and any loop domains entangled with it will both be stretched (b). Stress relaxation can then take place either by the reorganization of loop domains (c), or by the breaking of network crosslinks (d). Our data suggests that crosslink breaking occurs only for step strains beyond 3x elongation, which leads to irreversible chromosome stretching. Loop-domain reorganization is left as the main possibility for the slow relaxation we observe for step strains to less than 3x elongation.

A second and more plausible explanation for the stress relaxation is based on entanglement dynamics. Any scheme of chromosome folding must include two features: each half of a mitotic chromosome is made of a single, long (few cm in our case) chromatin fiber; and those fibers must be somehow be attached to themselves to keep the chromosome compacted. This implies the existence of 'ends' or 'loop domains' (Figure 5.6a), which have been observed in a number of ways (Paulson and Laemmli, 1977, Earnshaw and Laemmli, 1983). Such loops will behave as polymers tethered inside a polymer network. Following a step strain, they will be affinely stretched, contributing a large transient stress (Figure 5.6b). This stress will then relax as the extended loops pull out of the chromosome region in which they were originally embedded (Figure 5.6c). Following stress release, the loop domains will re-embed themselves into the relaxed chromosome by conformational diffusion.

5.9 Time-Scale Estimate of Chromatin Loop Dynamics

We can estimate the time-scale for this process by considering one loop, which initially will be in a random-walk-like conformation. A step strain of the chromosome will affinely deform the loop as well as the surrounding network in which it is embedded. Some of the stress contributed by the deformed loops can relax if they can regain a random-coil conformation. However, a loop can only do this by the torturous process of transfer of its entire length through the network 'pore' near its base (Figure 5.6d). In the small-deformation regime this process requires the loop end to diffuse along the path defined by its initial conformation (de Gennes, 1975). This process requires a time of roughly $\tau_0 e^{\alpha N}$ for a loop which is N segments long, where τ_0 is a chromatin persistence-length relaxation time of roughly 1 μsec, and where α is an order-unity constant. Assuming the relevant fiber is chromatin, we can estimate N from previous studies. Electron micrograph studies of histone depleted metaphase chromosomes found loop

domains of about 80 kb of DNA (Paulson and Laemmli, 1997, Earnshaw and Laemmli, 1983). The length of chromatin fiber containing 80 kb is at least 0.5 μm since DNA is compacted into chromatin by up to 50 times (van Holde, 1989). A length of 0.5 μm has about 15 segments, since chromatin has a persistence length of ~ 30 nm (Cui and Bustamante, 2000). Therefore, τ is on the order of seconds, which is consistent with the measured decay time.

We can understand why the decay is initially fast and then slows down to a final exponential decay in terms of this model, since part of the transient force can be relaxed quickly by partial changes of loop conformations (e.g. extension of only slightly constrained chromain segments). However, for all of the transient force to relax, topological barriers must be crossed, requiring a wide range of conformations to be explored, giving a slow final decay.

At even higher strains, some loops or crosslinks will break, leading to the irreversibility observed for steps of >3x initial length (Figure 5.6d). The log-time dependence of the force decays that was mentioned in section 5.4 for step-strains >6x can be understood in term of this model. There should be a broad range of free energy barriers to break chromatin connectors, which are crossed thermally as failure occurs. Each energy barrier, ε, should relax at the time $t = t_0\exp(\varepsilon/k_BT)$, implying the energy barriers crossed in time t are the barriers less than $\varepsilon = k_BT \ln(t/t_0)$. Assuming a flat distribution of energy barriers between the minimum energy barrier, ε_{min}, and the maximum energy barrier, ε_{max}, the fraction of broken connectors is $\frac{k_BT\ln(t/t_0)-\varepsilon_{\min}}{\varepsilon_{\max}-\varepsilon_{\min}}$. Each broken connector provides some additional length, and therefore the normalized change in length is the fraction of broken connectors. Thus, $\frac{\Delta L}{\Delta L_{final}} = \frac{k_BT\ln(t/t_0)-\varepsilon_{\min}}{\varepsilon_{\max}-\varepsilon_{\min}}$, where ΔL is the change in length of the chromosome following the step-strain and ΔL_{final} is the final change in

length. We can write down the force change, Δf, since it is related to the change in length by the force constant, so $\frac{\Delta f}{\Delta f_{final}} = \left(\frac{\varepsilon_{\min} - k_B T \ln(t/t_0)}{\varepsilon_{\max} - \varepsilon_{\min}} \right)$, where Δf is the total change in force, and is the form of the force decays for step-strains >6x.

5.10 Theory of Biofilament Bending Dynamics with Internal Viscosity

We have found that the dynamics of mitotic chromosome linear deformations indicate an internal viscosity η_i = 100 kg/m·sec. The internal viscosity will affect bending dynamics, since bending is simply stretching inhomogeneously across the chromosome cross-section. As discussed in chapter 4, the energy of a stiff filament of length L slightly bent from its straight equilibrium configuration is just the integral of its curvature-squared. The energy, to harmonic order in the transverse displacements as a function of contour length u(s), is (Landau and Lifshitz, 1986)

$$E = \frac{B}{2} \int_0^L ds \left(\frac{d^2 \mathbf{u}}{ds^2} \right)^2 = \frac{B}{2L} \sum_q q^4 \left| \mathbf{u}_q \right|^2 . \qquad (5.1)$$

For a filament with uniform and circular cross-section, the bending rigidity B is related to the Young modulus Y and filament cross-section radius r through $B = (\pi/4) Y r^4$. The final part of (5.1) is in terms of a complete set of orthonormal modes. For an infinite rod, where boundary conditions are unimportant, we can use the Fourier modes, $\mathbf{u}_q = \int ds\, e^{-iqs} \mathbf{u}(s)$. For finite-length rods, a different set of normal modes must be used (Rayliegh, 1945). The correct set of modes for a rod clamped at one and free at the other are described in Appendix A. However, the following discussion does not change for different sets of modes as long as they are orthogonal and complete. The thermal equilibrium amplitudes are

$$\left\langle u_q^a u_q^b \right\rangle = \frac{k_B T L}{B q^4} \delta^{ab}, \qquad (5.2)$$

where α and β =1,2 refer to the two components of u, which are discussed in more detail in Appendix A. Long filaments have random-walk conformations which will not consider; we will focus on the small-amplitude fluctuations occurring over filament segments L which are shorter than the persistence length, B/k_BT.

The dynamics of thermally excited bending modes is usually described with the Langevin equation, $B\frac{\partial^4 u}{\partial s^4} + \eta \frac{\partial u}{\partial t} = n(s,t)$ (Doi and Edwards, 1988). The first term accounts for the elastic restoring force from the energy of (5.1). The second term is the usual hydrodynamic drag force associated with motion of the filament cross-section through the surrounding fluid of viscosity ζ (geometrical factors and a weak correction from the nonlocal dependence of the hydrodynamic drag on motion of distant parts of the filament are straightforward to include, see Ref. (Harnau and Reineker, 1999)). The final n term is the random thermal noise with delta-function time correlations and wavenumber correlations that will be set to recover the equilibrium fluctuations (5.2). This gives the usual dynamical theory of filament fluctuations (Harnau and Reineker, 1999), with a relaxation time of $\tau_q \approx \zeta/Bq^4$ for the bending mode of wavenumber q.

A new ζ' term, proposed to include internal energy dissipation, changes this Langevin equation to

$$B\frac{\partial^4 u}{\partial s^4} + \eta \frac{\partial u}{\partial t} + \frac{\pi}{4}\eta' r^4 \frac{\partial}{\partial t}\frac{\partial^4 u}{\partial s^4} = n(s,t). \qquad (5.3)$$

The overall coefficient of this term $\zeta' r^4$ has the dimensions of viscosity×length^4, and thus ζ' is a parameter with viscosity dimensions. To see how the ζ' term arises, consider the free viscous relaxation of an initially stretched elastic rod, ignoring external hydrodynamic friction and

inertial terms. The extension strain $\Delta L/L = \varepsilon$ of the rod relaxes according to $\eta' \frac{\partial \varepsilon}{\partial t} + Y\varepsilon = 0$, as discussed in section 1.5, where ζ describes the internal friction which opposes instantaneous relaxation, and where Y is the Young modulus which drives the relaxation. This internal relaxation, ζ', is the same quantity discussed earlier in this chapter, which is about 100 kg/m·sec for mitotic chromosomes. The relaxation time ζ/Y is determined by balance of elastic and frictional forces. The rate of energy dissipation in a volume V of the rod is $(\partial E/\partial t)_{\text{friction}} = -V\zeta(\partial\varepsilon/\partial t)^2$.

Bending of this rod with local curvature κ generates stretching which is inhomogeneous across the rod cross-section, with extension towards the outside edge and compression towards the inside edge (Figure 5.7a). The average of the strain-squared across the rod cross-section is just $\langle \varepsilon^2 \rangle_{\text{cross-section}} = \kappa^2 r^2/4$. This identification is familiar from the connection between the usual elastic bending energy of a rod and the integral of its stretching free energy:

$$E_{bending} = \frac{B}{2}\int_0^L ds\kappa^2 = \frac{\pi Y r^2}{2}\int_0^L ds\left\langle \varepsilon^2 \right\rangle_{cross-section} \qquad (5.4)$$

The same identification allows us to write the rate of energy dissipation associated with the internal friction ζ:

$$\left(\frac{\partial E}{\partial t}\right)_{friction} = -\frac{\pi}{8}\eta' r^4 \int_0^L ds\left(\frac{\partial \kappa}{\partial t}\right)^2 \qquad (5.5)$$

Thus the rate of energy dissipation is proportional to the square of the time rate of change of local curvature. The energy dissipation rate can be used to find the equation of motion (5.3), following the Lagrangian formulation of frictional forces (Landau and Lifshitz, 1976).

A simple mechanical model can give an alternate justification of the energy dissipation rate (5.5), and therefore of the equation of motion (5.3). Consider a filament of cross-sectional

radius r, the exterior of which is a flexible cylindrical envelope filled with a highly viscous liquid medium of viscosity ζ. Running down the center of the tube is a backbone with static bending rigidity B (Figure 5.7b). If the time rate of change of curvature is $d\kappa/dt$, than flow of the liquid from the inside edge to the outside edge must occur. Near the middle of the rod, the velocity of this radial flow will be $v \approx r^2 d\kappa/dt$ (relative to the backbone), while at the edges of the rod, the fluid velocity must be zero. Therefore the velocity gradient in the liquid will be $r d\kappa/dt$, and the time rate of energy dissipation per length of rod will be $\approx \zeta r^4 (d\kappa/dt)^2$, essentially (5.5).

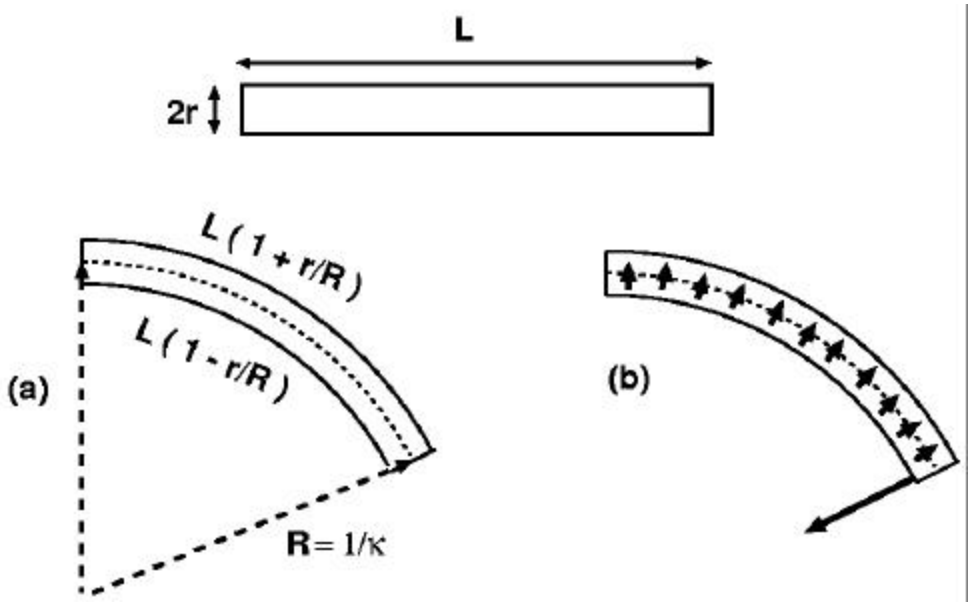

Figure 5.7
(a) The outer half of a bent rod is stretched, and the inner half is compressed. The magnitude of the strain at the rod edges in the bending plane is $|e| \approx \kappa r$, where κ is the rod curvature.
(b) Mechanical model for origin of internal viscosity of a biofilament: an elastic backbone is surrounded by a shell of liquid of large viscosity ζ. Changing the curvature by $d\kappa$ over time dt drives internal flow from the inner edge to the outer edge of the filament, with velocity gradients $\partial v/\partial r \approx r\, d\kappa/dt$. The energy dissipation rate per length of filament is therefore of order $\zeta r^4 (d\kappa/dt)^2$.

The above arguments amount to description of a biofilament as a thin piece of viscoelastic solid. One way to obtain a large $\zeta\!\!\!^{\cent}$ (relevant to the chromosomes of this thesis) is to have slow structural fluctuations, e.g. reptation of entangled polymers, or conformational changes which cross large energy barriers. A second way to obtain a large $\zeta\!\!\!^{\cent}$, which is relevant to filaments with gel-like internal structure, is the large dissipation associated with the flow of the surrounding fluid of viscosity ζ through narrow pores. For pores of diameter δ extending across the cross-section of a filament, the energy dissipation rate per length is $\approx \zeta(r^6/\delta^2)(\mathrm{d}\kappa/\mathrm{d}t)^2$. This reduces to (5.5), with an effective internal viscosity $\zeta\!\!\!^{\cent} \approx \zeta r^2/\delta^2$, which was previously discussed in section 5.7. For a filament of gel whose radius r is large compared to the diameter of the gel pores, the effective internal viscosity $\zeta\!\!\!^{\cent}$ can greatly exceed the viscosity ζ of the fluid, which surrounds and fills the filament.

After transformation with respect to contour length and time, the equation of motion (5.3) becomes

$$\left(Bq^4 + i\eta\omega + i\frac{\pi}{4}\eta' r^4 q^4 \omega \right) u_{q\omega} = n_{q\omega}, \qquad (5.6)$$

leading to the correlation function

$$\left\langle \left| u_{q\omega} \right|^2 \right\rangle = \frac{\left\langle \left| n_{q\omega} \right|^2 \right\rangle}{B^2 q^8 + \left(\eta + \frac{\pi}{4}\eta' r^4 q^4 \right)^2 \omega^2} \qquad (5.7)$$

Choosing delta-function time correlations for n(s,t) means that $\langle |n_{q\omega}|^2 \rangle$ is a function of q only. Transforming (5.7) back to equal times must recover (5.2), which fixes the noise correlation to be

$$\left\langle n^a_{q\omega} n^{b*}_{q\omega'} \right\rangle = 2\left(\eta + \frac{\pi}{4}\eta' r^4 q^4 \right) k_B T L \delta^{ab}\, 2\pi\delta(\omega + \omega') \qquad (5.8)$$

Therefore the correlation function is

$$\left\langle u^{a}_{qw} u^{b}_{qw'} \right\rangle = \frac{2k_B TL\left(\eta + \frac{p}{4}\eta' r^4 q^4\right)}{B^2 q^8 + \omega^2\left(\eta + \frac{p}{4}\eta' r^4 q^4\right)^2} \delta^{ab}\, 2\pi\delta(\omega + \omega') \qquad (5.9)$$

The relaxation times of the bending modes are therefore:

$$\tau_q = \frac{\eta + \frac{p}{4}\eta' r^4 q^4}{Bq^4} \qquad (5.10)$$

There are two wavenumber regimes, separated by a characteristic wavenumber $q^* = \left(\frac{4\eta}{p\eta'}\right)^{1/4} r^{-1}$. For long wavelengths, or $q << q^*$, the decay times are those of a stiff polymer damped by external hydrodynamic friction, $\langle |u_{q\omega}|^2 \rangle \propto 1/(B^2 q^8 + \zeta\omega^2)$, with mode relaxation times $\tau_q = \zeta/(Bq^4)$. In the opposite small-wavelength limit, $q >> q^*$, internal dissipation dominates and the correlator is $\langle |u_{q\omega}|^2 \rangle \propto q^{-4}[\omega^2 + 16B^2/(p\zeta\zeta' r^4)^2]^{-1}$. In this limit, the relaxation time is *wavenumber independent*, $\tau_q = p\zeta\zeta' r^4/4B$.

5.11 Mitotic Chromosome Bending Dynamics

The thermal fluctuations of single mitotic chromosomes used to measure the bending rigidity in chapter 4 show this wavenumber-independence for the bending relaxation time. In chapter 3 it was established that Y=300 Pa (Poirier *et al*, 2000), and earlier in this chapter it was shown that $\zeta' \approx 100$ kg/(m·sec) (Poirier *et al*, 2001). Since $\zeta'/\zeta \approx 10^5$, bending relaxation times should be constant for modes with wavelengths up to $2\pi(p\zeta\zeta'/4\zeta)^{1/4} r \approx 100$ microns. Since this is longer than the chromosomes themselves, we expect all bending modes to relax with the same lifetime $\approx \zeta'/Y \approx 0.3$ sec. The observed fluctuations, discussed in Chapter 4 and Appendix A (see Eq. A.9), are mainly due to thermal excitation of the smallest-wavenumber bending mode for a

rod clamped at one end and free at the other. This wavenumber is $q = 1.875/L \approx \delta/2L$ (Rayleigh, 1894 and Gittes *et al*, 1993), so the strategy is to study modes of different q using different-length chromosomes.

Three experiments on chromosomes were done with tip-to-pipette lengths of 7, 16.5 and 18.5 microns. The fluctuations of the chromosome of length L=18.5 microns were recorded at positions between chromosome tip and pipette are shown in Figure 5.8a. Figure 5.8b shows time series for amplitude $u(s)$ at a few points along this chromosome. The amplitudes are very small near the pipette, but grow rapidly as one moves toward the free end. Circles in Figure 5.9, inset show that the amplitude-squared follows the equilibrium law $\langle u(s)^2 \rangle \approx k_B T s^3/B$. (note only one of the two transverse components of u are measured). For this chromosome, B = 3×10^{-22} J·m.

Figure 5.8c,d shows the 7.0 micron chromosome, and its fluctuation time series near its tip, and near the pipette. As expected, the tip fluctuation amplitude is smaller than that of Figure 5.8b. The diamonds of Figure 5.9, inset indicate a bending rigidity close to that of the chromosome of Figure 5.8a. Squares in the inset of Figure 5.9 show similar data for a third chromosome of length 16.5 microns. This chromosome's thermal fluctuations are shown in Figure 4.2. The equilibrium fluctuations are all consistent with (5.2), with similar bending rigidities of about 10^{-22} J·m.

The time series of Figure 5.7b and 5.7d have similar fluctuation lifetimes. Plots of autocorrelation functions of the tip (largest) fluctuations for the three chromosomes (Figure 5.9) show the correlation time of 0.7 seconds to be nearly length-independent. If external hydrodynamic damping were the only dissipation mechanism (i.e. if ç¢=0 in (5.10)), the correlation time for the fluctuations of Figure 5.7d should be $(7.0/18.5)^4 \approx 0.02$ of that of Figure 5.7b. Instead, the fluctuation lifetime is nearly independent of chromosome length, and therefore

of bending mode wavenumber as expected from (5.10). Therefore mitotic chromosomes are a biofilament whose bending relaxation is dominated by internal viscosity.

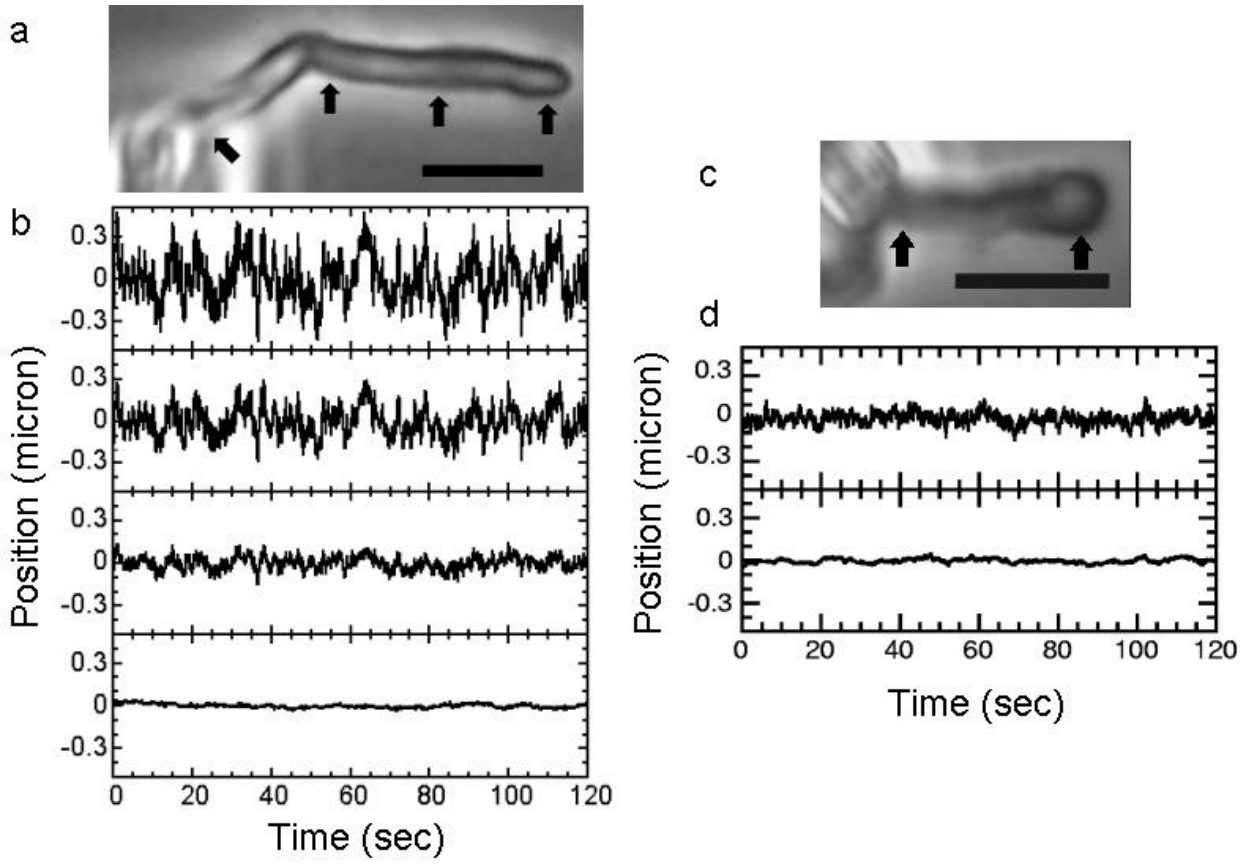

Figure 5.8
(a) Micromanipulated chromosome held at one end by a glass micropipette, with other end free. Total length of chromosome portion outside pipette is 18.5 microns. Bar = 5 ìm.
(b) Time series for amplitude *u* observed at a few points along the single mitotic chromosome of Figure 5.7a. The time series shown were measured at the points indicated by arrows in Figure 5.7a. Fluctuation amplitude grows with distance *s* from the anchored end.
(c) Shorter 7.0 micron chromosome attached to glass pipette. Bar = 5 ìm.
(d) Time series for fluctuations of shorter chromosome of (c) measured at the two points indicated by arrows in Figure 5.8a. Note that the characteristic time of fluctuations is similar to that of the long chromosome of Figure 5.7a-b.

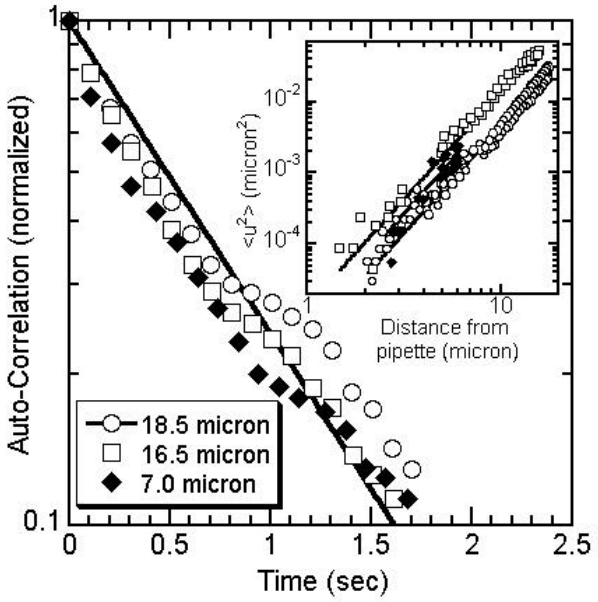

Figure 5.9 Autocorrelation functions for the free-end fluctuations of three chromosomes are independent of chromosome length. The 7.0 micron (diamonds) and 18.5 micron (circles) correlation functions come from the top time series of Figure 5.7b and 5.8b, respectively. The solid curve indicates the exponential $e^{-t/\hat{o}}$ with $\hat{o} = 0.7$ sec, the approximate timescale expected in the internal-viscosity-dominant regime of Eq. (5.9).

Inset: Mean-squared amplitude $\langle u^2 \rangle$ for time series as in Figure 2, versus length from anchored end, shows a cubic power law, as expected theoretically for thermal fluctuations of an elastic rod. The proportionality constant determines the bending rigidity B (see text). Diamonds, squares and circles show results for 7,0, 16.5 and 18.5 micron-long chromosomes.

5.12 Internal Viscosity May Also be Important for Other Biofilaments

Internal viscosity may play a central role in dynamics of other biofilaments. Actin filaments are composed of polymerized protein 'monomers', each ≈ 3 nm in radius. They have lengths of up to ≈ 10 microns, a cross-sectional radius of $r \approx 3$ nm and a bending rigidity $B \approx 7 \times 10^{-26}$ J · m (Gittes *et al*, 1993). We estimate the internal viscosity to be $ç¢ \approx B\hat{o}_0/r^4$ where $\hat{o}_0$ is the fluctuation time of conformational rearrangements at the cross-section scale. For actin, this time should be that associated with thermal fluctuations of the conformation of the individual protein

subunits, which are at least 10^{-9} sec (note that slow internal rearrangements of actin filaments have recently been proposed to explain the slow binding kinetics of certain polypeptides (Cruz *et al*, 1996)).

This (likely conservative) estimate gives $\zeta' > 1$ kg/m·sec, i.e. $\zeta'/\zeta > 1000$. The modes dominated by internal viscosity will therefore have wavelengths $< 2\pi/q^* = 2\pi(1000)^{1/4} \cdot 3$ nm $\approx$ 100 nm. These short-wavelength modes will relax together in a time $\tau^* = \zeta' r^4/B \approx 10^{-9}$ sec, i.e. essentially in the time required for the microscopic rearrangements at the actin monomer scale that are the origin of the internal viscosity. Recently developed diffusing-wave-spectroscopy experimental techniques (Palmer *et al*, 1999) may eventually be able to probe these short times.

5.13 Conclusions

We have found that mitotic chromosomes quickly stretched display a reversible elastic response with a relaxation time on the second time scale. This relaxation is not due to gel-draining dynamics, but is instead most likely due to the relaxation of chromosome 'loop' domains containing up to 80 kb of DNA. While the observation of loop domains by dynamical relaxation of chromosomes is indirect, these results indicate that loop domains are present at physiological conditions. In addition, they suggest that mitotic chromosomes are not folded in the precise fashion of globular proteins or other biopolymers organized by sequence-specific interactions. Instead we are led to a model of relatively loosely self-tethered chromatin, which admits rapid flow of small molecules in and out of the chromosome volume, and permits large chromatin domains to change conformation by slowly sliding between their neighboring fibers.

The mitotic chromosome internal friction is quantified by an internal viscosity of $\eta' =$ 100 kg/m·sec, and is important for understanding the time correlations of mitotic chromosome thermal bending fluctuations. The term $\eta' r^4 \partial/\partial t(\partial^4 u/\partial s^4)$ is added to the Langevin equation and

predicts that time correlations are wavenumber independent for $q > 0.05$ ìm^{-1} or wavelengths < 100 ìm. Mitotic chromosomes are no more than 20 ìm long, so we expect all time correlations to decay with the same characteristic time of $\tau \approx \eta/Y = 0.3$ sec. We find that thermal fluctuations of mitotic chromosomes are independent of q with a correlation time of about 0.7 sec.

Biofilaments with intermediate (≈ 30 nm) thicknesses, e.g. bundles of actin filaments or 'stress fibers', may provide excellent experimental systems for further exploration of internal viscosity effects. Also, similar phenomena can be expected for the short-wavelength bending fluctuations of thin shells of soft materials; for example, biological membranes 'decorated' with relatively thick layers of proteins or other biopolymers (Helfer *et al*, 2000).

Part of this chapter has been published as Poirier *et al*, 2001.

CHAPTER 6

EFFECTS OF IONIC CONDITIONS ON MITOTIC CHROMOSOMES

Introduction 6.1

A powerful tool used to study chromosome (and particularly chromatin) structure is its perturbation by varying ionic conditions. The reason for the importance of electrostatic interactions to chromatin structure is simply that DNA itself is highly negatively charged, and the attractive part of histone-DNA interactions is largely due to electrostatic attraction. Changes in univalent ion concentration change the range of electrostatic interactions, and can be used to 'tune' their strength. Di- and multivalent ions can also do this, but at relatively low concentration can also mediate *attractive* interactions between like-charged macromolecules (Gelbart *et al*, 2000), essentially by forming ionic 'bridges'.

In this chapter, a wide range of salt conditions, including conditions far from physiological concentrations, is used to perturb mitotic chromosome structure. The reason for exposing the chromosome to extreme, unphysiological conditions is to learn about native chromosome structure by observation of how it is disrupted. The results of the experiments of Maniotis *et al*, 1997 and Bojanowski *et al*, 1998 show that mitotic chromosomes dramatically unfold when exposed to ~500 mM NaCl and ~200 mM $MgCl_2$. This suggests that temporary exposure of mitotic chromosomes to strong shifts in ionic strength can cause large-scale unfolding of chromosomes, which is apparently reversible (i.e. the mitotic chromosomes were observed to regain a native-like conformation). We therefore used shifts in ionic conditions to develop techniques that use force measurement as a probe of chromosome structure during biochemical experiments on single mitotic chromosomes. A general result of these experiments is that in comparison to the cytoskeleton and other cell structures, mitotic chromosomes are

remarkably durable, and capable of drastic structural change. Upon return to physiological ionic strengths they are also able to regain near-native structure and elastic response, even after exposure to extreme charge densities.

By combining the basic idea of the studies of Maniotis *et al* and Bojanowski *et al* with elasticity measurements of chromosomes we plan to quantitatively answer the following questions:

(1) How does the degree of decondensation (assayed using changes in visible size and elastic response) of mitotic chromosomes vary with ionic strength, and with valence of the cations used?

(2) What is the timescale for ionic-strength chromosome decondensation to occur (assayed through dynamic measurement of tension changes in a chromosome)?

(3) How reversible are ionic-strength decondensation-condensation cycles (assayed using measurements of elasticity before and after ionic strength exposures)?

(4) How isotropic is ionic-strength-mediated decondensation, and can any evidence of an internal 'scaffold' structure (e.g. a directly observable structure, or a lower limit on the degree to which chromosome elastic response is reduced by ion exposure) be observed?

We find, in agreement with Maniotis *et al*, 1997, that high concentrations of either NaCl or $MgCl_2$ induce dispersion of the chromosome, into a 'cloud' of chromatin fibers much larger than the initial chromosome, and with a much lower contrast in the phase microscope. For sufficiently large ion concentrations, the tension supported by the chromosome can be reduced to zero. Associated with this increase in size is a decrease in the tension that the chromosome initially supported. The dynamics of these reactions are very rapid; decondensation occurs in a few seconds and the recondensation occurs in less than a second.

Effects of lower salt concentrations on chromosome elasticity depend on the valence of the ion used. 30 mM NaCl induces a drop in the measured force and density in a few seconds. Once the chromosome is returned to physiological conditions the force returns to the original value in about 1 second. 10 mM $MgCl_2$ induces the opposite effect; there is an increase in the force and the volume decreases in about 1 second. Hexaminecobalt trichloride has a similar but more pronounced effect to $MgCl_2$, causing a five-fold increase in the force and reducing the chromosome to 2/3 of its original volume. Thus, in general we have found that low concentrations of multivalent ions can induce hypercondensation of mitotic chromosomes.

Our results show that shifts in ionic strength can cause the chromosome's internal structure, which supports the applied force, to be completely disrupted. In the case of low concentrations of di- or trivalent cations, chromosomes become hypercondensed and become elastically stronger. These effects are in close correlation with effects observed for chromatin fibers, and lead us to the conclusion that the main cause of the large-scale effects that we observe is modulation of the electrostatic portion of nucleosome-nucleosome interactions. Thus, charge interactions play a crucial role in maintaining large-scale mitotic chromosome structure.

A number of general observations come out of our experiments as well. The rapidity with which we can unfold and refold chromosomes indicates that the chromatin in a prometaphase chromatid has a large amount of conformational freedom allowing for its dynamic unfolding and refolding. Remarkably, this unfolding and refolding does not lead to large changes in chromosome elasticity, suggesting that the initial native state does not have a highly ordered structure. We find that 1/3 of the volume of a native metaphase chromosome can be rapidly 'squeezed out', again indicating a relatively loose native organization of chromatin fibers.

Finally, we find no evidence for a mechanically solid internal mitotic 'scaffold': ion-driven chromosome decondensation is essentially isotropic (inconsistent with a loops-hanging-from-scaffold picture). Furthermore, when electrostatic interactions are screened away, the chromosome completely unfolds, leaving no mechanically solid structure. The general behavior of the mitotic chromosome is therefore essentially that of a crosslinked network of chromatin fibers, with no global organization of the crosslinking elements.

6.2 Review of How Ionic Conditions Affect Chromatin

The effect of changing ionic conditions on chromatin structure and nucleosome-nucleosome interactions has been widely studied. Increasing the concentration of NaCl above 500 mM causes the successive dissociation of histones from the chromatin fiber (van Holde, 1989) on a time scale of an hour (Yager *et al*, 1998). This is due to the reduction in strength of electrostatic interactions that occurs at high univalent ionic strength. Lowering the concentration of NaCl to 10 mM converts the 30 nm chromatin fiber to the 10 nm 'beads on a string' chromatin fiber, thanks to the electrostatic repulsion of adjacent nucleosomes that occurs at low univalent ionic strength. However, addition of ~1 mM of $MgCl_2$ maintains the 30 nm fiber at 10 mM NaCl (Ausio *et al*, 1984; Zlatanova *et al*, 1998), thanks to attractive nucleosome-nucleosome interactions mediated by the divalent ions. Above ~1 mM $MgCl_2$, chromatin fibers begin to aggregate and stick to each other (Borochov *et al*, 1984), again due to divalent-cation-induced attractive interactions. Higher valence ions such as hexaminecobalt trichloride (a trivalent cation) show this ability to compact chromatin and cause aggregation at lower concentrations than divalent ions (Sen and Crothers, 1986, Smirnov *et al*, 1988).

Since variation in ionic conditions change nucleosome-nucleosome interactions and the structure of isolated chromatin fibers in micromanipulation experiments, the elastic properties of

chromatin should also be affected. Cui and Bustamante, 2000, studied the elasticity of isolated chromatin fibers in micromanipulation experiments, and showed how various concentrations of NaCl affected their elastic response. They found at 5 mM NaCl chromatin fibers adopt an extended, 10 nm-fiber-like form, which deforms continuously from its random-coil initial state, with a positive curvature in the force-extension response rather similar to that of dsDNA. In this low-ionic-strength regime, chromatin fiber was observed to behave rather like a flexible polymer, showing no tendency for nucleosomal aggregation. At higher concentrations of 40 and 150 mM NaCl the chromatin fiber was seen to exhibit a transition 'plateau' in its force-extension response, which could be understood as mechanically-driven unfolding of the initially condensed 30 nm fiber, to the uncondensed 10 nm fiber. The results of those experiments are thus in good accord with previous biochemical and biophysical experiments on isolated chromatin fibers at low and physiological salt concentrations.

Changes in ionic conditions have also been observed to affect the cellular organization of chromatin fibers, in interphase nuclei and in mitotic chromosomes. The effects of KCl and $MgCl_2$ on interphase chromosomes in isolated nuclei are consistent with studies of ionic effects on isolated chromatin fibers (Arronson and Woo, 1981). Inside isolated nuclei, chromatin is most condensed at about 200 mM KCl and gradually disperses for concentrations above and below 200 mM. In contrast, the same authors observed that $MgCl_2$ induces a sharp compaction at 1 mM and the chromatin stays compacted until about 50 mM where the chromatin gradually disperses again.

One of the best-known experiments using ions to perturb chromosome structure was use of 1 M NaCl to histone-deplete metaphase chromosomes, which were then observed with the electron microscope (Paulson and Laemmli, 1977). Loops of about 80 kb of DNA were

observed emanating from a dense protein core, leading to the proposal of a scaffold model for mitotic chromosome structure. This scaffold was also found to undergo a lateral aggregation in the presence of 5 mM $MgCl_2$ (Earnshaw and Laemmli, 1983). Although intuitively appealing, the interpretation of these experiments depended on the assumption that the histone-depletion reaction and subsequent preparation for electron microscopy did not substantially alter the proposed scaffold organization.

A recent experiment (Maniotis *et* al, 1997) pursued an approach similar to that of Paulson and Laemmli, but while observing the chromosomes in physiological buffer using light microscopy. Maniotis et al showed that mitotic chromosomes extracted from cells using glass needles could be made to rapidly decondense and recondense when either 500 mM $MgCl_2$ or 1 M NaCl was pipetted into the cell culture dish (Maniotis *et al*, 1997). Similar results were found for chromosomes *in vivo*, where extracellular addition of 410 mM NaCl or 65 mM $MgCl_2$ caused cycles of decondensation-condensation of the mitotic chromosomes *inside* Bovine Capillary endothelial cells (Bojanowski and Ingber, 1998).

6.3 NaCl Always Reversibly Decondenses and Softens Mitotic Chromosomes

Isolated chromosomes were extended to an initial force of 0.4 nN and then sprayed with 30 mM to 500 mM of NaCl for 10 sec. Time series of images were acquired at 10 frames per second for 40 seconds; the spray was initiated about 5 seconds into the time series (Fig 6.1a,b). Following the initiation of the 10 sec spray the force reduction equilibrated in about 2 sec. The final change in force was determined by averaging the last 5 sec of the spray. Increasing the distance between the chromosome and the spray pipette reduced the concentration of ions. This was calibrated following the experiment as described in section 2.16. Spray experiments with 15 different concentrations were done.

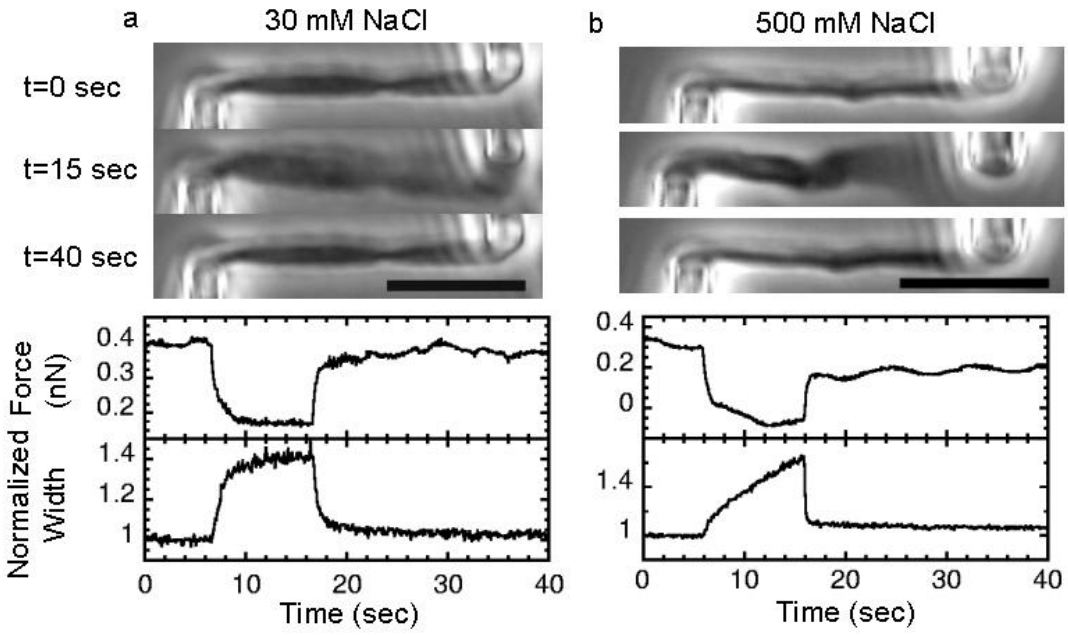

Figure 6.1 Images of combined chemical-micromechanical experiments with 30 mM NaCl (6.1a) and 500 mM NaCl (6.1b). The images show the chromosome before, during and after an exposure to the different ionic conditions. The plots show the time series of the force the chromosome supports and width of the chromosome. For 30 mM and 500 mM NaCl, the force decreases and the width increase. The time scale of the response of the chromosome to the ionic shifts occurs on the second time scale, and shows the internal structure of a mitotic chromosome can be rapidly changed. Bars = 10 μm.

Table II

Effects of ionic conditions on chromosome elasticity

Ion	Maximum Concentration	Exposure Time	Initial force Constant	Final force Constant	Change in Force constant	% Change in force constant
Na^{+}	30 mM	60 sec	0.43 nN	0.54 nN	+0.11 nN	+26%
Na^{+}	300 mM	20 sec	0.32 nN	0.49 nN	+0.17 nN	+53%
Na^{+}	600 mM	20 sec	0.37 nN	0.67 nN	+0.30 nN	+80%
Na^{+}	2000 mM	30 sec	0.55 nN	0.65 nN	+0.10 nN	+27%
Na^{+}	2000 mM	270 sec	0.55 nN	0.26 nN	-0.29nN	-53%
Mg^{+2}	20 mM	60 sec	0.75 nN	1.39 nN	+0.64 nN	+85%
Mg^{+2}	100 mM	60 sec	0.42 nN	0.38 nN	-0.04 nN	-10%
Mg^{+2}	300 mM	20 sec	0.67 nN	0.72 nN	+0.05 nN	+07%
Ca^{+2}	10 mM	60 sec	0.94 nN	1.14 nN	+0.20 nN	+21%
$Co(NH_3)_6^{+3}$	40 mM	20 sec	0.78 nN	0.35 nN	-0.35 nN	-55%
$Co(NH_3)_6^{+3}$	200 mM	40 sec	0.54 nN	0.38 nN	-0.16 nN	-30%

NaCl always induced a decrease in the measured force (Fig 6.2). Concentrations below 500 mM of NaCl slightly decreased the force and density of the chromosome (Fig 6.2). The maximum force and density occurs around 100 mM of NaCl. After the chromosome was returned to physiological salt concentrations, the force constant was measured. Below 600 mM NaCl, the force constant of the chromosome returns to a larger value (Table II).

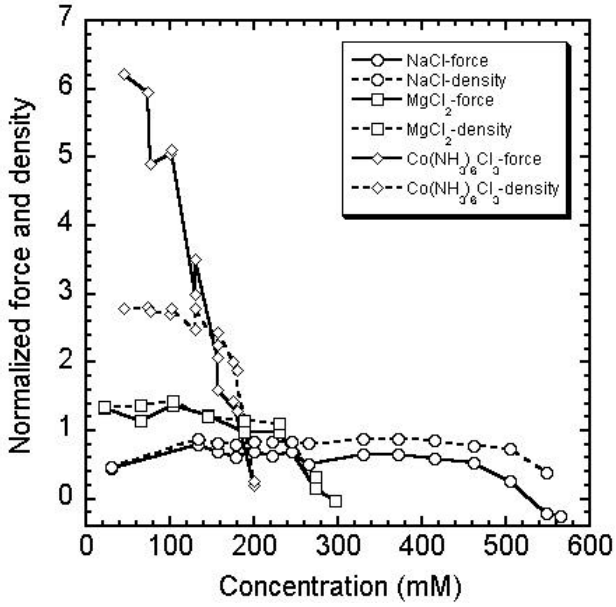

Figure 6.2 The normalized force (solid line) and density (dashed line) of mitotic chromosomes vs. concentration of NaCl ( ), $MgCl_2$ ( ) and $Co(NH_3)_6Cl_3$ ( ). The normalized force and width measurements are the steady-state force or density during a salt exposure divided by the initial force or density before the exposure. Since the force and density are normalized, the value of 1 implies no change is induced. NaCl always causes a decrease in the force and density with a minimum change at about 150 mM. However, $MgCl_2$ and $Co(NH_3)_6Cl_3$ cause an increase in the force and density for concentrations below 100 mM and a decrease in force and density above 150 mM. The absolute value of the concentration measurements have an uncertainty of about ±50% since the overall scale of spray concentration curves described in section 2.17 is known to within a factor of two. However, the relative concentrations have about a ±10% uncertainty because the shape of the calibration curve is known to this accuracy. These results are qualitatively similar to the behavior of other charged biopolymers, dsDNA (Gosule and Schellmann, 1976) and actin (Tang and Janmey, 1996), and indicate that the chromatin inside mitotic chromosomes behaves as a charged biopolymer.

We also exposed mitotic chromosomes to 2 M NaCl and observe the same decondensation. For short exposures of 10-40 seconds, the chromosome fully recondenses with an increase in the force constant (Table 1). However, following exposures of > 250 seconds, the chromosome does not fully recondense and is irreversibly changed. The length is more than doubled, the force constant is reduced by more than half (Table 1) and the contrast in the phase microscope is reduced. The reduction of the force constant by about 2 times is very dramatic since the length increased by more than 2 times (the force constant is defined as the force required to double the chromosome length). Therefore, the chromosome is completely different following the longer exposures of 2 M NaCl. We emphasize that this irreversible behavior does not occur for the short exposures (10 sec) of lower ionic strength, which are the main focus of this paper.

6.4 $MgCl_2$ Reversibly Decondenses and Hypercondenses Mitotic Chromosomes

Chromosomes were extended so they supported a force of about 0.5 nN and were then exposed to between 10 and 300 mM of $MgCl_2$. Again, the force was monitored at a rate of 10 frames per second for 40 seconds, where the spray was initiated 5 seconds into the time series (Figure 6.3a,b). Below 100 mM $MgCl_2$, the force and density increased by about 20% (Figure 6.2). Between 100 and 200 mM $MgCl_2$, there is an initial increase in force (Data not shown), which then reduces back to the initial force (Figure 6.2). 10 mM $CaCl_2$ also caused an increase in force identical to 10 mM $CaCl_2$. Larger concentrations were not studied because at higher $CaCl_2$ concentrations, calcium phosphate forms at the tip of the spray pipette.

The force increase at 10 mM $MgCl_2$ is also seen as the concentration is increased to 300 mM (Figure 6.3b). The force plot in Figure 6.3b has a spike in the force as the spray is initiated. The force then drops to zero as the concentration of $MgCl_2$ increases through 10 mM to 300 mM.

This spike occurs in less than a second, which is faster than the internal response time discussed in chapter 5. Once the concentration is increased above 200 mM, the force drops nearly to zero, indicating complete loss in the ability for the chromosome to support force (Figure 6.2 and 6.3b).

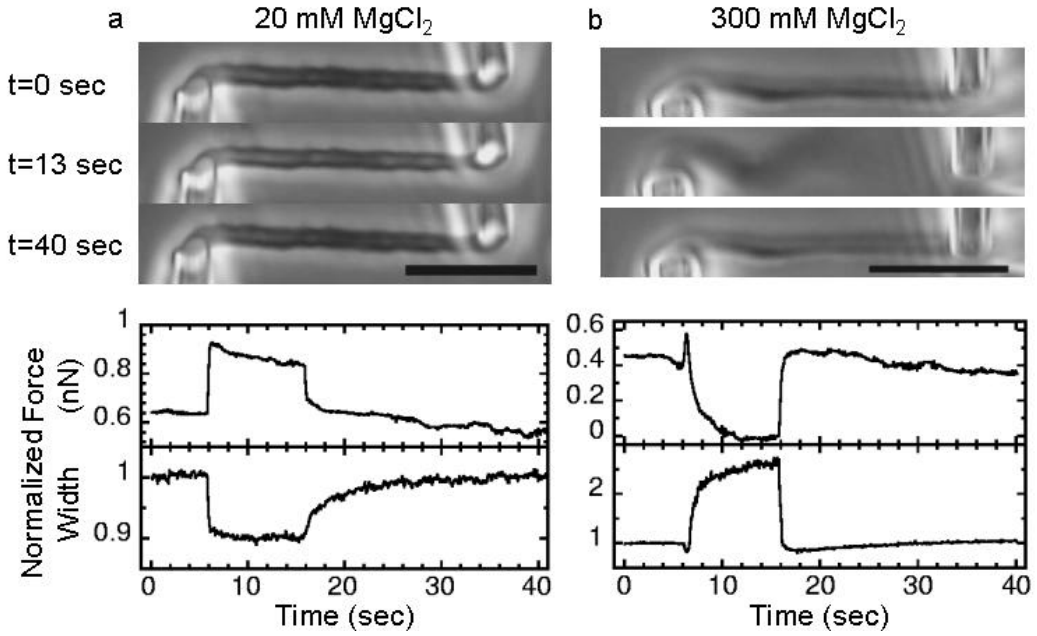

Figure 6.3 Images, force and width response to 20 mM $MgCl_2$ (a), 300 mM $MgCl_2$ (b). 20 mM $MgCl_2$ induces an increase in the force and decrease in width, and 300 mM $MgCl_2$ causes a decrease in force and increase in width. Also, as the $MgCl_2$ is increased to 300 mM through 20 mM, there is a transient increase in the force. Bars = 10 ìm.

Following a return to physiological salt conditions, the force constant was measured. Over this range of $MgCl_2$ concentrations, the force constant did not change by more than a factor of 2, indicating approximately reversible unfolding-refolding behavior.

6.5 Hexaminecobalt Trichloride Decondenses and Hypercondenses Mitotic Chromosomes

Using hexaminecobalt trichloride allows us to study how the cation valence affects chromosome condensation. Mitotic chromosomes were stretched so that they initially supported about 0.2 nN of force and then exposed to concentrations between 40 mM and 200 mM. Below 150 mM $Co(NH_3)_6Cl_3$, the force increases about five times, from 0.2 nN to 1 nN (Figure 6.4). This is qualitatively similar to $MgCl_2$, however the effect is quantitatively much larger. The time for the chromosome to hypercondense and the time for the chromosome to return to the native condensed state are very different (Figure 6.4). The increase in force occurs in a fraction of a second while the decrease in force occurs on the minute time scale. This is likely due to a large energy barrier for the $Co(NH_3)_6^{+3}$ to dissociate from the chromosome. Also, after 40 mM $Co(NH_3)_6^{+3}$ diffuses away, the chromosome force constant is reduced by 50% (table II) and indicates this trivalent ion irreversibly affects chromosome structure.

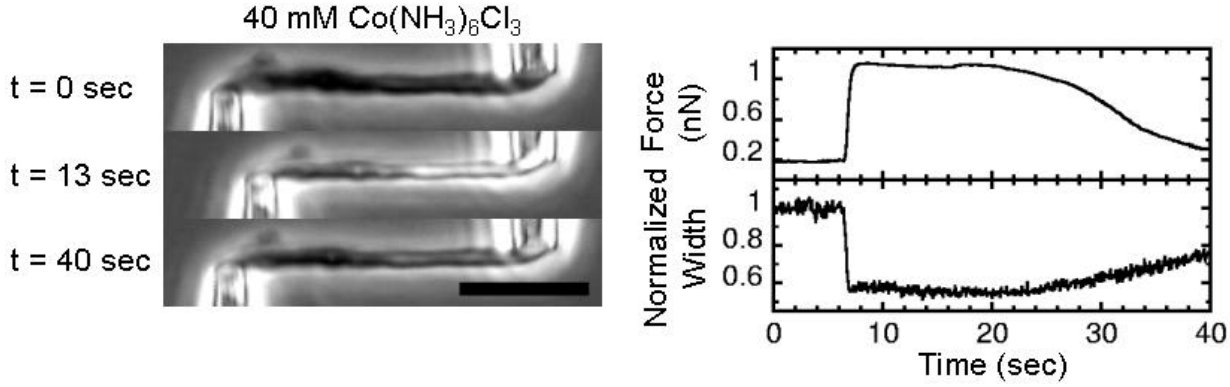

Figure 6.4 Images, force and width response of a mitotic chromosome to an exposure of 40 mM $Co(NH_3)_6Cl_3$. $Co(NH_3)_6Cl_3$, is similar to $MgCl_2$ in terms of the qualitative response of the chromosomes however the magnitude of the change in force and width are about 5 times larger. Bar = 10 ìm.

Between 150 and 200 mM this increase in force is reduced and at 200 mM the force drops to zero indicating the chromosome has lost the ability to support force (Figure 6.2). Following the exposure to 200 mM $Co(NH_3)_6Cl_3$ the force constant is reduced by about 30%, indicating the chromosome did not fully recondense.

6.6 The Force Supported by a Chromosome is Related to Density

For each time series the width, length and a force were measured. By assuming the chromosome width is similar in both the horizontal and vertical directions, we calculated the volume of the chromosome, which is inversely proportional to the average chromosome density. Figure 6.2 plots how the force and density is related to the concentration of various ions. The density increases or decreases when the force increases or decreases, respectively. This implies that the denser the chromosome is the more force it is able to support. However, density and force are not proportional, as can be seen for hexaminecobalt trichloride. The force continues to increase while the density is remaining constant for decreasing concentration. This plateau in the density is likely due to the chromosome reaching its maximum degree of compaction.

6.7 Unconstrained Chromosomes Expand and Contract Isotropically

We independently measured the chromosome width and length for chromosomes held in one pipette while the other end was free (Figure 6.5). A chromosome was isolated as described in Material and Methods and then exposed to increasing concentrations of NaCl or hexaminecobalt trichloride. NaCl concentrations of 150 mM, 200 mM, 300 mM and 400 mM and hexaminecobalt trichloride concentrations of 5 and 40 mM were used. Figure 6.5 shows that the decondensation and hypercondensation of mitotic chromosomes is roughly isotropic.

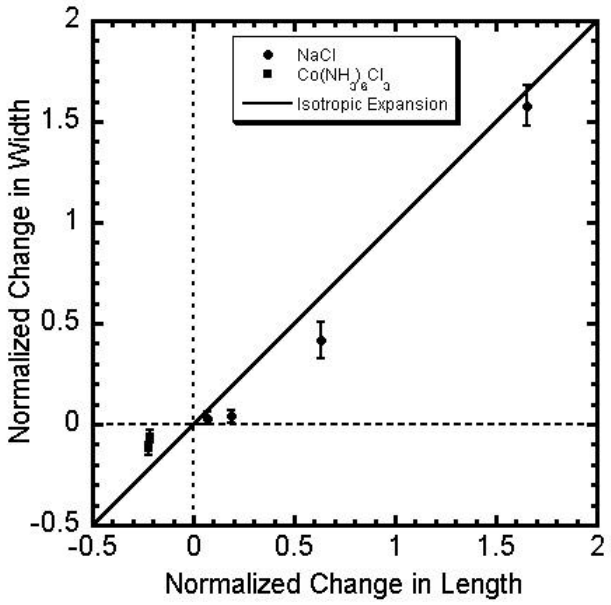

Figure 6.5 Salt-driven isotropic decondensation and hypercondensation of mitotic chromosomes. NaCl ( ) decondenses and hexaminecobalt trichloride ( ) hypercondenses mitotic chromosomes similarly to what is expected for isotropic contraction and expansion (solid line) and is not consistent with what is expected for chromatin loops tethered to a protein scaffold. This response is consistent with a crosslinked polyelectrolyte gel. Also, the maximum condensation by hexaminecobalt trichloride shows that mitotic chromosomes are at least 1/3 aqueous solution.

6.8 Hexaminecobalt Trichloride Reduces Chromosome Volume by 1/3.

Figure 6.2 shows that the density approaches a plateau while the force continues to increase as the concentration of hexaminecobalt trichloride is decreased below 100 mM. Again, this implies the chromosome is reaching a maximum density. At these concentrations, Figure 6.5 shows that a hypercondensed, unconstrained chromosome has a normalized change in length of 0.8 and normalized change in width of 0.9. This implies a decrease in volume by 1/3. Also, after the concentration of $Co(NH_3)_6^{+3}$ is returned to zero, chromosome returns to its original volume with a similar force constant (Table 6.1). This suggests the hypercondensation involves the

expulsion of aqueous solution and that the native mitotic chromosome is at most 2/3 DNA and protein and that at least 1/3 is essentially water.

6.9 The Shifts in Ionic Conditions Mainly Perturb Chromatin Structure

We have shown that chromosome structure can be rapidly and reversibly hypercondensed and decondensed by shifts in ionic conditions on the second time scale. Combining these results with previous salt studies of chromatin and chromosomes allow us to understand how changes in ionic conditions perturb chromosome structure. The simplest explanation is that the rapid shifts in ionic conditions mainly perturb the chromatin level of structure. This is consistent with the reversibility in both the force constant and size of the chromosome.

6.9.1 Effects of NaCl Concentrations Below 30 mM

30 mM concentrations of NaCl cause a decrease in the force supported by a mitotic chromosome and a decrease in chromosome density (Figure 6.2). This can be understood in terms of how low concentrations of NaCl ions affects chromatin structure. It was previously shown (van Holde, 1989) that chromatin structure is gradually converted from the 30 nm fiber to the 10 nm fiber as NaCl concentrations are reduced below 75 mM. The elements maintaining chromosome condensation are not permanently interfered with since there is little permanent change in chromosome force constant or size. Therefore, low NaCl concentrations partially unfold chromatin fibers while the higher order chromosome structure is relatively undisrupted.

6.9.2 Effects of NaCl Concentrations Above 500 mM

Mitotic chromosomes are unable to support tension and the density dramatically decreases above 500 mM NaCl. This is where core histones begin to be removed from nucleosomes (van Holde, 1989). However, histone removal must be done by gradually increasing the NaCl concentration over a period of at least an hour. A rapid increase of NaCl

concentration to above 500 mM does not remove core histones from nucleosomes for at least 40 minutes (Yager, *et al,* 1989). However, experiments exposing chromatin fibers to 500 mM NaCl for short periods show a shift in the sedimentation coefficient, which is due to a destabilizing of the nucleosome without removal (van Holde, 1989).

The decondensation of mitotic chromosomes observed for a NaCl concentration of 500 mM is therefore likely due to destabilization of chromatin fiber structure. Higher levels of mitotic chromosome structure are not permanently removed by this salt treatment since the chromosome returns to a similar size and force constant following the removal of the salt treatment. We do, however, observe effects consistent with histone removal at longer exposures (4 minutes) of higher NaCl concentration (2 M).

6.9.3 Effects of Multivalent Ion Concentrations Below 20 mM

Low concentrations (~10 mM) of multivalent ions cause an increase in the force supported by a chromosome and a decrease in its width. It was previously shown that chromatin aggregates above 1 mM of $MgCl_2$ (Borochov *et al,* 1984) and 0.01 mM Hexaminecobalt Trichloride (Sen and Crothers, 1986, Smirnov *et al,* 1988). This suggests that the decrease in volume and increase in force are due to an induced attraction between chromatin fibers, which is mediated by the multivalent ions.

This attraction is consistent with aggregation of other biopolymers such as DNA (Gosule and Schellmann, 1976) and actin (Tang and Janmey, 1996). Bloomfield, 1991, Ray and Manning, 1994 and Nguyen, Rouzina and Shklovskii, 2000, have described theories that explain this aggregation. Mitotic chromosomes are another biopolymer in which multivalent ions induce like-charged polymers to attract each other.

6.9.4 Effects of Multivalent Ion Concentrations Above 200 mM

Mitotic chromosomes are unable to support an applied force and increase in width by 2 times (Figure 6.3b) for multivalent ion concentrations above 200 mM. The increase in width and reduction of force is similarly to 500 mM NaCl. There has been less study of the effect of high concentrations of multivalent ions on chromatin structure. Aaronson and Woo, 1981 used turbidity to measure the compaction of chromatin within rat liver nuclei by $MgCl_2$. They find that between 2 and 30 mM of $MgCl_2$ the chromatin is maximally compacted and that over 100 mM it appears to decondense. These results suggest that the decondensation at 200 mM is due to destabilization of the chromatin fibers, analogous to the decondensation at 500 mM NaCl.

6.10 Conclusions

By monitoring chromosome elasticity while locally changing ionic conditions, we are able to assay structural changes within a mitotic chromosome. The observed structural changes show that electrostatic interactions clearly play a crucial role in maintaining native mitotic chromosome structure. Disruption of electrostatic interactions leads to rapid and isotropic swelling behavior that would be expected of a crosslinked polyelectrolyte gel. Cobolt hexamine trichloride is able to reduce chromosome volume by 2/3, indicating they are at least 1/3 aqueous solution. The rapid and reversible reorganization suggests that mitotic chromosome structure is not highly ordered in the sense that each region of chromatin does not have a regulated folded pattern. Finally, the isotropic swelling supports the idea that there is no globally anisotropic structure within mitotic chromosomes. There is no remnant elasticity after chromatin is unfolded, or any anisotropic swelling behavior, as should occur for unfolding of chromatin loops off of an underlying stiff scaffold.

CHAPTER 7

EFFECTS OF dsDNA-CUTTING ENZYMES ON MITOTIC CHROMOSOMES

7.1 Introduction

This chapter describes microdigestion experiments, which combine micromechanical force measurement with microfluidic enzyme digestion and allow us to study the internal organization of single newt (*N. viridescens*) chromosomes. These experiments are similar in spirit to the microspray experiments described in chapter 6, because force measurement is used to monitor structural changes within a single mitotic chromosome. However, instead of just changing ionic strength, the chromosome is exposed to enzymes that have well-characterized DNA cutting properties. The enzymes used were micrococcal nuclease and 8 different restriction enzymes and can be thought of as nanometer sized scissors, which exclusively cut DNA.

Micrococcal nuclease cuts both dsDNA and ssDNA at any accessible site. This enzyme has proven to be a powerful tool in the study of chromatin. It is used to isolate nucleosomes from chromatin since it only cuts the exposed linker DNA between nucleosomes (van Holde, 1989). The DNA wrapped around the core histones is protected against cutting since it is pasted to the histones (Polach and Widom, 1995). Micrococcal nuclease is active in our cell culture medium with the addition of 1 mM of $CaCl_2$, making it a straightforward tool to combine with our force measuring techniques.

Exposing mitotic chromosomes to 1-10 nM micrococcal nuclease first removes the native elastic response, and then goes on to completely disintegrate single mitotic newt chromosomes. A concentration of 1 nM is used because this provides about 1 molecule per micron^3, so there are no more than hundreds of molecules near and within the chromosome. Furthermore, if the digestion is stopped before the chromosome shows any morphological change, multiple

extension-retraction cycles reduce the chromosome elastic constant by more than a factor of ten, and chromatin islands appear as the chromosome is extended. These islands are connected in series by thin fibers, which can be cut by micrococcal nuclease. These experiments show there is no internal non-DNA protein `scaffold' that provides the mechanical integrity of metaphase chromosomes, and instead indicate that chromosomes are networks of chromatin.

Restriction enzymes also cut dsDNA, however they are 'restricted' to cutting at a specific sequence. As discussed in section 2.19, most recognize a 4 to 8 bp sequence and cut dsDNA leaving either single strand overhangs, or blunt ends (no ssDNA overhangs). The varying degree of sequence specificity allows control over the number of cuts being made. The restriction enzymes used here all cut dsDNA leaving blunt ends, eliminating the complication of base pairing between cut ends. Restriction enzymes that recognize a 4 bp sequence cut apart mitotic chromosomes confirming the micrococcal nuclease results, even though they cut 256 times less frequently. We went on to use restriction enzymes, which recognize a 6 bp sequence with variable specificities. These allow us to estimate that cuts of at least every few kb completely cut up the chromosome and that cuts less frequently than every 50 kb do not affect chromosome elasticity. These results confirm the micrococcal nuclease result that mitotic chromosomes are a network without an internal non-DNA protein scaffold and indicate that chromatin in metaphase chromosomes is constrained by isolated chromatin-crosslinking elements spaced by at least 50 kilobases of dsDNA.

7.2 Digestion of Single Mitotic Chromosomes with Micrococcal Nuclease

All of the experiments describe in this chapter were done with experimental setup, version 3, where a mitotic chromosome was isolated and attached to micropipettes as described in section 2.7.2. The native elastic response of single chromosomes was measured, and then

microdigestion experiments were done as described in section 2.17. The chromosome was extended to ~1.5 times its relaxed length with ~0.3 nN of force. 1-10 nM micrococcal nuclease in 60% PBS with 1 mM $CaCl_2$ was then microinjected from a third 3-micron-diameter micropipette ~10 microns from the chromosome (Figure 7.1a). Images were acquired at 10 frames/sec before, during and after each enzyme exposure; this records pipette positions (and therefore force and extension) and chromosome morphology.

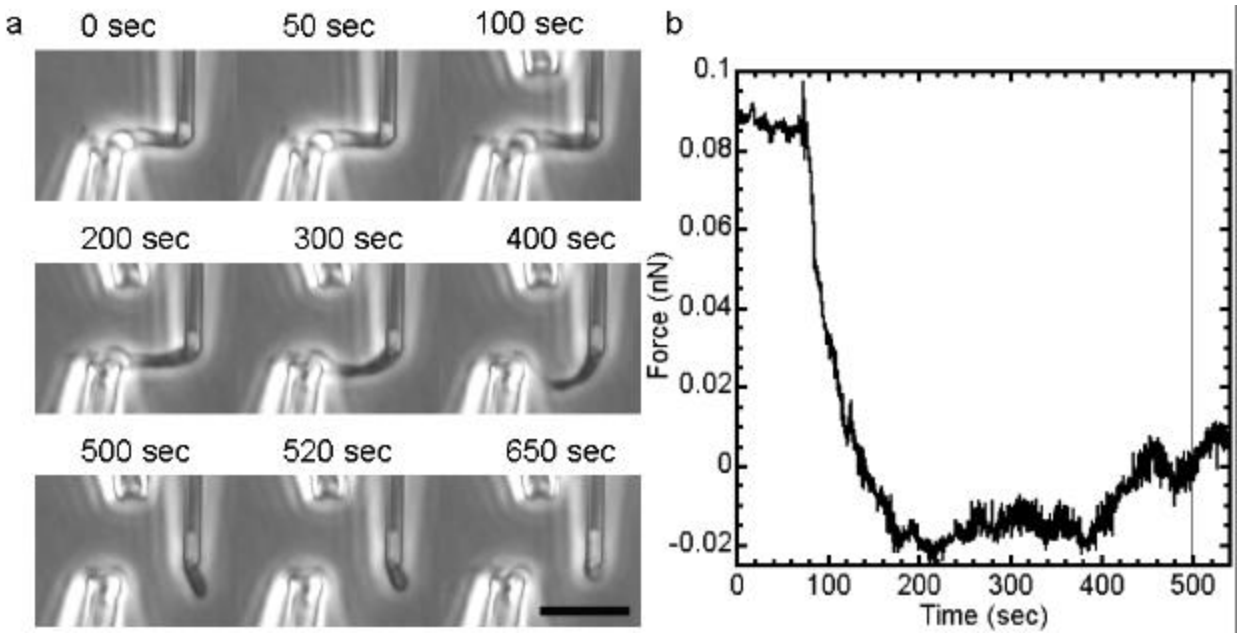

Figure 7.1 Response of a mitotic chromosome microdigested with 1 nM of micrococcal nuclease in 60% PBS with 1 mM $CaCl_2$. The chromosomes was put under 0.1 nN of force before microdigestion. Micrococcal nuclease completely relaxes the applied force before the there is any apparent change in chromosome morphology as viewed by phase contrast microscopy. This shows that a large-scale protein scaffold does not exist within mitotic chromosomes.
(a) Phase images of the chromosome being digested by micrococcal nuclease. The time in each image is the time it was captured and corresponds to the times series of (b). Bar = 10 ìm.
(b) Time series of the force supported by the chromosome during the nuclease digestion. The thin vertical line indicates the time at which the chromosome was completely cut through.

Micrococcal nuclease (MN) at concentrations of 1 to 10 nM cause the force to drop to zero in about 60 seconds (Figure 7.1b). This indicates there is a drastic reduction in elastic modulus, which occurs before any apparent morphological (Figure 7.1a) change in the chromosome. After an additional 60 seconds the chromosome 'thins' and then after 500 seconds is completely severed. This basic experiment has been repeated with enzyme concentrations of 1 to 100 nM and initial tensions of 0.1 to 1 nN, with the same result.

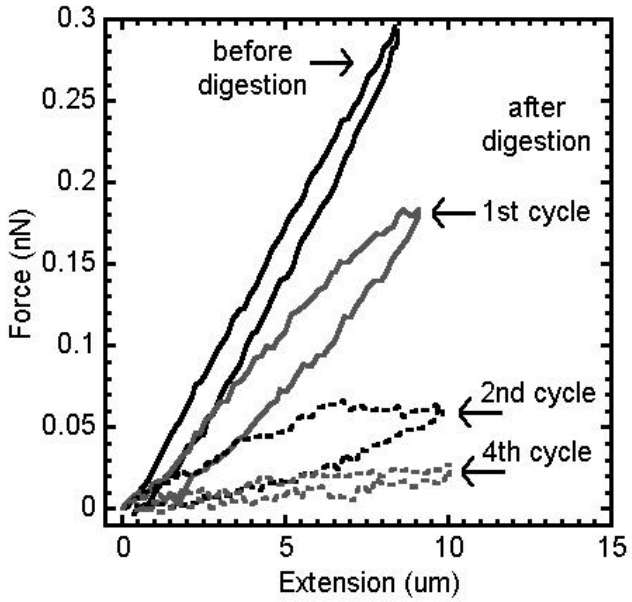

Figure 7.2 A newt mitotic chromosome was digested with 10 nM of Micrococcal nuclease for 90 sec and then subjected to 4 extension-retraction cycles. The chromosome's force constant was reduced after each extension-retraction cycle, resulting in a reduction by more than a factor of 10.

A second type of experiment was then done where 10 nM MN digestion was stopped after 90 sec, before 'thinning' was observed. At this point, morphology is unchanged. The chromosome was then repeatedly extended and retracted. Before digestion, a chromosome can be repeatedly extended and retracted without any change in its elastic response (chapter 3). By

contrast, after mild MN digestion, repeated extension-retraction cycles cause the force constant to be reduced by more than a factor of 10 (Figure 7.2). Even more striking, the chromosome no longer extends homogeneously; instead, relatively dense domains connected by thin fibers appear (Figure 7.4, t=0 sec). These thin fibers connecting the islands were extended with forces of about 30 pN and then exposed to 10 nM of nuclease, which immediately cuts the thin fiber (Figure 7.3, 7.4). This shows that mitotic chromosome's contiguous structural element is DNA, not protein.

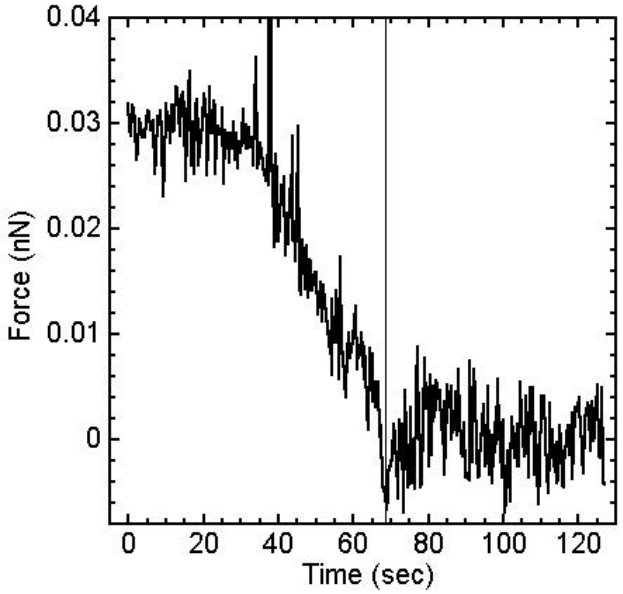

Figure 7.3 Following the 90 sec digestion and the 4 extension retraction cycles, the chromosome was extended to 40 microns and then microdigested again with 10 nM nuclease while monitoring the force. The digested chromosome does not elongate homogeneously, instead there are blobs connected by thin fibers. This time series of the digestion experiment shown shows the thin fiber is cut by nuclease. The microdigestion began at ~60 seconds. The thin vertical line indicates when the fiber was severed.

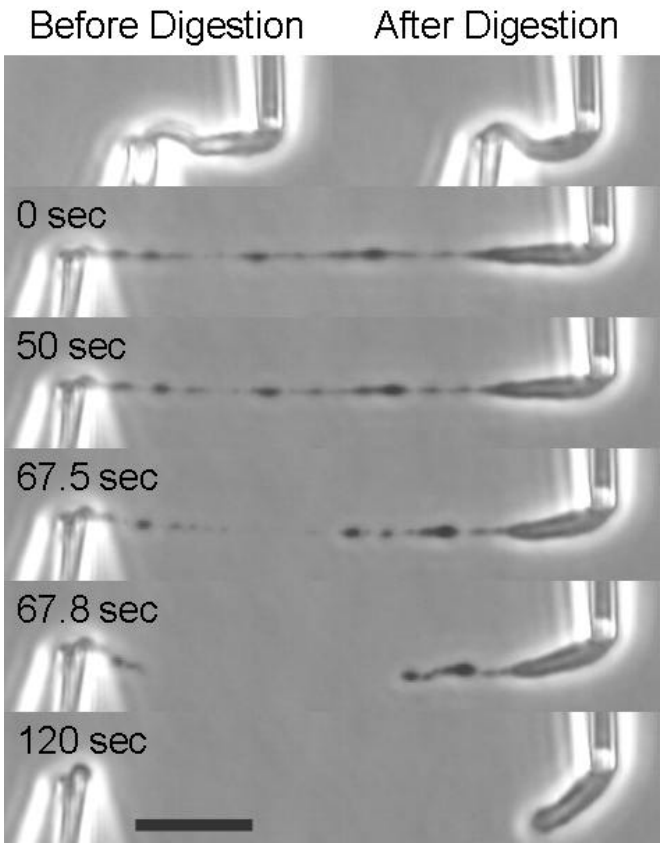

Figure 7.4 The images labeled before digestion and after digestion are of the chromosome unextended before and after the 90 sec microdigestion and 4 extension retraction cycles shown in Figure 7.2. The images labeled with a time are of the experiment shown in Figure 7.3. The chromosome (after the 90 sec microdigestion and extension retraction cycles) was extended to ~40 ìm and supported a force of ~30 pN. The times correspond to the time series in Figure 7.3. Bar = 10 micron.

7.3 Digestion of Single Mitotic Chromosomes with Restriction Enzymes

In order to estimate the average DNA length between DNA cuts, further experiments were done with blunt-cutting restriction enzymes. These enzymes cleave dsDNA at specific sequences, and therefore with a given statistical frequency. We used enzymes with 4- and 6-base recognition sequences. Again, chromosomes were extended to about 1.5 times native length, (force ~0.5 nN), and were then sprayed with an enzyme concentration of 0.4 to 1.2 units/ul

enzyme in the appropriate reaction buffer (in each case Tris-HCl pH 7.5 to 8, 50 to 100 mM NaCl , 5 to 10 mM $MgCl_2$). One unit of restriction enzyme is defined as the amount required to completely digest 1 ìg of λ DNA in 50 ìl of the recommended buffer in 1 hour at 37 C. This is a concentration of 0.02 unit/ìl. Unfortunately, the companies were unable to provide both the molecular weight and specific activity, so we are unable to determine the enzymes molarity. However, this is not very important since comparing results with the same unit activity takes in account differences in enzyme activity. The activity of each restriction enzyme preparation was assayed as described in section 2.19. Digestion assays were done with either 0.02 ìg/ìl of pBR322 (Promega) or 0.01 ìg/ìl of lambda DNA (Promega) at 25 C for 15, 30 and 60 minutes; results were analyzed using gel electrophoresis (Figure 2.7). In each case digestion was complete by 30 minutes, with no excess cutting ('star activity').

Experiments with Alu I (AG^CT, Promega) produce results similar to MN. Alu I exposure causes the force to completely relax after 30 sec, and then after 200 sec completely cuts the chromosome. Hae III (GG^CC, Roche) gave similar results (data not shown). These enzymes cut bare, random-sequence DNA on average once every 4^4=256 bases, or with a frequency 1/256 that of MN, and still leads to compete disintegration of the chromosome.

To make less frequent dsDNA cuts, we went on to use restriction enzymes that recognize more specific sequences than Alu I and Hae III. However, higher specificity requires longer sequences, which may cause the enzyme to have less access to exposed DNA. This will reduce the number of cuts made by more than what is expected statistically. To control for this we used the restriction enzyme, Cac8 I (GCN^NGC, New England Biolabs, note N denotes 'any base'). The Cac8 I recognition sequence has the same statistical frequency on a random-sequence of DNA ($1/4^4$ = 1/256) as Alu I and Hae III, but requires a 6-base DNA region to be exposed. Cac8

I only partially reduces the applied force (Figure 7.5), and after spraying for 60 minutes the force constant converges to 40% of its native value (Figure 7.6). The rate of force reduction by Cac8 I is 1/10 that of Alu I and Hae III, indicating that the increase in recognition sequence size has reduced cut frequency by about 10 times.

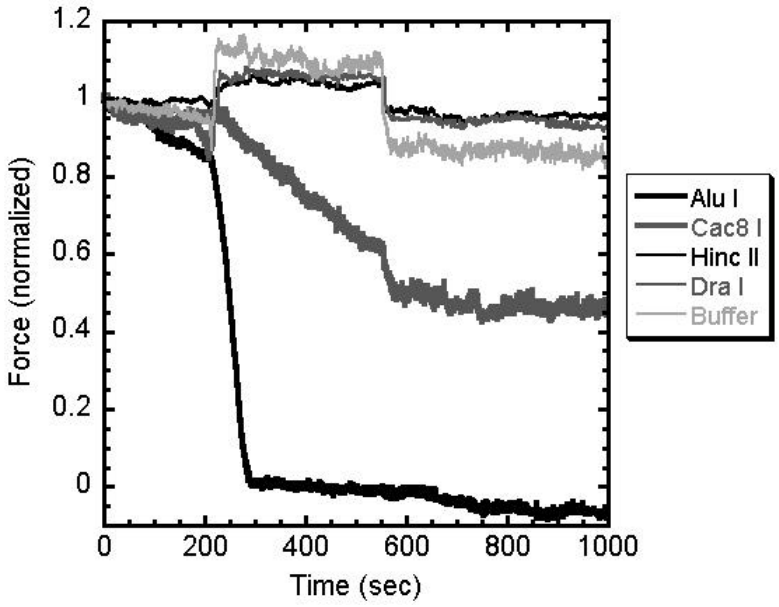

Figure 7.5 The force supported by a chromosome before, during and following a 350 sec exposure to various restriction enzymes. The force is in units of the initial applied force, which ranged between 0.2 and 0.8 nN. Alu I AG^CT (thick-black) relaxes the force in about 30 sec; Cac8 I GCN^NGC (thick-gray), only partially reduces the force; Hinc II GT(T/C)^(A/G)AC (thin-black) and Dra I TTT^AAA (thin-gray) induce an increase in force which is purely a buffer effect (thin-light gray). These results indicate that mitotic chromosome have a network structure with ~50 kb of dsDNA between crosslinks.

The more specific restriction enzymes used recognize a 6 bp sequence, requiring similar access to DNA as Cac8 I. We used Hinc II (GT(T/C)^(A/G)AC, Roche), which cuts a random DNA sequence once every 4^5 = 1024 bases, and therefore expect only 1/4 of the force reduction

as for Cac8 I. Hinc II causes no detectable reduction in the chromosome force constant within our force resolution of 10 pN (Figure 7.5). Experiments with Hind II (GT(T/C)^(A/G)AC, Roche) produce the same result (data not shown). Even rarer 6-base-footprint enzymes Dra I (TTT^AAA, Promega, Figure 7.5), Stu I (AGG^CCT, New England Biolabs, data not shown) and Pvu II (CAG^CTG, Promega, data not shown), which cut random DNA once every 4^6 = 4096 bases, also do not produce observable force relaxation.

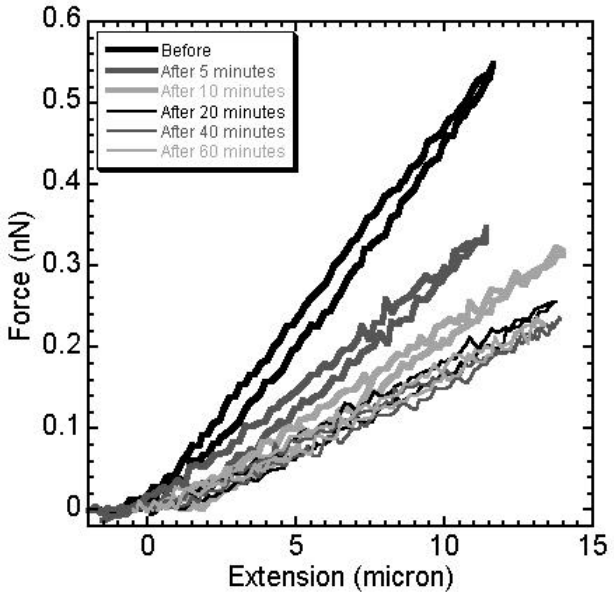

Figure 7.6 The force response after increasing exposure times of Cac8 I. The thick black plot is the force response before any digestion with Cac8 I. The additional plots are the force response following digestion with of the same chromosome with 1.2 units/îl of Cac8 I for a total of 5 (thick dark gray), 10 (thick light gray), 20 (thin black), 40 (thin dark gray) and 60 (thin light gray) minutes. The force response of the chromosome converges to a total reduction of 60%. This shows that Cac8 I has cut all of the accessible DNA within the chromosome and that a total of 60% of the force supporting elements have been severed in a chromosome cross-section.

Table III

Restriction enzyme effects on chromosome elasticity

Restriction Enzymes Name	Recognition Sequence	Statistical Frequency for bare dsDNA	Effect on Chromosomes Elasticity
Alu I	AG^CT	1 in 256	Completely cut apart
Hae III	GG^CC	1 in 256	Completely cut apart
Cac8 I	GCN^NGC	1 in 256	Reduces modulus by 60%
Hinc II	GT(T/C)^(A/G)AC	1 in 1024	No Effect
Hind II	GT(T/C)^(A/G)AC	1 in 1024	No Effect
Dra I	TTT^AAA	1 in 4096	No Effect
Pvu II	CAG^CTG	1 in 4096	No Effect
Stu I	AGG^CCT	1 in 4096	No Effect

We note that the increase in force during spraying seen in the force traces for the less effective cutters is mainly due to the reactions buffer's 6–10 mM Mg^{+2} ions, which is similar to the results in chapter 6. Figure 7.5 includes a force trace for reaction buffer with no enzyme, indicating that after spraying is complete, chromosome elastic response returns to its native value. Therefore the irreversible effects observed when an enzyme is used are due to the enzyme and not the buffer itself.

7.4 Mitotic Chromosomes have a Network Architecture Without a Large-Scale Protein Scaffold

Micrococcal nuclease and 4 bp restriction enzymes eliminate a chromosome's ability to support a force, even before any morphological change occurs. A protein scaffold with emanating chromatin loops should remain structurally sound after many cuts in dsDNA are made. Also, short exposures to micrococcal nuclease cause chromatin islands attached by thin fibers to appear and these thin fibers can be cut by micrococcal nuclease. Thus, our enzyme

experiments are inconsistent with a scaffold picture, and rule out a large-scale protein scaffold model for mitotic chromosome structure.

The reduction in elasticity by both micrococcal nuclease and 4 bp restriction enzymes directly shows that the force-supporting element within a mitotic chromosome is DNA. This implies that mitotic chromosomes must have an organization with isolated chromatin-chromatin 'crosslinks'. In other words, we must conclude that mitotic chromosomes have a 'network' architecture. This network model is also supported by the blob-link structure of Figure 7.2b, which shows the expected result for extension of a network after random scission of its links to nearly where it is broken into disconnected pieces.

7.5 dsDNA cuts every 3 kb Completely Disassemble a Mitotic Chromosome

Microdigestion with micrococcal nuclease, Alu I and Hae III demonstrates that chromosomes have a network architecture. The additional results of restriction enzymes with 6 bp recognition sites allow for an estimate of the total number of cuts made by the dsDNA cutting enzymes, providing information about the chromosome network. The main difference between the restriction enzymes used is their recognition sequences, which must be the reason for the wide range of force reduction in Figure 7.5. The two main differences in the recognition sequences used are the statistical frequency of occurrence and the length of the sequence. Both of these changes should affect the number of dsDNA cuts made within a mitotic chromosome. Figure 7.5 demonstrates that restriction enzymes with either a longer recognition site or a more specific recognition site reduce the enzymes effect on chromosome elasticity and therefore reduces the number of dsDNA cuts within a mitotic chromosome. Both Alu I and Hae III recognition sites are 4 bp in length and without redundancy so they each occur on average 1 in every $(1/4)^4$ = 256 times in a random DNA sequence. Cac8 I recognition sequence is 6 bp but

recognizes 16 different 6 bp sequences and therefore a Cac8 I recognition site will also occur on average every 1 in 256 times. Thus, the only difference between either Alu I or Hae III and Cac8 I is the length of the recognition sequence.

Surprisingly this difference in length of 2 bp causes tremendous differences on how chromosome elasticity and morphology are affected. Alu I and Hae III completely cut the chromosome apart while Cac8 I only cuts enough to reduce the modulus by 60% with no change in chromosome morphology. In addition, the cut rates at similar unit concentrations differ by 10 times. Based on this difference in rates we estimate that Alu I cuts 10 times more often than Cac8 I.

Statistically we know that Alu I cuts dsDNA 1 in 256 bp, however within a mitotic chromosome not all of the DNA will be accessible. Results of Polach and Widom, 1995 and 2001 show that the cut rate of a restriction enzyme at site within a nucleosome is reduced by 2 to 4 orders of magnitude as compared with dsDNA alone. Based on this we estimate the DNA available to be cut within a mitotic chromosome is the ratio of the linker DNA length of 20-40 bp divided by the nucleosome repeat length of about 200 bp, i.e. ~10%. We are assuming the maximum amount of accessible DNA; therefore, these estimates of cuts per length should be interpreted as an upper bound. Alu I cut on average 1 in 256 bp of the accessible DNA, it cuts a total of roughly one cut every 3 kb (12 nucleosomes). Thus, this frequency of dsDNA cuts is sufficient to completely disassemble a mitotic chromosome.

7.6 Mitotic Chromosomes are Crosslinked Every 50 kb

As mentioned above, Cac8 I cuts dsDNA within a mitotic chromosome about 1/10 as often as Alu I. This order of magnitude difference is surprising, although not completely unexpected since the length of the Cac8 I recognition sequence is 6 bp instead of 4. The estimate

that Alu I cuts 1 in every 3 kb implies that Cac8 I cuts 1 in every 30 kb. For a network architecture, reduction in force constant to 40% of native requires cutting of 60% of the links. Based on the estimate that Cac8 I cuts once per 30 kb, we estimate the length of chromatin between crosslinks in the mitotic chromosome to be 50 kb.

This also predicts that cuts less than once per 50 kb should have little affect on chromosome elasticity. This is what is seen for Hinc II and Hind II, which cut 4 times less frequently than Cac8 I or every 80 kb. Also, Dra I, Pvu II and Stu I, which cut 16 times less frequently than Cac8 I or every 320 kb have no effect on chromosome elasticity.

7.7 Conclusions

By combining dsDNA cutting enzymes with force measurement, we are able to directly observe large-scale changes in mitotic chromosome structure. The results of micrococcal nuclease, Alu I and Hae III show that dsDNA cuts more frequently than 1 in 3 kb completely disassemble mitotic chromosomes, proving that a large-scale protein scaffold does not exist within a mitotic chromosome. Instead, our results show that mitotic chromosomes can be considered to be a crosslinked network of chromatin. Experiments using restriction enzymes of differing specificity and recognition site length indicate that the average spacing between crosslinks is at least 50 kb.

CHAPTER 8

CONCLUSIONS

8.1 Interpreting Mitotic Chromosome Elasticity

Now that the elasticity of mitotic chromosomes is characterized, we need to interpret it in a biologically meaningful way by making conclusions about mitotic chromosome structure. To do this, we will first summarize the main results of this thesis. This is followed by a discussion of independent measurements that provide similar results. We will then discuss why mitotic chromosomes extracted from cells are representative of *in vivo* mitotic chromosome structure. This is vital for interpreting our results, since we are trying to understand *in vivo* mitotic chromosome structure. Based on these results a model of mitotic chromosome structure is described. Finally, additional experiments are suggested, which should provide new and exciting results.

8.2 Summary of the Experimental Results

- Young's modulus, $Y = 300$ Pa.
- Poisson ratio, $\sigma = 0.1$
- Bending rigidity, $B = 1\times10^{-22}$ J·m
- Internal viscosity, $\eta' = 100$ kg/m·sec
- Volume fraction, $\phi = 0.7$
- Extensions of less than 3 times the relaxed length are reversible.
- Extensions beyond 30 fold exhibit a force plateau at 15 nN.
- The 15 nN force plateau converts the chromosome to a disperse ghost-like state with little change in chromatin structure
- Mitotic chromosomes have an overall isotropic structure.

- dsDNA cuts more frequent than once every 3 kb cause a mitotic chromosome to disintegrate even under low applied force.
- dsDNA cuts less frequent than once every 50 kb do not affect mitotic chromosome structure.

8.3 Consistencies between Independently Measured Results

Some of the results listed in section 8.2 are supported by two or three independent measurements. The observed global isotropy is supported by three independent measurements. The Young's modulus and bending rigidity are consistent with $B = \frac{p}{4} R^4 Y$, which is based on the assumption that the structure is isotropic. Shifts in ionic conditions cause mitotic chromosomes to swell and contract isotropically. The Poisson ratio of 0.1 indicates the bulk and shear moduli are similar, which again indicates isotropy.

The internal viscosity measurement is inferred from two independent measurements. Both the step-strain relaxation time of 2 seconds and bending thermal fluctuation correlation time of 0.7 sec imply an internal viscosity of h' = 100 kg/m·sec.

The regime over which a mitotic chromosome can be extended reversibly is measured in both chapter 3 and 5. In chapter 3, we found that slow extensions beyond 3–fold display hysteresis, and that subsequently the relaxed length are permanently increased. In chapter 5, we found that decay times increase for step-strain experiments beyond 3-fold extensions and the chromosome is again permanently lengthened.

8.4 Extracted Chromosome Structure is Similar to *In Vivo* Structure

An advantage of these force-measuring techniques over the traditional electron microscopy studies is the chromosome is never removed from aqueous solution. However, the ideal experiments would be measurement of chromosome structure and elasticity *in vivo*. As

discussed earlier in section 1.3, chromosome structure may be affected by moving the chromosome to the cell culture buffer, which differs from the *in vivo* environment. Therefore, we first must address the question of whether the *in vivo* mitotic chromosome structure is altered by the extraction before using these results to understand the native structure. There are four lines of evidence that show the structure is not drastically changed by the extraction and change of surrounding solution. First, there is no obvious change in the chromosome when it is moved from the cell into the culture medium as viewed by either phase or DIC microscopy. Second, the cell culture medium has a 100 mM univalent salt concentration, a low concentration of divalent metal ions and a pH of 7.4, similar to physiological conditions. Third, the stretching elasticity of extracted and *in vivo* chromosomes are similar based on the combined results from Chapter 3 and Nicklas, 1983. Fourth, the bending rigidities of extracted and *in vivo* chromosomes are similar based on results from Chapter 4 and experiments of Marshall *et al*, 2001. We therefore conclude that mitotic chromosomes extracted into the cell culture medium are structurally representative of *in vivo* chromosomes.

8.5 A Model of Mitotic Chromosome Structure

In this section, a model of mitotic chromosome structure is presented (Figure 8.1). This model is based on the results listed in section 8.2 and is essentially a network containing crosslinks every 50 kb between which chromatin is in a highly folded state that is maintained by proteins.

The starting point of the model is with the smallest and largest length scales within a mitotic chromosome. The shortest length scale is 30 nm, the diameter of chromatin fiber, which is the lowest-level organization of dsDNA maintained throughout the cell cycle. Thus, the 30 nm chromatin fiber is the basic building block of this model. The largest length scale comes from the

restriction enzymes microdigestion experiments, which show that cuts less frequent than about 50 kb do not affect chromosome elasticity and structure. The dsDNA length of 50 kb can be converted to a distance since there are about 10^6 kb of dsDNA within a volume of 50 μm^3 for a newt mitotic chromatid (Bennett, 1977). This gives a spacing of 0.1 μm.

Next, we rule out the scaffold type model where a non-DNA structure organizes chromatin into loops. There are three lines of evidence against the scaffold model. First, as discussed in section 8.3, chromosomes are relatively isotropic, which is contrary to the inherently anisotropic scaffold model. Second and most compelling, is the microdigestion result that cuts in dsDNA cause the chromosome to loss its force supporting structure before large scale structural changes are observed in the microscope. This shows that DNA is the contiguous mechanical element of the mitotic chromosome structure and that a non-DNA scaffold does not exist within mitotic chromosomes. Third, when microdigestion is stopped so there is around 5 to 50 kb of dsDNA per cut, islands with invisible fibers connecting them are pulled out of the chromosome. In addition, dsDNA-cutting enzymes cut the invisible fibers. Cuts in dsDNA would not convert a scaffold structure to this observed island-thin fiber structure. To understand the microdigestion experiments, we conclude that large-scale mitotic chromosome structure involves chromatin fibers linked together by proteins, i.e. a network structure. A network crosslinked every 50 kb easily explains the microdigestion results (Figure 8.1). This gives an average spacing of 0.1 μm per crosslink and a total of 50,000 crosslinks within the newt mitotic chromosome volume of 50 μm^3.

The simplest type of network is an entropic gel. However, as discussed in chapters 1 and 3, an entropic gel model is ruled out by the combination of the 3-fold reversible and linear extensibility and the Young's modulus of 300 Pa. Instead of entropic random-walk-type folding

of chromatin, proteins most likely maintain the chromatin between crosslinks in a more tightly folded state (Figure 8.1). This proposed folding protein should occur about every 3 kb since dsDNA cuts at this frequency disintegrate the chromosome. Assuming there are about 6 nucleosomes in a chromatin fiber cross-section, this folding protein occurs every 30 nm along the chromatin fiber.

This model is similar to the hierarchical folding structure proposed by Belmont *et al*, 1987. The essential difference between their model and the one proposed here is the organization of the intermediate structure into a network, rather than a purely linear folding scheme.

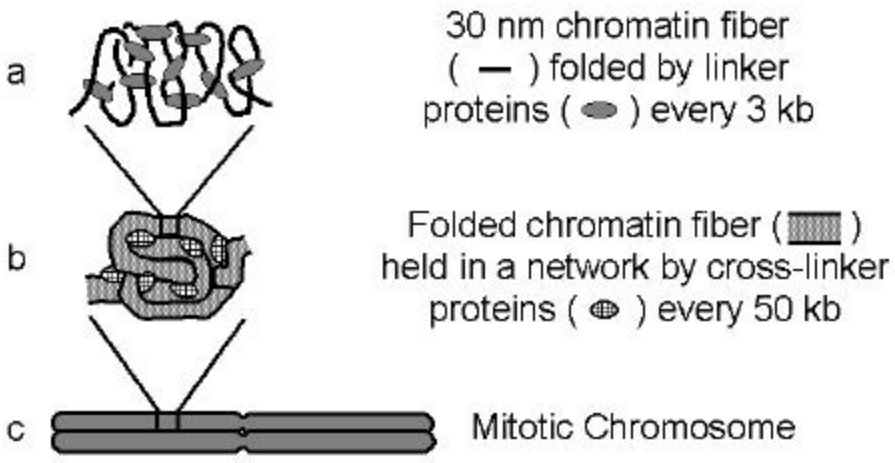

Figure 8.1 A model of mitotic chromosome structure. This model has two levels of folding. The 30 nm chromatin fiber is fold by a protein occurring every 3 kb. This fold fiber is then crosslinked every 50 kb by a second crosslinking protein.

The questions of the identity of this chromatin-folding protein which occurs every 3 kb, and how it folds chromatin are not yet addressed by our experiments. However, it is possible that the chromatin-folding protein is condensin, since they are found every 5 kb within mitotic

chromosomes (Kimura *et al*, 1999 and Hirano, 2000). Figure 8.1 shows a relatively disordered chromatin folding pattern; however, the model of Kimura *et al*, 1999, which proposes that condensins helically folds up DNA (Figure 1.6) could be the folding scheme between crosslinks.

The identity of the crosslinking protein that occurs every 50 kb is also not addressed here. One possibility is the extremely large protein titin, which is reported to be in mitotic chromosomes (Machado, 1998) and required for chromosome structure (Machado, 2000). Another possibility is this crosslinking protein has yet to be discovered.

Our model is consistent with the stretching response of mitotic chromosomes described in chapter 3. There are three regimes observed for the elastic response of mitotic chromosomes. Up to three-fold extensions reversibly deform the chromosome with a stretch modulus of 300 Pa. Extension-retractions between 3x and 30x show hysteresis and irreversibly elongate the chromosome. A force plateau of 15 nN is observed at an extension beyond 30x and converts the chromosome into a disperse ghost-like state, where the volume is increased by 20 times.

The highly folded structure provides the mitotic chromosome 3-fold extensibility and the value of the stretch modulus. A rough estimate of the stretch modulus for this folding model is the energy required to deform the folding protein to release additional chromatin length divided by the volume occupied by one chromatin folding protein. The energy scale should be on the order of a few k_BTs, about 10^{-20} Joules. The chromatin folding protein concentration is roughly the number of cuts that disintegrates a mitotic chromosome, i.e. 1 per 3 kb, which has an average spacing of about 50 nm. This indicates a Young's modulus of $Y \approx \frac{1\times10^{-20}\ J}{\left(5\times10^{-8}\ m\right)^3} \approx 100$ Pa, which is similar to the experimental modulus of 300 Pa.

The onset of irreversibility at a 3-fold extension occurs at a force of about 3 nN. At this force the crosslinking proteins begin to be irreversibly unfolded. Since they have an average

spacing of 0.1 microns, there are about 300 crosslinks in a chromosome cross-section. This gives a force of 10 pN per crosslink, which is the typical force required to start irreversibly changing protein secondary structure (Kellermayer *et al.*, 1997).

The total work done in the irreversible stretching regime of a 3-fold to 30-fold extension is $1x10^9$ k_BT: the area under the curve in Figure 3.5 from 3x to 30x extension. The work done per crosslink is thus 2×10^4 k_BT, since there are 50,000 crosslinks within a mitotic chromosome. There are about 10 times more chromatin folding proteins than crosslinking proteins, so most of the work is done on the chromatin folding proteins at 2×10^4 k_BT of work for each. Since the work done unfolding a protein by force is roughly 2 k_bT per residue (Kellermayer *et al.*, 1997), we estimate the average size of the chromatin folding protein to be about 1×10^3 aa. This number is very similar the 1200 amino acids comprising the condensin proteins SMC2 and SMC4.

The 15 nN plateau force (Figure 3.5) is likely due to the disassociation of the crosslinking proteins from the chromatin fiber. Again, since there are about 300 (now unfolded) crosslinks supporting the 15 nN of force in a chromosome cross-section, there is about 50 pN of force per crosslink. This force is similar to the force scale required to drive proteins off DNA (Bennick *et al*, 2001).

These force and energy threshold arguments show our proposed model is consistent with the observed mitotic chromosome elastic response. It also supports the suggestion made earlier that condensins are the chromatin folding proteins since they are calculated to have an average size of 1000 aa. Therefore, the chromosome force-extension behavior is consistent with reversible then irreversible unfolding and then finally disassociation of condensin-SMCs and an unknown crosslinking protein, which could be titin (Machado *et al.*, 1998).

There are at least two questions about this model. First, this model does not obviously produce a final rod-like shape observed for mitotic chromosomes. Without additional constraints, the final shape of the chromosome should be sphere-like. However, this model could produce rods instead of spheres, if there are enough initiation points along each chromosome. Each initiation point would be locally sphere-like, however enough initiation points will induce a linear organization of spheres, which is rod-like. In addition, there is evidence that the chromosomes are anchored within the nucleus (Marshall *et al*, 1997) and possibly to the nuclear envelope (Marshall *et al*, 1996). This will also localize the sphere-like organization, forcing a line of small spheres, which is again rod-like.

The second question is that this model does not provide an obvious way to help disentangle of the two sister chromatids, which must occur for the two to be separated during anaphase. Topo II is the protein which disentangles the two chromosome copies (Holm, 1994), and the details of how the network is organized needs to bias Topo II toward disentanglement of the two sister chromatids. However, there is evidence that dissentanglement is done earlier in prophase making this less of a problem (Sumner, 1991).

8.6 Future Experiments

There are many additional experiments that could be done with the current experimental setup and should provide additional information about mitotic chromosome structure. Comparing bulk modulus measurements to those made in this thesis should be extremely interesting. A measurement of the bulk modulus could be done as suggested by Marko and Siggia, 1997, with polyethylene glycol added to the buffer surrounding an isolated chromosome. This polymer should exert a concentration dependent osmotic pressure at all points on the chromosome surface. Whether or not the chromosome deforms isotropically, and the response as the osmotic

pressure is increased would be extremely interesting. Based on the value of the Poisson ratio, we expect the bulk modulus to be similar to the Young's modulus of 300 Pa.

As mentioned in section 1.5, we have not considered twist deformations. A twist deformation is volume conserving and therefore a pure shear. The twist rigidity, C is proportional to the shear modulus, μ, and for an isotropic rod is $C = (\pi/2)\mu R^4$ (Landau and Lifshitz, 1986). This is analogous to the relation between the bending rigidity and Young's modulus, as discussed in chapter 4. A measurement of the twist rigidity would directly test various chromosome structure models. A scaffold structure should have a much lower twist rigidity than what is expected from the twist-shear relation, while a network type structure should obey the twist-shear relation. Based on our results and model, a twist rigidity similar to the bending rigidity is expected, i.e. 10^{-22} J·m.

A twist deformation could be done with this setup by allowing the pipette to rotate, as in DNA experiments of (Leger *et al*, 1999), where they rotate a pipette to twist a dsDNA molecule. The major difficulty is measuring the applied torque. One possibility is to observe the shape of the chromosome for various amounts of twist. When the twist energy becomes comparable to the bending energy, the chromosome will undergo a supercoiling instability, which provides an estimate of the twist rigidity. A second possibility is to observe thermal twist fluctuations, similarly to how the bending rigidity was measured in chapter 4. This could be done by adhering sub-micron size beads to the surface and observing the bead fluctuations.

A third type of elastic deformation would be to extend the chromosome perpendicular to its axis, and could be done by sandwiching a chromosome between two pipettes, translating one of the pipettes while observing bending of the other. This would again address how homogenous mitotic chromosome structure is.

In section 2.9, it was mentioned that extracted chromosomes are usually attached end to end by invisible fibers. It would be very interesting to characterize the elastic properties of these fibers. These thin fibers are sensitive to nuclease (Maniotis *et* al, 1997) and our preliminary experiments indicate them to be very extensible suggesting DNA is highly folded within this fiber. Additional experiments may show these fibers contain chromatin folded in a manner similar to the folded state found within mitotic chromosomes.

It may be possible to pull a chromatin fiber or the proposed intermediate fiber out of a mitotic chromosome with micron sized beads labeled with an antibody for either histones or SMCs. A pipette could hold the labeled bead and monitor the force as an attached fiber is pulled out providing additional information on how chromatin is folded within a mitotic chromosome.

Additional microdigestion experiments should be done with restriction enzymes that cut dsDNA and leave ssDNA overhangs. Our preliminary experiments show that Msp I, which cuts a 4 bp site and leaves a 2 bp overhang, does not disintegrate mitotic chromosomes like Hae III and Alu I, which have the same size recognition site and statistical cut frequency. Understanding how the ssDNA overhangs change the effect of restriction enzymes on chromosome elasticity will provide additional structural information.

Microspray experiments with enzymes other than dsDNA cutters should be straightforward and extremely interesting. Some specific suggestions of enzymes to use are:

- Trypsin, which cuts proteins at any serine or arginine.
- Proteinase K, which cuts proteins between almost any amino acid.
- Protein phosphatase, which dephosphoralates serine and threonine residues.
- Topoisomerase I, which relaxes twist in dsDNA.

Elasticity experiments with either trypsin or proteinase K would demonstrate proteins overall role in maintaining chromosome structure. We expect an effect since Maniotis *et al*, 1997 showed that groups of mitotic chromosomes disperse when exposed to trypsin and then recondense when exposed to histone H1. There is evidence that the phosphoralation of certain histones plays a role in chromosome condensation (Hirano, 2000). Single-chromosome elasticity measurements during an exposure to a protein phosphatase may indicate aspects of chromosome structure that depend on protein phosphoralation. Combining elasticity experiments with exposures of Topoisomerase I should indicate if supercoiling plays a structural role. There are models that propose supercoiling as a means of condensing mitotic chromosomes (Koshland and Strunnikov, 1996). Preliminary experiments with Topo I show no effect on chromosome elasticity, indicating dsDNA within mitotic chromosomes is not highly torsionally constrained.

In section 1.7, it was mentioned that combining fluorescence imaging with elasticity measurements should provide structural information. In collaboration with Dr. Tatsuya Hirano's lab, preliminary experiments where single mitotic chromosomes were labeled with fluorescent anti-bodies for XCAP-E (a *Xenopus* SMC) show helical arrangement with additional coils appearing as the chromosome is extended. More experiments with these antibodies may help in understanding condensins role in maintaining chromosome structure.

Experiments that selectively disrupt condensin function would be extremely interesting. Previous experiments by Hirano and Mitchison, 1994 show that adding antibodies for XCAP-E to a *Xenopus* mitotic extract causes condensed sperm chromatin to puff up. We attempted a similar experiment by labeling both newt and *Xenopus* mitotic chromosomes with anti-XCAP-E. However, we did not observe the same puffing, instead a slight increase in elasticity was observed. It may be possible to more effectively disrupt XCAP-E's function with Chromophore-

assisted laser inactivation (Beerman and Jay, 1994). This involves labeling XCAP-E with an antibody, which has a fluorophore that when exposed to a laser beam of a certain wavelength generates hydroxyl radicals, which cut proteins by hydrolysis (Liao *et al*, 1994).

Observation of how an inhomogeneous fluorescence pattern in a mitotic chromosome changes as it is elongated would probe mitotic chromosome structure. Inhomogeneous labeling could be done by first labeling an isolated chromosome with fluorescent anti-histone as in chapter 3 or with the dsDNA dye, DAPI, and then photobleaching a fluorescent band. This would make a line along the cross-section of the chromosome and the shape of this line could be observed as the chromosome is stretched. A more sophisticated way to inhomogeneously label chromosomes is to bead load fluorescent dUTP into a cell, which then is incorporated into the chromosomes during S-phase (Manders *et al*, 1999). Ms. Chee Xiong is currently doing this in the Marko lab. Due to sequence inhomogeneities along the DNA, a speckled pattern should be produced, similar to speckling observed on statistically labeled microtubules (Waterman-Storer and Salmon, 1997). A change in the speckle pattern could be observed as the chromosome is stretched.

Ultimately, we would like to transfect either the TVI or A6 cell lines with the GFP labeled *lac*-repressor gene and multiple *lac*-operator arrays (Robinett *et al*, 1996 and Belmont, 2001). This would label the chromosomes with fluorescent spots, which could be tracked as the chromosome is stretched. Additional uses of GFP technology such, as GFP-condensin would be extremely interesting.

8.7 Final Remarks

This thesis characterizes the elasticity of mitotic chromosomes and shows that elasticity measurements provide a sensitive assay for structural changes within mitotic chromosomes. Not

only do elasticity measurements provide structural information, but also by combining them with biochemical techniques, we are able to make direct observations of mitotic chromosome structure. In addition to the studies of this thesis, there are many possibilities for further micromechanical-biochemical studies of mitotic chromosomes.

APPENDICES

Appendix A

Thermal Bending Fluctuations of a Rod

Here we show how the bending rigidity is related to thermal fluctuations, in the limit where those fluctuations are small. The chromosome is considered to be a uniform straight rod of length L that lies along the x-axis and undergoes small fluctuations u ($u << L$) in the y direction. Fluctuations in the z-direction play no role in our analysis and may be ignored.

The position of the rod is described by the vector $\vec{r}(s)$, where s is the position along the rod. For the case that $u << L$, $s \approx$ x, the tangent vector $\hat{t} \approx \hat{x}$ and the curvature $\kappa \approx \frac{d^2u}{dx^2}$. The equation of motion for the case of hydrodynamically damped stiff rod is $B\frac{\partial^4 u}{\partial x^4} + \eta\frac{\partial u}{\partial t} = 0$ (Gittes *et al*, 1993). In chapter 5, a more general case will be discussed which includes not only hydrodynamic damping, but damping due to internal viscous losses. The equation of motion for this turns out to be, $B\frac{\partial^4 u}{\partial x^4} + \eta\frac{\partial u}{\partial t} + \eta'\frac{\partial}{\partial t}\frac{\partial^4 u}{\partial x^2} = 0$.

For either case, the time dependence of u is $e^{-t/\tau}$, which can be factored out, resulting in the form (Rayleigh, 1945)

$$\frac{d^4u(x)}{dx^4} = \frac{k^4}{L^4}u(x). \qquad \text{(A.1)}$$

The general form of the solution is

$$u_k(x) = N\,[A\sin(k\alpha) + B\sinh(k\alpha) + C\cosh(k\alpha) + D\cosh(k\alpha)], \text{ (A.2)}$$

where $\alpha = x/L$ and N is the normalization constant. We are considering a straight rod which is clamped at $x = 0$ and free at $x = L$, and has the four boundary conditions:

Appendix A (continued)

$$(1)\qquad u_{x=0}=0 \qquad\qquad (2)\qquad \left(\frac{du}{dx}\right)_{x=0}=0$$

$$(3)\qquad \left(\frac{d^2u}{dx^2}\right)_{x=L}=0 \qquad\qquad (4)\qquad \left(\frac{d^3u}{dx^3}\right)_{x=L}=0$$

These boundary conditions determine A, B, C and D. It is easier it see how to satisfy the boundary conditions if we rewrite Eq. (A.1) as

$$u(x)=N\begin{bmatrix} A'(\sin k\alpha+\sinh k\alpha)+B'(\sin k\alpha-\sinh k\alpha) \\ +C'(\cos k\alpha+\cosh k\alpha)+D'(\cos k\alpha-\cosh k\alpha)\end{bmatrix}. \quad \text{(A.2)}$$

Right away one sees that B.C. (1) and (2), require A' and C' to be zero. After some arithmetic, one finds B.C. (3) and (4) set B' = (sin(k) − sinh(k)) and D' = (cos(k) + cosh(k) where k has discrete values determined by

$$\cos k\cdot\cosh k=-1. \qquad \text{(A.3)}$$

The first six values of k are k_1=1.8751, k_2=4.6941, k_3=7.8548, k_4=10.9955, k_5=14.1372 and k_6=17.2788 (Raleigh, 1945), and for large k_n, it becomes $(2n-1)\pi/2$. Therefore,

$$u(x)=N\begin{bmatrix}(\sin k-\sinh k)(\sin k\alpha-\sinh k\alpha) \\ +(\cos k+\cosh k)(\cos k\alpha-\cosh k\alpha)\end{bmatrix} \qquad \text{(A.4)}$$

and the normalization constant, N, is

$$N^2=\frac{1}{4k}\begin{bmatrix}(\sin k-\sinh k)^2[(\sinh 2k-\sin 2k)-4(\cosh k\sin k-\sinh k\cos k)] \\ +(\cos k+\cosh k)^2[4k+(\sinh 2k-\sin 2k)-4(\sinh k\sin k-\cosh k\cos k)] \\ +2(\sin(k)-\sinh(k))(\cos(k)+\cosh(k))[\cosh 2k-\cos 2k-4\sinh k\sin k]\end{bmatrix}. \quad \text{(A.5)}$$

Appendix A (continued)

The set of u_k are orthogonal (Raleigh, 1945) and complete since it is the set of eigenfunctions to the self-adjoint differential operator, $\frac{d^4}{dx^4}$, with the above boundary conditions. Now we can consider the case of a rod subjected to thermal fluctuations. We can write down the shape of a deformed rod deformed as a sum of the bending modes, $u = \sum_k a_k u_k$. The bending energy is described by $E = \frac{B}{2}\int_0^L ds\,\boldsymbol{k}^2 \approx \frac{B}{2}\int_0^L dx\left(\frac{d^2u}{dx^2}\right)$. After plugging in for the curvature, we find

$$E = \frac{B}{2}\sum_{k,l}\frac{k^2}{L^2}\frac{l^2}{L^2}a_k a_l L\int_0^1 d\boldsymbol{a}\,\boldsymbol{k}_k(\boldsymbol{a})\boldsymbol{k}_l(\boldsymbol{a}), \qquad \text{(A.6)}$$

$$\text{where } \boldsymbol{k}_k(x) = N\left[\begin{array}{l}(\sin k - \sinh k)(-\sin k\boldsymbol{a} - \sinh k\boldsymbol{a}) \\ +(\cos k + \cosh k)(-\cos k\boldsymbol{a} - \cosh k\boldsymbol{a})\end{array}\right]. \qquad \text{(A.7)}$$

Like u_k, $\boldsymbol{k}_k$ is also orthonormal, so

$$E = \frac{B}{2}\sum_{k,l}\frac{k^2l^2}{L^3}a_k a_l\boldsymbol{d}_{kl} = \frac{B}{2}\sum_{k,l}\frac{k^4}{L^3}a_k^2 \qquad \text{(A.8)}$$

Since the energy is quadratic for each bending mode, k, the equipartition theorem tells us that $\langle a_k^2\rangle = \frac{k_BTL^3}{Bk^4}$ and $\langle a_k a_l\rangle = 0$ for $k \neq l$. Note that for $L << B/k_BT$, these amplitudes are small, and that the lowest k mode dominates by a factor ~3^4.

We can now calculate $\langle u^2\rangle$

$$\langle u^2\rangle = \frac{k_BTL^3}{B}\sum_k\frac{u_k(x)}{k^4} = \frac{k_BTL^3}{B}f(x/L). \qquad \text{(A.9)}$$

Appendix A (continued)

Numerical analysis shows that the function *f(x/L)* is within 1.5 percent of $\frac{32x^3}{\pi^4 L^3}$ for $0<x<L$. We can therefore approximate Eq. (A.9) with $\left\langle u^2 \right\rangle = \frac{32K_B T x^3}{\pi^4 B}$.

Appendix B

Newt Lung Cell Culture Protocols

Newt Cell Culture Medium (NCCM)

- Combine
  - 250 ml of L-15 (CellGro
  - 40 ml of FBS (BioWhittaker)
  - 210 ml of Pure water (BioWhittaker)
  - 5-5.5 ml of Pen/Strep
- Filter sterilize.
- Store at 4 C.

Preparing Dialysis Filters

- Store the dialysis filter at 4 C.
- Cut out twelve 6 cm diameter circles from the dialysis filters with a clean surgical blade.
- Wash a 250 ml beaker with EtOH and rinse with clean water.
- Fill the beaker with 50 ml of autoclaved water.
- Soak the circles overnight in the water at 4 C.
- Transfer the circles to a beaker with NCCM and soak them for 24 hours at 4 C.
- The dialysis filter circles can be stored for up to 2 weeks in NCCM at 4 C.

Cleaning and assembling cell culture dishes

- Turn on the hot plate to melt a beaker of paraffin.
- Wash 6 culture dishes (60x15 mm, Falcon) with a 3 cm diameter hole cut out of the bottom thoroughly with soap and water, followed by through rinsing.
- Wash 6 teflon rings with soap and water followed by thorough rinsing.
- Clean nine 4 cm diameter #1 cover glass (Fisher) with Sparkle.
- Soak the culture dishes, teflon rings and cover glass for 1-2 hours in 70% EtOH.
- Use the Nitrogen gas to dry off the culture dishes, cover glass and teflon rings
- Use a pasteur pipette to apply a ring of melted on the inside of each culture dish
- Place a cover glass on top of the wax, which has solidified by now.
- Place the culture dish on the hot plate, this will melt the wax. The melted wax will then wet the cover glass and culture dish. This will glue and seal the cover glass to the culture dish.
- UV irradiate the teflon rings, assembled culture dishes and lids for 30-60 minutes.
- Be sure to flip the teflon rings so that both sides are UV irradiated.
- The dishes and rings can be used immediately are stored in a clean pipette tip box.

Appendix B (continued)

Dissecting the newt

- Soak surgical scissors, forceps, dissection pan, and scapul in 70% EtOH for at 2 hours.
- Dry with Nitrogen.
- Submerge a male Newt (Notophthalmus viridescens, Connecticut Valley) in 300 ml of 1 mg/ml tricaine (Acros) for 20 minutes. This kills the Newt.
- Rinse the newt with deionized water to remove excess gunk.
- Place the newt on its back and pin down the legs, arms and tail.
- With the surgical scissors make an incision under the abdominal region, between the two legs.
- Make two incisions along both sides of the newt, from the leg to the arm.
- Pull the abdominal skin up over the head and the pin it down.
- With the tweezers move the organs around to look for the lungs, taking care not to puncture them.
- Pull out each lung up with the tweezers using the scissors to cut any connective tissue.
- Place each lung into a culture dish with a thin layer of NCCM.
- Cut off tissue which is still attached to the lungs with the scapul
- Cut the lungs into 1 mm^2 pieces with the scapul.
- Transfer the 1 mm^2 pieces into a new cell culture dish with 10 ml of NCCM
- Add 100 µl of stock fungazone to the dish.
- Incubate the lung fragments in NCCM over night at room temperature.

Growing the newt lung cell cultures

- With a transfer pipette place 3-5 newt lung fragments into a clean cell culture dish with a glass bottom.
- Place a dialysis filter circle over the lung fragments. Be sure the fragments are in the center of the dish with a space of a few mm between each fragment.
- Gently press on each lung fragment with the tip of the transfer pipette to help them stick to the glass.
- Place a teflon ring over the dialysis filter.
- Fill the dish with NCCM.
- Add 100 µl of fungazone, 5 µg/ml.
- Repeat this for the other five cell culture dishes with glass bottoms.
- Keep the dish at room temperature (~25 C).
- After 3-5 days cells begin to migrate out onto the glass.
- After the 5-7 days carefully remove the dialysis filter and replace the NCCM.
- Mitotic activity is typically greatest after 7-10 days.
- After 14 days the mitotic activity has stopped the culture dishes can be disposed into a Biohazard container.

Appendix C

Amphibian Cell Line Protocols

Cell Freezing

- Start with a 250 ml flask which is ~90% confluent with the cells.
- Pipette off Cell Culture Medium (NCCM).
- Add 10 ml of 60% PBS and wait 30-60 seconds.
- Pipette off 60% PBS
- Add 3 ml of 0.15% Trypsin in 60% Hanks Buffered Saline Solution.
- Wait 60 secs.
- Pipette of 2 ml of the 0.15% Trypsin.
- Wait till most of the cells are come off the surface, 3 to 5 minutes.
- Add 9 ml of NCCM with 5% DMSO
- Pipette NCCM with 5% DMSO and cells 5 times. Be gentle because the DMSO causes the cell membrane to become fragile.
- Divide cell supension into 6 cryotubes with 1.5 ml each.
- Put the tubes into a styrofoam contain and the put into –80 C freezer overnight.
- Remove the tubes from the –80 C freezer and put into liquid N_2.
- A day after to putting the frozen cells into N_2, thaw 1 tube and check that a culture starts again.

Cell Thawing

- Warm the heat bath to 37 C.
- Add 10 ml of NCCM to a 75 ml flask.
- Remove 1 tube of cells frozen in liquid N_2.
- Gently shake the tube of cells in the 37 C heat bath.
- Once the cell suspension has thawed, add it to the 75 ml flask.

Subculturing A6 and TVI cell lines

- Wait till the culture is 90% confluent in the original flask.
- Add 10 ml of NCCM to two 70 ml cell culture flasks with vented caps.
- Remove the NCCM from the original flask.
- Add 6 ml of 60%PBS to the flask with cells.
- Gently rock the flask for 30 seconds.
- Pipette off the 60% PBS
- Add 1 ml of 0.15%trypsin in 60%HBSS
- Incubate for 2 to 5 minutes and flick the bottom of the flask to help knock the cells off the surface. If the cells are not coming off incubating at 35 C may help.
- Add 5 ml of NCCM

Appendix C (continued)

- Pipette the NCCM with cells up and down 10 times. This helps break up clumps of cells into individual cells.
- Add between 0.3 and 1.5 ml of the cell suspension to each new flask. (Recommend adding 0.3 ml to one flask and 1 ml to the second flask.)
- If the cap to the flasks are vented, screw them on tight. If the cap is not vented, leave the cap loose so air can exchange between the flask and the room.

Replacing culture medium

- Cell culture medium should be replaces every 2-3 days for A6 cells and every 5-7 days for TVI cells.
- Warm NCCM to room temperature.
- Remove the NCCM (about 10 ml).
- Add 10 ml of NCCM.

Appendix D

Microdishes

Microculture dishes

- Each dish is made from 2 silicon rings with an outer diameter of 2.56 cm and a wall thickness of 1 mm (020, McMaster) and a 35x50 mm #1 cover glass (Fisher).
- 6 rings have a 2.5 mm gap cut out of it. The other 6 rings have a v cut out of the bottom, which is 2.5 mm at the bottom and ends about 2/3 from the top of the ring.
- Wash the 6 cover slides with sparkle
- soak the cover glass and silicon rings in 70% ETOH for 1 hour.
- The rings and glass are then dried with nitrogen.
- A ring with the gap is place on a cover slide and a ring with a v is place on the gap ring with the v and gap aligned.
- The rings are attached to the glass and each other with paraffin.
- The side opening is lined with paraffin.
- After assembly, the dishes are UV irradiated for 30 minutes and then stored in a clean, UV irradiated pipette tip box.

Starting cell cultures in microdishes

- Rinse an old 1-200 ìl pipette box and rack with 70% ethanol for 1 hour
- UV irradiate the box and rack for 30 minutes.
- Put the rack in the box and place 2 microdishes on the rack and UV irradiate for 30 minutes.
- Pipette in to the bottom of the box 25 ml of clean water. Subculture a 90% confluent 70 ml flask of TVI or A6 of cells.
- Place 2-5 drops of the cell suspension produced from subculturing and then add 1.0-1.5 ìl of NCCM to each dish. Usually 2 drops are put into one microdish and 5 drops are put into the other microdish.
- Replace the NCCM every 1-2 days. The cells usually spread out after 2-3 days for TVI and 1-2 days for A6 cells after which they are ready for experiments. The cell cultures in the microdishes become over grown after 7-10 days for TVI and 3-5 days for A6.

Setting up a microdish for an experiment

- Place a microdish on a microscope plate with a mount to hold a micropipette.
- With the 1000 ìl pipetter, scrap off a 1mm wide area with goes from the side opening of the dish to the center.
- Wash the microdish with some NCCM and then fill the dish with 1.5 ml of NCCM.
- Prepare a force measuring pipette filled with 60% PBS (Biowhittaker).
- Align the side opening of the dish with the pipette mount and fix the microdish to the microscope plate with scotch tape.
- Slide the force pipette through the side of the dish.

- Attach tubing to a reservoir to the force measuring pipette.
- Place the microscope plate on the microscope.
- While viewing with the 10x objective, position the force measuring pipette 20-30 ìm above the glass where the cells have been removed.
- Prepare two stiff pipettes, one filled with 10 mg/ml BSA in 60% PBS and the other with the tip filled with 0.05% Triton-X (FisherBiotech) in 60% PBS.
- The force measuring pipette position should be tracked for 60 seconds to check if there is much drift. The level of the microscope plate should be adjusted so that the drift is reduce to < 0.01 ìm/sec.
- Set the stage position to zero so that the force pipette can be moved back into view after a chromosome is isolated.

Appendix E

Separating Labeled Antibody From Free Dye

Prepare of Micro-Spin columns

- Store at 4 C (DO NOT FREEZE)
- Invert the column sharply several times to resuspend the settled gel and remove any bubbles. Snap off the tip and place the column in a 2.0 ml microcentrifuge tube. Now remove cap.
- Centrifuge for 2 minutes in a microcentrifuge at 1000x(g).
- Place the column in a clean 1.5 ml microcentrifuge and add 500 µl of Blocking Solution (5 mg/ml BSA in PBS).
- Centrifuge for 2 minutes at 1000x(g).
- Repeat steps 4 and 5.
- Place the column in a clean 1.5 ml microcentrifuge and add 500 µl of PBS.
- Centrifuge for 2 minutes at 1000x(g).
- Repeat steps 7 and 8 twice.
- Load the about 20-30 ìl of the labeling reaction solution onto the column and spin at 1000x(g) for 4 minutes.
- The labeled protein is in the tube and the free dye is still in the column. 1-2 weeks storage, keep at 4 C; 1-2 months storage, keep at –20 C; longer then 2 months storage keep in Liquid Nitrogen.

Appendix F

Pipette Fabrication

Borosilicate pipettes with 1 mm outer diameter and 0.7 mm inner diameter (WPI) are pulled by a micropipette puller (P-97, Sutter). These pipettes have a ramp value = 467. The force measuring pipette are made with the following settings:

Heat = ramp value + 40, Pull = 150, Vel. = 160, Time = 47, Pressure = 500.

The stretching pipettes are pulled with the following settings:

Heat = ramp value – 17, Pull = 100, Vel. = 120, Time = 50, Pressure = 500.

After the micropipettes are pulled, a micropipette forge cuts the tip to have an inner diameter of about 2 microns. The forge is a standard microscope with a 10X objective, and with a 0.5 mm-long, 0.1 mm-diameter platinum wire (Fisher) mounted below the lens and connected in series to a power supply with a power resister (16 Ohm, 150 Watt). A small bead of borosilicate glass is melted onto the platinum wire while the current = 3.5 A. Before each cut, the current is set to 3.5 Amp for 1 minute, during which the wire is glowing. The current is then set to about 2.2 A, so that the wire expands out but is not glowing. The micropipette is then brought into contact with the glass bead, and the current is then turned off. The wire retracts, resulting in a clean break at the point where the pipette was in contact with the glass bead (Brown and Flaming, 1986).

CITED LITERATURE

Aaronson, R.P. and Woo E. Organization in the cell nucleus: divalent cations modulate the distribution of condensed and diffuse chromatin. *J. Cell Biol.* 90:181-186, 1981.

Adolph, K.W. *Chromosomes and Chromatin*, Boca Raton, CRC Press, 1988.

Alberts, B., Bray, D., Lewis, J., Raff, M., Roberts, K. and Watson, J. *Molecular Biology of the Cell*, New York, Garland Press, 1994.

Arbe, A., Monkenbusch, M., Stellbrink, J., Richter, D., Farago, B., Almdal, K. and Faust R. Origin of internal viscosity effects in flexible polymers: A comparative neutron spin-echo and light scattering study on poly(dimethylsiloxane) and polyisobutylene *Macromolecules* 34:1281-90, 2001.

Ausio, J., Borochov, N., Seger, D. and Eisenberg, H. Interaction of chromatin with NaCl and $MgCl_2$. *J. Mol. Biol.* 177:373-398, 1984.

Beermann, A.E.L. and Jay, D.G. Chromophore-assisted laser inactivation of cellular proteins. *Meth. Cell Biol.* 44:715-732, 1994.

Belmont A.S., J. W. Sedat, D. A. Agard, A Three-dimensional approach to mitotic chromosome structure: evidence for a complex hierarchical organization. *J. Cell Biol.* 105:77-92, 1987.

Belmont, A.S. Visulaizing chromosome dynamics with GFP. *Trends Cell Biol.* 11:249-256, 2001.

Bennett, M.D. The Time and Duration of Meiosis. *Phil. Trans. Roy. Soc. Lond.* B277:201-226, 1977.

Bennick, M.L., Leuba, S.H., Leno, G.H., Zlatanova, J., De Grooth, G.H. and Greve, J. Unfolding individual nucleosomes by stretching single chromatin fibers with optical tweezers. *Nat. Struc. Biol.* 8:606-610 2001.

Biggins, S., A.W. Murray. 1998. Sister chromatid cohesion in mitosis. *Curr Opin Cell Biol.* 10, 769-775.

Bloomfield V.A. Condensation of DNA by multivalent cations: considerations on mechanism. *Biopolymers* 31:1471-1481, 1991.

Bojanowski, K. and Ingber, D.E. Ionic control of chromosome architecture in living and permeabilized cells. *Exp. Cell Res.* 244:286-294, 1998.

Bojanowski, K., Maniotis, A.J., Plisov, S., Larsen, A.K. and Ingber, D.E. DNA topoisomerase II can drive changes in higher order chromosome architecture without enzymatically modifying DNA. *J. Cell. Biochem.* 69:127-142, 1998.

Borochov, N., Ausio J. and Eisenberg, H. Interaction and conformational changes of chromatin with divalent ions. *Nucleic Acids Res.* 12:3089-3096. 1984.

Boy de la Tour, E. and Laemmli, U. K. The metaphase scaffold is helically folded: sister chromatids have predominantly opposite helical handedness. *Cell* 55:937, 1988.

Brown, K. T. and Flaming, D. C. *Advanced Micropipette Techniques For Cell Physiology*, New York, John Wiley & Sons, 139-141, 1986

Bustamente, C., J.F. Marko, E.D. Siggia, and S. Smith. Entropic elasticity of lambda-phage DNA. *Science* 256:1599-1600. 1994.

Burlingame, R.W., Love, W.E., Wang, B.C., Hamlin, R., Nguyen, H.X. and Moundrianakis, E.N. Crystallographic structure of the octomeric hitone core of the nucleosome at a resolution of 3.3 A. *Science* 228:546-553, 1985.

Champoux, J.J. DNA topoisomerase: structure, function and mechanism. *Annu. Rev. Biochem.* 70:369-413, 2001.

Claussen, U., Mazur, A., and Rubstov, N. Chromosomes Are Highly Elastic and Can Be Stretched. *Cytogenet. Cell Gen.* 66:120-125. 1994.

Cluzel, Ph., Lebrun, A., Heller, C., Lavery, R., Viovy, J-L., Chatenay, D. and Caron, F. DNA: an extensible molecule. *Science* 271:792-794, 1996.

Cruz, E.M. and Pollard, T.D. Kinetics and thermodynamics of phalloidin binding to actin filaments from three divergent species. *Biochemistry* 12:14054-61, 1996.

Cui, Y. and Bustamante, C. Pulling a single chromatin fiber reveals the forces that maintain its higher-order structure. *Proc. Natl. Acad. Sci. USA* 97:127-132, 2000.

De Gennes, P. G. Reptation of stars. *J. Phys. (Paris)* 36:1199-1203, 1975.

P. G. de Gennes *Scaling Concepts in Polymer Physics*, Ithica, New York, Cornell University Press, 230-233, 1979.

Dietzel S. and Belmont, A.S. Reproducible but dynamic positioning of DNA within chromosomes during mitosis. *Nat. Cell Biol.* 3:767-770, 2001.

Doi, M. and Edwards, S.F. *Theory of Polymer Dynamics*, Oxford, Oxford University Press, 91-99,1988.

Earnshaw, W.C. and Laemmli, U.K. Architecture of metaphase chromosomes and chromosome scaffolds. *J. Cell Biol.* 96:84-93, 1983.

Fritzsche, W. and Henderson, E. Mapping Elasticity of Rehydrated Metaphase Chromosomes by Scanning Force Microscopy. *Ultramicroscopy* 69:191-200, 1997.

Fritzsche, W. Salt-dependent chromosome viscoelasticity characterized by scanning force microscopy-based volume measurements. *Microsc. Res. Tech.*44:357-362, 1999.

Geissler, E. and Hecht, A. M. The poisson ratio in Polymer gels 2. *Macromolecules* 14:185-188, 1981.

Gelbart, W.M., Bruinsma, R.F., Pincus, P.A. and Parsgian, V.A. DNA-inspired electrostatics. *Physics Today* 53:38-44, 2000.

Gittes, F., Mickey, B., Nettleton, J. and Howard, J. Flexural rigidity of microtubules and actin filaments measured from thermal fluctuations in shape. *J. Cell Biol.* 120:923-34 1993.

Gosule, L.C. and Schellmann, J.A. Compact form of DNA induced by spermidine. *Nature* 259:333-335, 1976.

Guacci, V., Koshland, D. and Strunnikov, A. A direct link between sister chromatid cohesion and chromosome condensation revealed through the analysis of MCD1 in *S. cerevisiae. Cell* 91:47-57, 1997.

Hagerman, P.J. Flexibility of DNA. *Annu. Rev. Biophys. Bio.* 17: 265-286, 1988.

Harnau, L. and Reineker, P. Equilibrium and dynamical properties of semiflexible chain molecules with confined transverse fluctuations. *Phys. Rev. E* 60:4671-6, 1999.

Hegner, M., Smith S.B. and Bustamante, C. Polymerization and mechanical properties of single RecA-DNA filaments. *Proc. Natl. Acad. Sci. USA* 96:10109-14 1999.

Heck, M.M. Condensins, cohesins, and chromosome architecture: How to make and break a mitotic chromosome. *Cell* 91:5-8, 1997.

Helfer, E., Harlepp, S., Bourdieu, L., Robert, J., MacKintosh, F.C. and Chatenay, D. Microrheology of biopolymer-membrane complexes, *Phys. Rev. Lett.* 85:457-460 2000.

Hirano, T. and Mitchison, T.J. Topoisomerase II does not play a scaffolding role in the organization of mitotic chromosomes assembled in *Xenopus* egg extracts. *J. Cell Biol.* 120:601-612, 1993.

Hirano, T. and Mitchison, T.J. A heterodimeric coiled-coil protein required for mitotic chromosome condensation *in vitro*. *Cell* 79, 449-458, 1994.

Hirano, T. SMC Protein Complexes and Higher-Order Chromosome Dynamics. *Curr. Opin. Cell Biol.* 10:317-322, 1998.

Hirano, T. Chromosome cohesion, condensation, and separation. *Annu. Rev. Biochem.* 69:115-144, 2000.

Hohenadl, M., Storz, T., Kirpal, H., Kroy K. and Merkel, R. Desmin filaments studied by quasi-elastic light scattering, *Biophys. J.* 77:2199-209, 1999.

Holm, C. Coming undone: how to untangle a chromosome. *Cell* 77:955-957, 1994.

Horowits, R. and Podolsky, R.J. The positional stability of thick filaments in activated skeletal muscle depends on sarcomere length: evidence for the role of titin filaments. *J. Cell Biol.* 105:2217-2223, 1987.

Houchmandzadeh, B., Marko, J. F., Chatenay, D. and Libchaber, A. Elasticity and structure of eukaryote chromosomes studied by micromanipulation and micropipette aspiration. *J. Cell Biol.* 139:1-12, 1997.

Houchmandzadeh, B. and Dimitrov, S. Elasticity measurements show the existence of thin rigid cores inside mitotic chromosomes. *J. Cell Biol.* 145:215-223. 1999.

Kellermayer, M. S. Z., Smith, S. B., Granzier, H. L. and Bustamante, C. Folding-unfolding transitions in single titin molecules characterized with laser tweezers. *Science* 276:1112-1116, 1997.

Kimura, K., Rybenkov, V.V., Crisona, N.J., Hirano, T., Cozzarelli, N.R. 13S condensin actively reconfigures DNA by introducing global positive writhe: implications for chromosome condensation. *Cell* 98:239-248, 1999.

Kleckner, N. Meiosis: how could it work? *Proc. Natl. Acad. Sci. USA* 93:8167-8174, 1996.

Klug, A., Rhodes, D., Smith, J., Finch, J.T. and Thomas, J.O. A low resolution structure for the histone core of the nucleosome. *Nature* 287:509-516, 1980.

Koshland, D. Mitosis: Back to the Basics. *Cell* 77:951-954, 1994.

Koshland, D. and Strunnikov, A. Mitotic chromosome condensation. *Annu. Rev. Cell Dev. Biol.* 12:305-333, 1996

Landau, L.D. and Lifshitz, E.M. *Fluid Mechanics*, New York, Pergamon Press, 58-64, 1987.

Landau, L.D. and Lifshitz, E.M. *Theory of Elasticity*, New York, Pergamon Press, 1986.

Landau, L.D. and Lifshitz, E.M. *Mechanics*, New York, Pergamon Press, 74-77, 1976

Larson, R.G. *The Structure and Rheology of Complex Fluids*, New York, Oxford University Press, 12-18, 1999.

Laskey, R.A., Mills, A.D. and Morris, N.R. Assembly of SV40 chromatin in a cell-free system from Xenopus eggs. *Cell* 10:237-243, 1977.

Leger, J.F., Robert, J., Bordieu, L., Sarkar, A., Chatenay, D. and Marko, J.F. Structural transformations of a twisted and stretched DNA. *Phys. Rev. Lett.* 83:1066-1069, 1999.

Lemon, K.P. and Grossman, A.D. Movement of replicating DNA through a stationary replisome. *Mol. Cell.* 6:1321-1330, 2000.

Leno, G.H. 1998. Cell-free systems to study chromatin remodeling. *Methods Cell Biol.* 53:497-515, 1998.

Lever, M.A., Th'ng, J.P.H., Sun, X. and Hendzel, M.J. Rapid exchange of histone H1.1 on chromatin in living human cells. *Nature* 408:873-876, 2000.

Liao, J.C., Roider, J. and Jay, D.G. Chromophore-assisted laser inactivation of proteins is meiated by the photogeneration of free radicals. *Proc. Natl. Acad. Sci. USA* 91:2659-2663, 1994.

Losada, A., Hirano, M. and Hirano, T. Identification of *Xenopus* SMC protein complexes required for sister chromatid cohesion. *Genes & Dev.* 12:1986-1997, 1998.

Love, A.E.H. *A Treatise on the Mathematical Theory of Elasticity,* New York, Dover, 1944.

Luger, K., Mader, A.W., Richmond, R.K., Sargent, D.F. and Richmond, T.J. Crystal structure of the nucleosome core particle at 2.8 A resolution. *Nature* 389:251-60, 1997.

Machado, C., Sunkel, C.E. and Andrew, D.J. Human autoantibodies reveal titan as a chromosomal protein. *J. Cell Biol.* 141:321-333, 1998.

Machado, C. and Andrew, D.J. Chromosomes and Muscles. *J. Cell Biol.*151:639-651, 2000.

Manders, E.M.M., Kimura, H. and Cook, P.R. Direct imaging of DNA in living cells reveals the dynamics of chromosome function. *J. Cell Biol.* 144:813-821, 1999.

Maniotis, A.J., Bojanowcki, K. and Ingber, D.E. Mechanical continuity and reversible chromosome disassembly within intact genomes removed from living cells. *J. Cell Biochem.* 65:114-130, 1997.

Marko, J.F. and Siggia, E.D. Stretching DNA *Macromolecules* 28:8759-70 1995.

Marko, J.F. and Siggia, E.D. Polymer models of meiotic and mitotic chromosomes. *Mol. Biol. Cell* 8:2217-31. 1997.

Marko, J.F. *DNA under high tension: overstretching, undertwisting and relaxation dynamics*. *Phys. Rev. E* 57:2134-2149, 1998.

Marshall,W.F., Dernburg, A., Harmon, B., Agard, D.A., Sedat, J.W. Specific interactions of chromatin with the nuclear envelope: Positional determination within the nucleus in *Drosophila melanogaster*. *Mol. Biol. Cell* 7:825-842, 1996.

Marshall,W.F., Straight, A., Marko, J.F., Swedlow, J., Dernburg, A., Belmont, A., Murray, A.W., Agard, D.A. and Sedat, J.W. Interphase chromosomes undergo constrained diffusional motion in living cells. *Curr. Biol.* 7:930-939, 1997.

Marshall,W.F., J.F. Marko, D.A. Agard and J.W. Sedat. Chromosome elasticity and mitotic polar ejection force measured in living *Drosophila* embryos by four-dimensional microscopy-based motion analysis. *Curr. Biol.* 11:1-20, 2001.

Melby, T., Ciampaglio, C. N., Briscoe, G. and Erickson, H. P. The Symmetrical Structure of Structural Maintenance of Chromosomes (SMC) and MukB Proteins: Long, Antiparallel Coiled Coils, Folded at a Flexible Hinge. *J. Cell Biol.* 142:1595-1604. 1998.

Michaelis, C., Ciock, R. and Nasmyth, K. Cohesins: chromosomal proteins that prevent premature separation of sister chromatids. *Cell* 91:35-45 1997.

Micheli, T., Gunjan, A., Hock, R., Bustin, M. and Brown, D.T. Dynamic binding of histone H1 to chromatin in living cells. *Nature* 408:877-881, 2000.

Nicklas, R. B. Measurements of the Force Produced by the Mitotic Spindle in Anaphase. *J. Cell Biol.* 97:542-548, 1983.

Nicklas, R.B. How cells get the right chromosomes. *Science* 275:632-637, 1997.

Nguyen, T.T., Rouzina I., and Shklovskii, B.I. Reentrant condensation of DNA induced by multivalent counterions. *J. Chem. Phys.* 112:2562-2568, 2000.

Palmer, A., Xu, J., Kuo, S.C. and Wirtz, D. Diffusing wave spectroscopy microrheology of actin filament networks. *Biophys. J.* 76:1063-71 1999.

Paulson, J. R. and Laemmli, U. K. The structure of histone-depleted metaphase chromosomes. *Cell* 12:817-828, 1977.

Pearson, C.G., Maddox, P.S., Salmon, E.D. and Bloom, K. Budding yeast chromosome structure and dynamics during mitotis. *J. Cell Biol.* 152:1255-1266, 2001.

Pingoud, A.P. and Jeltsch, A. Structure and function of type II restriction endonucleases. *Nucleic Acids Res.* 29:3705-3727. 2001.

Poirier, M., Eroglu, S., Chatenay, D. and Marko, J.F. Reversible and irreversible unfolding of mitotic newt chromosomes by applied force. *Mol. Biol. Cell.* 11:269-76 2000.

Poirier, M.G., Nemani, A., Gupta, P., Eroglu, S. and Marko, J.F. Probing chromosome structure with dynamic force relaxation. *Phys. Rev. Lett.* 86:360-363, 2001.

Polach, K.J. and Widom, J. Mechanism of protein access to specific DNA sequences in chromatin: a dynamic equilibrium model for gene regulation. *J. Mol. Biol.* 254:130-49, 1995.

Robinett, C.C., Straight, A., Li, G., Willhelm, C., Sudlow, G., Murry, A. and Belmont, A.S. *In vivo* localization of DNA sequences and visualization of large-scale chromatin organization using lac operator/repressor recognition. *J. Cell Biol.*135:1685-1700, 1996.

Ray, J. and Manning, G. An attractive force between two rodlike polyions mediated by the sharing of condensed counterions. *Langmuir* 10:2450-2461, 1994.

Reese D.H., T. Yamada, and R. Moret. An Established Cell Line from the Newt *Notophthalmus viridescens*. *Differentiation* 6:75-81, 1976.

Reif, M., Guatel, M., Oesterhelt, F., Fernandez, J. M. and Gaub, H. E. (1997) Reversible Unfolding of Individual Titin Immunoglobulin Domains by AFM. Science 276, 1109-1112.

Rayleigh, J.W.S. *The Theory of Sound*, New York, Dover, 256-305, 1894.

Rieder, C. L. and Hard, R. Newt lung epithelial cells: cultivation, use, and advantages for biomedical research. *Int. Rev. Cytol.* 122:153-220, 1990.

Rieder, C.L. and Salmon, E.D. The vertebrate cell kinetochore and its roles during mitosis. *Trends Cell Biol.* 8:310-318, 1998.

Schmidt, F.G., Hinner, B., Sackmann, E. and Tang, J.X. Viscoelastic properties of semiflexible filamentous bacteriophage. *Phys. Rev. E* 62:5509-17. 2000.

Sen D. and Crothers, D. Condensation of chromatin: role of multivalent cations. *Biochemistry* 25:1495-1503, 1986.

Skibbens, R.V., Skeen V.P., and Salmon, E.D. Direction instability of kinetochore motility during chromosome congression and segregation in mitotic newt lung cells: a push-pull mechanism. *J. Cell Biol.* 122:859-875, 1993.

Smith, S. B., Finzi, L. and Bustamante, C. Direct Mechanical Measurements of the Elasticity of Single DNA Molecules by Using Magnetic Beads. *Science* 258:1122-1126, 1992.

Smith, S.B., Cui, Y.J. and Bustamante, C. Overstretching B-DNA: The elastic response of individual double-stranded and single-stranded DNA molecules. *Science* 271:795-799, 1996.

Smirnov, I.V., Dimitrov, S.I. and Makarov, V.L. Polyamine-DNA interactions. Condensation of chromatin and naked DNA. *J. Biomol. Struct. Dyn.* 5:1149-1161, 1988.

Smythe, C., and J.W. Newport. Systems for the study of nuclear assembly, DNA replication, and nuclear breakdown in *Xenopus laevis* egg extracts. *Methods Cell Biol.* 35:449-468, 1991.

Strick, T.R., Allemand J.F., Bensimon, D. and Croquette, V. The elasticity of a single supercoiled DNA molecule. *Science* 271:1835-1837, 1996.

Strick, T., Allemand, J.-F., Croquette, V. and Bensimon, D. The manipulation of single biomolecules. *Physics Today* 54(10):46-51, 2001.

Strunnikov, A.V., Larionov, V.L. and Koshland, D. SMC1: an essential yeast gene encoding a putative head-rod-tail protein is required for nuclear division and defines a new ubiquitous protein family. *J. Cell Biol.*123:1635-1648, 1993.

Sullivan, K.E. and Kay, S.A. *Methods in Cell Biology, Green Fluorescent Proteins*, London, Academic Press, 1999.

Sumner, A.T. Scanning electron microscopy of mammalian chromosomes from prophase to telophase. *Chromosoma*, 100:410-418, 1991.

Sutani, Y. and Yanagida, M. DNA renaturation activity of the SMC complex implicated in chromosome condensation. *Nature* 388:798-801, 1997.

Tang, J.X. and Janmey, P.A. The polyelectrolyte nature of f-actin and the mechanism of actin bundle formation. *J. Biol. Chem.* 271:8556-8563, 1996.

Thoma, F., Bergman, L. W. and Simpson, R. T. Nuclease Digestion of circular TRP1ARS1 chromatin reveals positioned nucleosomes separated by nuclease-sensitive regions. *J. Mol. Biol.* 177:715-733, 1984.

Tskhovrebova, L., Trinick, J., Sleep, J.-A. and Simmons, R.-M. Elasticity and unfolding of single molecules of the giant muscle protein titin. *Nature* 387:308-312, 1997.

Tumbar, T. and Belmont A.S. Interphase movements of a DNA chromosome region modulated by VP16 transcriptional activator. *Nat. Cell Biol.* 3:134-139, 2001.

van Holde, K. E. *Chromatin*, New York, Springer-Verlag, p. 343, 1989.

Watermann-Storer, C.M. and Salmon, E.D. How microtubles get fluorescent speckles. *Biophys. J.* 75:2059-2069, 1998.

Watson, J.D. and Crick, F.H.C. Molecular structure of nucleic acids. A structure for deoxyribose nucleic acid. *Nature* 171:964-967, 1953.

Widom, J. Chromosome structure and gene regulation. *Physica A* 244:497-509, 1997.

Widom, J. Structure, dynamics, and function of chromatin *in vitro*. *Annu. Rev. Biomol. Struct.* 27:285-327, 1998.

Yager, T.D., McMurray, C.T. and van Holde, K.E. Salt-induced release of DNA from nucleosome core particles. *Biochemistry* 28:2271-2281, 1989.

Yin, H., Pruyne, D. Huffaker, T.C. and Bretscher, A. Myosin V orientates the mitotic spindle in yeast. *Nature* 406:1013-1015, 2000.

Zlantanova, J., Leuba S.H. and van Holde, K. Chromatin fiber structure: morphology, molecular determinants, structural transitions. 74:2554-66, 199

VITA

NAME: Michael Guy Poirier

EDUCATION: B.S., Truman State University (formerly Northeast Missouri State University), 1995
M.S., University of Illinois at Chicago, 1997

PROFESSIONAL MEMBERSHIP: American Physical Society
American Society of Cell Biology.

ABSTRACTS: Biophysical Characterization of Structure and Elasticity of Mitotic Chromosomes, American Society for Cell Biology Annual Meeting, Dec. 13-17, 2000.

Elasticity Measurements Reveal Differences Between In Vivo and In Vitro Assembled Chromosomes, FASEB summer research conference 2000, Yeast Chromosome Structure, Aug. 19-24, 2000.

Microelasticity of Single Mitotic Chromosomes, American Physical Society March Meeting, March 20-24, 2000.

Elasticity of Metaphase Chromosomes, Biophysical Society Annual Meeting, Feb. 13-17, 1999.

PUBLICATIONS: Poirier, M., Eroglu, S., Chatenay, D. and Marko, J.F. Reversible and irreversible unfolding of mitotic newt chromosomes by applied force. *Mol. Biol. Cell* 11:269-276, 2000.

Poirier, M.G., Nemani, A., Gupta, P., Eroglu, S. and Marko, J.F. Probing Chromosome structure with dynamic force relaxation. *Phy. Rev. Lett.* 86:360-363, 2001.

Poirier, M.G., Manhait, T. and Marko, J.F. Reversible hypercondensation and decondensation of mitotic chromosomes studied using combined chemical-micromechanical techniques. *J. Cell. Biochem*., in press.

Sarkar, A., Eroglu, S., Poirier, M.G., Nemani, A., Gupta, P. and Marko, J.F. Dynamics of chromosome compaction during mitosis. *Exp. Cell. Res*. in press.

Poirier, M.G., Eroglu, S. and John F. Marko, J.F. The bending rigidity of mitotic chromosomes. Submitted.

Poirier, M.G., and Marko, J.F., Effect of internal friction on biofilament dynamics, Submitted.

Poirier, M.G. and Marko, J.F. Metaphase chromosomes are chromatin networks with no contiguous protein scaffold. In preparation.

MICROMECHANICAL BIOCHEMICAL STUDIES OF MITOTIC CHROMOSOME ELASTICITY AND STRUCTURE

Michael Guy Poirier, Ph.D.
Department of Physics
University of Illinois at Chicago
Chicago, Illinois (2001)

The structure of mitotic chromosomes was studied by combining micromechanical force measurements with microfluidic biochemical exposures. Our method is to use glass micropipettes attached to either end of a single chromosome to do mechanical experiments in the extracellular buffer. A third pipette can be used to locally 'spray' reactants so as to carry out dynamical mechanical-chemical experiments. The following elastic properties of mitotic chromosomes are found: Young's modulus, Y = 300 Pa; Poisson ratio, σ = 0.1; Bending rigidity, $B = 1\times10^{-22}$ J·m; Internal viscosity, η' = 100 kg/m·sec; Volume fraction, ϕ = 0.7; Extensions of less than 3 times the relaxed length are linear and reversible; Extensions beyond 30 fold exhibit a force plateau at 15 nN and convert the chromosome to a disperse ghost-like state with little change in chromatin structure; Mitotic chromosomes are relatively isotropic; dsDNA cuts of at least every 3 kb cause the a mitotic chromosomes to fall apart; dsDNA cuts less frequently than every 50 kb do not affect mitotic chromosome structure. These results lead to the conclusion that mitotic chromosomes are a network crosslinked every 50 kb between which chromatin is fold by chromatin folding proteins, which are likely to be condensins.